# Progression of Mitochondrial Network Dysfunction in Cardiomyocytes and the Arrhythmogenic Implications: A Computational Study

**by**

**Brent Millare**

**A dissertation submitted to The Johns Hopkins University**

**in conformity with the requirements for the degree of**

**Doctor of Philosophy**

**Baltimore, Maryland**

**June, 2018**

# Abstract

Dense, tightly coupled networks, found throughout nature are vulnerable to cascading failure, where a small increase in stress can create a decrease in performance across the whole network. Mitochondria exist as dense networks within cardiomyocytes to meet the large energetic demands of heart function but are vulnerable to excessive oxidative stress such as during ischemia/reperfusion. Arrhythmia are observed in hearts exposed to oxidative stress and they occur just after the mitochondrial network within the tissue fails, suggesting an arrhythmogenic role of mitochondrial failure. This work investigates the mechanisms underlying the progression of mitochondrial network failure and how this failure can scale to the whole heart.

A computational modeling approach was used to study the complex systems existing at multiple spatial and temporal scales. First, a mitochondrial network model was developed, where mitochondria were coupled by diffusion of reactive oxygen species (ROS) including superoxide and hydrogen peroxide. The simulation results revealed that while superoxide was important for propagating mitochondrial depolarizations across the network, diffusion of hydrogen peroxide was required for extending the failure region

to the rest of the network. Failure of the network could not occur until depletion of the network's scavenging capacity, which superoxide alone could not induce because of its periodic release.

Second, a ventricular myocyte model that included a mitochondrial component was incorporated into a 2D tissue model to study how oscillation of mitochondrial membrane potential can create reentry. A large enough region of tissue with depolarized mitochondria had lower ATP levels, and activated ATP sensitive potassium channels that reduced their excitability and shortened their action potential duration (APD). Upon repolarization of the mitochondria, the tissue became excitable and an existing propagating wave was able to spontaneously propagate in reverse, creating reentry.

Together, these findings demonstrate the link between mitochondrial failure and arrhythmia, through the emergence of complex, arrhythmogenic spatiotemporal patterns of excitability. This research provides new potential targets for pharmaceutical intervention that may be used to prevent post-ischemic arrhythmia such as from a myocardial infarction.

# Thesis Committee

## Primary Readers

Natalia Trayanova (Primary Advisor)
Professor
Department of Biomedical Engineering
Johns Hopkins Whiting School of Engineering
Johns Hopkins Whiting School of Medicine

Brian O'Rourke
Professor
Department of Cardiovascular Medicine
Johns Hopkins Whiting School of Medicine

## Alternate Readers

Raimond Winslow
Professor
Johns Hopkins Whiting School of Engineering
Johns Hopkins Whiting School of Medicine

# Acknowledgments

This work would not be possible without my supportive family. Even though they are on the other coast, I always feel connected to them. Thank you my friends for the wonderful years we shared together in graduate school. Thank you Lanlan, my girlfriend, for your inspirational stories and nourishing delicious food you cooked for me. Thank you Dr. Raimond Winslow for providing me with research advice. Thank you Dr. Brain O'Rourke for showing me the interesting world of mitochondria. Finally, thank you Dr. Natalia Trayanova for being patient with me and helping me develop my skills as a scientist and communicator.

# Table of Contents

**Table of Contents** vi

**List of Tables** x

**List of Figures** xi

**1 Background and Motivation** 1

1.1 Mitochondria . . . . . 1

1.1.1 Mitochondrial Structure . . . . . 2

1.1.1.1 Outer Membrane . . . . . 4

1.1.1.2 Intermembrane Space . . . . . 4

1.1.1.3 Inner Membrane . . . . . 4

1.1.1.4 Matrix . . . . . 5

1.1.2 ROS Production . . . . . 6

1.1.3 ROS Scavenging . . . . . 7

1.2 Heart . . . . . 8

1.2.1 Cardiac Electrophysiology . . . . . 8

1.2.2 Arrhythmia . . . . . 12
1.3 Role of Mitochondria in Cardiac Arrhythmia . . . . . 15
1.3.1 Ischemia/Reperfusion . . . . . 15
1.3.2 Mitochondrial Network Failure . . . . . 16
1.3.3 Network Communication Mechanisms . . . . . 17
1.3.4 Mitochondrial Failure and Electrophysiology . . . . . 20

**2 General Methods** **27**
2.1 Computational Modeling . . . . . 27
2.2 Mitochondrial Models . . . . . 27
2.2.1 Single Mitochondrion . . . . . 27
2.2.2 Network . . . . . 28
2.3 Cardiac Electrophysiology Modeling . . . . . 28
2.4 Single Myocyte . . . . . 28
2.5 Cardiac Tissue . . . . . 29

**3 Mitochondrial network dysfunction** **32**
3.1 Introduction . . . . . 32
3.2 Methods . . . . . 36
3.2.1 Computational Model Summary . . . . . 36
3.2.2 Oxidative Stress Stimulation Protocol . . . . . 40
3.3 Results . . . . . 41
3.3.1 Mitochondrial Network Response to ROS Stimulus . . 41

3.3.2 Mechanisms Driving Mitochondrial Network Failure Patterns . . . 46
3.3.3 Dependence of Mitochondrial Network Response on ROS Stimulus Makeup . . . 50
3.4 Discussion . . . 52
3.4.1 Hydrogen Peroxide Communication & Accumulation Enables SO Accumulation & Communication . . . 54
3.4.2 Delay in Network Response to Oxidative Stress is from Scavenging Capacity Depletion Time Course . . . 56
3.4.3 Modeling Variations in Mitochondrial Network Failure Behavior . . . 58
3.5 Appendix . . . 60
3.5.1 Methods . . . 60
3.5.1.1 Mitochondrial Model Additions . . . 60
3.5.1.2 Computational Methods . . . 62
3.5.2 Model Equations . . . 63

**4 Effect of Multiple Non-coherent Clusters of Oscillating Mitochondria on Electrical Propagation** **84**
4.1 Introduction . . . 84
4.2 Methods . . . 86
4.2.1 Computational Model . . . 86
4.2.2 Simulation Protocol . . . 87

4.2.3 Phase Distribution Algorithm . . . . . 90
4.3 Results . . . . . 91
4.3.1 Formation of Inexcitable Region . . . . . 91
4.3.2 Recovery of Mitochondrial Energetics Induces Spontaneous Arrhythmia . . . . . 92
4.3.3 Dynamic Excitability of Small Clusters Induces Spontaneous Arrhythmia . . . . . 95
4.4 Discussion . . . . . 99
4.4.1 Limitations . . . . . 102
4.4.2 Future Directions . . . . . 103

**5 Conclusion** **109**

5.1 Summary of findings . . . . . 109
5.2 Future directions . . . . . 110

# List of Tables

3.1 **Propagating Wave Depolarization Start Times (seconds)** . . . 54

# List of Figures


1.1 Components of Mitochondria . . . . . 3

1.2 Ion currents of a cardiac action potential . . . . . 10

1.3 Types of Reentry . . . . . 13

3.1 Mitochondrial arrangement in a myocyte . . . . . 35

3.2 Model Schematics . . . . . 38

3.3 ROS Stimulated Mitochondrial Network Without $H_2O_2$ Diffusion 42

3.4 ROS Stimulated Mitochondrial Network with $H_2O_2$ diffusion 44

3.5 Evolution of the Region Vulnerable to Failure and Regions of ROS Accumulation in the Mitochondrial Network . . . . . 47

3.6 Evolution of $H_2O_2$ Accumulation and $H_2O_2$ Scavenging Capacity Depletion in the Mitochondrial Network . . . . . 51

3.7 Variations in Mitochondrial Network Oscillation Frequency and Timing Depending on the ROS Stimulus Makeup . . . . . 53

4.1 ECME-RIRR Model Schematic . . . . . 88

4.2 Tissue Slab Protocol Scheme . . . . . 89

4.3 Parameterization of Mitochondrial Oscillation State . . . . . 90
4.4 Effect of reactive oxygen species (ROS)-induced regional mitochondrial depolarization on metabolic sink formation and electrical wave propagation . . . . . 93
4.5 Effect of recovery of mitochondrial inner membrane potential ($\Delta\Psi_m$) on electrical propagation . . . . . 94
4.6 Electrical wave, mitochondrial inner membrane potential ($\Delta\Psi_m$) recovery, and $I_{KATP}$ during waveback breakthrough . . . . . 96
4.7 Reentry from the side . . . . . 96
4.8 Iterative phase distribution gGeneration . . . . . 97
4.9 Electrical wave propagation with generated mitochondrial oscillation phase distributions . . . . . 98
4.10 Dynamic excitability of small tissue clusters . . . . . 99

# Chapter 1

# Background and Motivation

## 1.1 Mitochondria

Mitochondria are required for the survival of practically all eukaryotic organisms. They are dedicated cellular organelles that efficiently provide energy to the cell in the form of adenosine triphosphate (ATP) derived from glucose and fatty acid substrates. Oxidative phosphorylation is the highest yielding ATP generating processes found in nature and is present in mitochondria and aerobic bacteria. Like bacteria, mitochondria are roughly 1 um in diameter in most cells, however, they can vary widely in shape, size, and structure (Wiemerslage and Lee, 2016; Frey and Mannella, 2000). Further, their organization can vary depending on the tissue and cell type. For example, in neuronal cells, their arrangement is sparse, whereas in cardiac cells, they form a dense lattice (Brian O'Rourke et al., 2007). Given that a by-product of the respiration process from mitochondria is the production of reactive oxidative species (ROS) that can damage the cell, the accumulation of ROS from densely packed mitochondria can have a large impact on the function of the cell. ROS are also

important for regulation and controlled cell death (apoptosis) such as during embryonic development in animals, but excessive ROS can lead to pathophysiological behavior of the cell and necrosis. Mitochondria have ROS scavenging systems to keep the levels in check and the dysfunction of these systems can lead to pathophysiological cell behavior. Further, accumulation of damage from ROS requires that the population of mitochondria in the cell repair, tear down, or build new mitochondria through a complex process of biogenesis, mitochondrial fission, and fusion. Cells that have a larger energetic demand, such as cardiac myocytes, require more mitochondria, and regulation of all the described processes becomes more important. Since calcium is used for the contraction of muscles, which is a energetically demanding process, calcium is also important for regulating mitochondrial function. However, mitochondria are also important in regulating calcium for the cell. Thus, mitochondria are intimately tied to the functions of the cell and are important to study.

### 1.1.1 Mitochondrial Structure

Like the cell membranes of almost all living organisms, mitochondrial membranes are composed of phospholipid bilayers and proteins. Unlike most organelles, mitochondria have two membranes instead of one, an inner and outer membrane (Figure 1.1). The regions at or within the outer membrane are discussed.

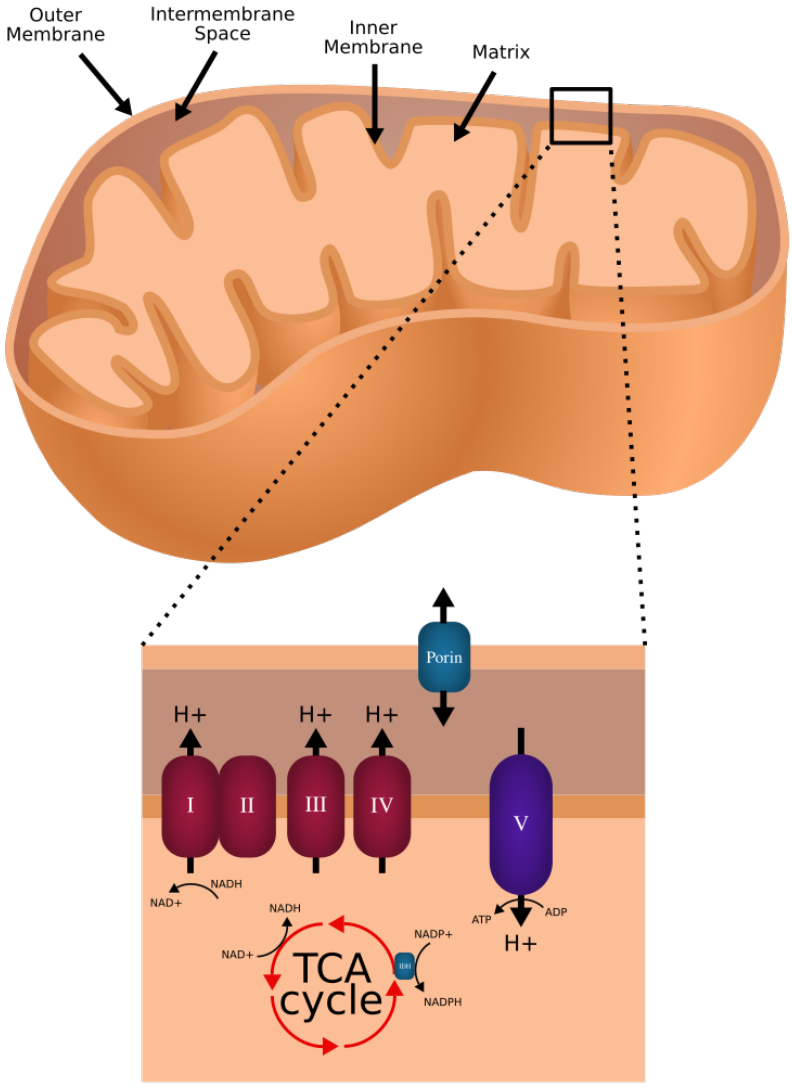


**Figure 1.1: Components of Mitochondria** The inset shows components of the electron transport chain in the inner membrane and how they are coupled to the tricarboxylic acid cycle.

#### 1.1.1.1 Outer Membrane

The outer membrane is relatively permeable since small molecules (<5000 daltons) can cross the membrane in both directions via channels called porins, which includes the voltage dependent anion channel. Larger proteins can enter through with the coordinated effort of translocase proteins (Schatz, 1996; Neupert, 1997). Release of the cytochrome c from the inside of the mitochondria and other inner components of the mitochondrion can induce apoptosis or necrosis. The outer membrane can also interact with the endoplasmic reticulum to aid in calcium signaling between the two organelles.

#### 1.1.1.2 Intermembrane Space

This is the relatively thin space formed between the outer and inner mitochondrial membrane. Since the outer membrane is permeable to small molecules, the concentrations of these small molecules is the similar to those in the cytosol, however, the concentration of protons will be higher in this space due to the pumping of the protons out of the matrix and into the intermembrane space via protein complexes, as part of the electron transport chain (ETC), located in the inner membrane. Also, incoming large proteins must have a special sequence in order to be transported through the outer and inner membranes.

#### 1.1.1.3 Inner Membrane

In contrast to the outer membrane, the inner membrane is not permeable to most ions and small molecules, apart from calcium. Most of the ions and

molecules require special membrane transporters to enter or exit the matrix. The electric transport chain consists of protein complexes that reside in the inner membrane. Complexes I, II, III, and IV, produce a proton gradient (an electrochemical gradient which is both an electrical and pH gradient) across the inner membrane, which then is used by complex V, ATP synthase, to produce ATP. The impermeability of the membrane is important for the efficiency of ATP generation by reducing the leakage of protons across the membrane and maintaining the mitochondrial membrane potential ($\Delta\Psi_m$). The inner membrane is arranged with many folds that increase the surface area to volume ratio, which is important for optimizing the ratio of electron transport chain machinery vs the citric acid cycle machinery.

#### 1.1.1.4 Matrix

The inner membrane encloses the matrix space. Mitochondria have their own machinery to produce RNA and proteins. The citric acid cycle is located in the matrix and is the series of chemical reactions that convert the stored energy derived from carbohydrates, fats, and proteins into intermediates that are used to power the electron transport chain and oxidative phosphorylation. The cycle consumes acetyl co-enzyme A and water to form the main products, which are reduced nicotinamide adenine dinucleotide (NADH) and carbon dioxide. The generated intermediates of the cycle may also be used for different functions. Malate and isocitrate are used by malic enzyme and NADP+-dependent isocitrate dehydrogenase respectively, to produce nicotinamide adenine dinucleotide phosphate (NADPH), which is used to drive reactions that scavenge of ROS. The theoretical maximum yield of a single

glucose molecule is 38 ATPs but the actual efficiency is reduced from the costs of transport and leakage of protons.

### 1.1.2 ROS Production

ROS can be produced in cells from a wide range of mechanisms. Ultraviolet light is a form of ionizing radiation that can completely remove an electron from a molecule and thus form a free radical, which is highly reactive and can damage many components of the cell. While sunlight exposure is a large source of exogenous ROS, the largest source of endogenous ROS is from the mitochondria. The electron transport chain involves the a series of electron donor/accepter reactions. An electron is passed to a successively more electronegative acceptor, with oxygen being the final acceptor. Oxygen is ideally reduced to water but electrons that leak from this process prevent proper full pairing and instead form ROS intermediates. The most unstable ROS is superoxide, followed by hydroxyl, and then hydrogen peroxide. A small percentage of electron leak is normal for mitochondria and forms basal level of ROS production. Increase of electron chain reduction does increase the production of ROS but the ROS scavenging system can compensate for this increase. In fact, a decrease in activity increases ROS production because the elctron donor sites become more reduced. Metabolic stress such as during ischemia/reperfusion, increases the level of ROS production. ROS can impair mitochondrial and cell function by damaging DNA, and oxidizing lipids and proteins. The resulting damage can induce further electron leakage and scavenging depletion, creating a vicious cycle of ROS overload.

### 1.1.3 ROS Scavenging

To deal with the intrinsic ROS production of the electron transport chain, mitochondria have sophisticated ROS scavenging systems. Superoxide is highly reactive but is quickly converted to hydrogen peroxide by superoxide dismutase (SOD). SOD is located in the mitochondrial matrix and the cytosol. Hydrogen peroxide is less reactive than superoxide but can more easily diffuse throughout the cell because of the lack of charge. Catalase is an enzyme that converts hydrogen peroxide into water. It exists throughout most cells but is not present in heart mitochondria. To improve the scavenging of hydrogen peroxide, mitochondria have an energetically driven scavenger, glutathione peroxidase. Glutathione peroxidase uses the reducing potential of glutathione to convert hydrogen peroxide into water. The resulting oxidized glutathione can then be reduced by glutathione reductase, which is energetically driven by NADPH. NADPH levels are maintained by nicotinamide nucleotide transhydrogenase, malic enzyme and NADP+-dependent isocitrate dehyrogenase, which are driven by the metabolic intermediates of the citric acid cycle. NADPH also drives the reduction of thioredoxin through thioredoxin reductase, which contributes to hydrogen peroxide scavenging through thioredoxin-dependent peroxiredoxins. Because NADH and NADPH production both depend on the TCA cycle, under conditions of high energy demand, activation of the TCA cycle, for example by calcium, is important for both ATP production and ROS scavenging.

## 1.2 Heart

The heart is composed of electrically coupled muscle cells that form the main chambers of the heart, which are the left and right versions of the atria and ventricles. The cardiac muscle cells contract in response to an electrical stimulus. Cardiac myocytes are electrically coupled via gap junctions and electrical signals can propagate throughout the tissue. Uncoordinated contraction of the chambers does not result in sufficient blood flow to meet the metabolic demands of the organism and thus a complex coordinated electrical conduction system is necessary to coordinate the contractions. Regular temporally spaced contractions are initiated by electrical signals from pacemaker cells in the sinoatrial node. These signals rapidly propagate throughout the remaining tissue through a complex network of Purkinje fibers composed of specialized signal carrying cells. Proper timing of the relaxation of the heart is also necessary to properly refill the chambers of the heart with new blood.

### 1.2.1 Cardiac Electrophysiology

Cardiac cells coordinate contraction by communicating using electrical signals called action potentials, which are complex transient fluctuations in voltage across the cellular membrane. The voltage is formed due to the different concentration of ions between outside and inside of the cell, resulting in a difference in charge like in a capacitor. Specialized proteins called ion channels are embedded in the membrane and are selectively permeable to different ions. At any given moment, the net flow of ions going in and out of the cell are determined by the combination of the conductivity of the

ion channels and a balance between the flux due to the voltage across the membrane (the transmembrane potential), and flux due to diffusion from the difference in concentration across the membrane. Controlled changes in the ion channel conductance changes the current and results in controlled changes in the transmembrane potential because of the capacitance of the cell. The complex action potential shape is produced by the fluxes of different ion types through their corresponding channels, exchangers, and pumps (Figure 1.2). The characteristic shape consists of a depolarization, plateau, repolarization, and resting components.

Neighboring cardiac cells are connected by gap junctions permeable to ions. Neighboring cell currents induce neighboring changes in transmembrane potential, allowing signals to propagate from cell to cell. These changes in electric potential travel across the heart faster than signals from changes in chemical concentration from just chemical diffusion. Because of the additional capacitance of the neighboring cell, the induced voltage change is reduced for each additional cell and limits the maximum communication distance. Further propagation of the electrical signal requires active enhancement.

There is an abundance of sodium ion channels that open in response to a positive change in transmembrane potential. Since the resting transmembrane potential of the cell is around -80mV and the concentration of sodium ions is larger outside the cell, opening a sodium ion channel results in a positive current that raises the transmembrane potential of the cell. Thus, a positive feedback loop exists to ensure a positive change in transmembrane potential, and then electrical propagation between cells. The positive change in voltage

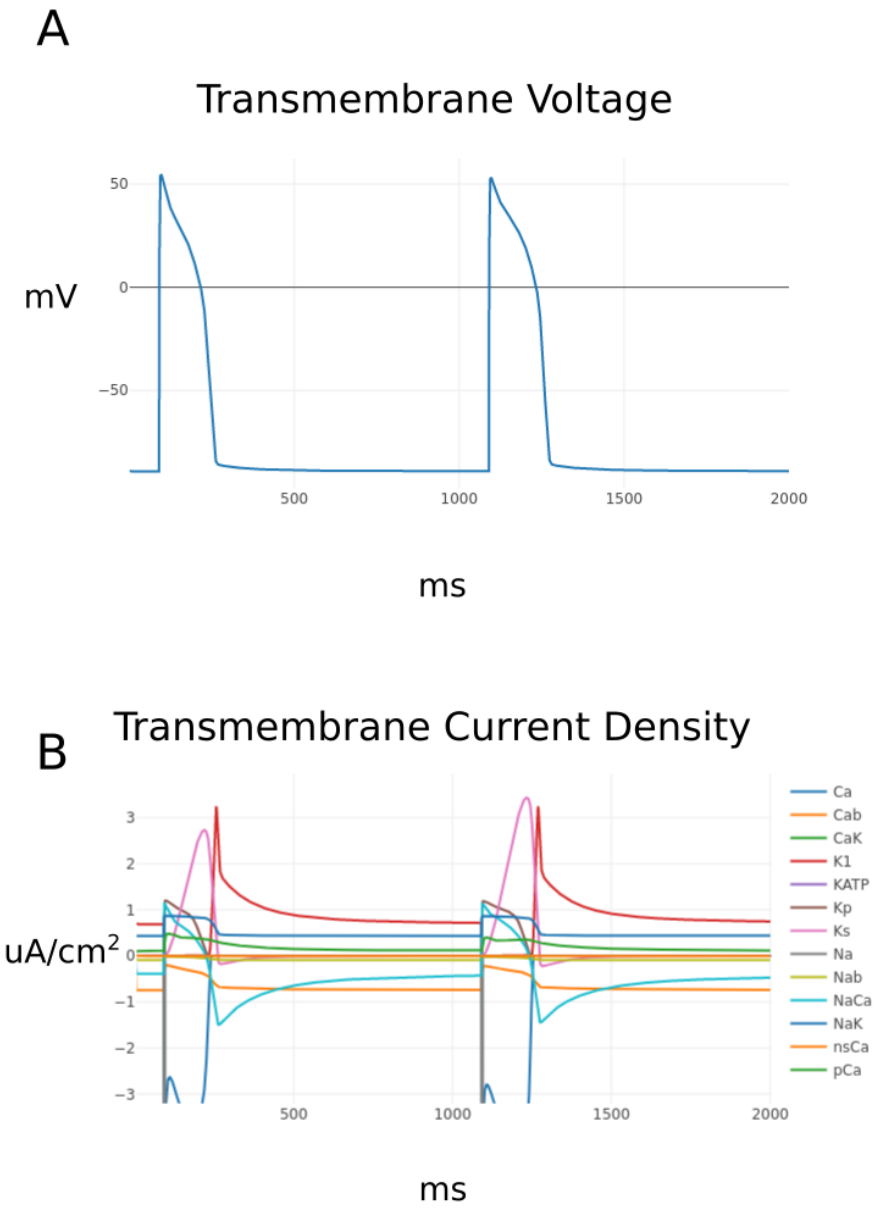


**Figure 1.2: Ion currents of a cardiac action potential** **A.** Normal voltage profiles of an action potential from a guinea pig cardiomyocyte model. **B.** Current contributions of the different ion channels, exchangers, and pumps.

is called a depolarization because the resting potential is negative and the end of the changed potential is closer to zero. If the sodium channel remained open, the voltage would quickly approach the Nernst potential of sodium, which is around 60mV, resulting in no more net flux of sodium ions across the membrane. However, the sodium channel has inactivation components that decrease conductance after seeing the positive voltage. This decrease from inactivation occurs more slowly than the increase from activation, thus creating a transient influx of sodium that still results in a positive change in transmembrane potential. The sodium current is responsible for the rapid upstroke of the action potential.

The contraction mechanisms that physically shorten the cell are activated by an increased calcium concentration. The myocyte has two main pathways for calcium influx, the L-type calcium channel and the sodium calcium exchanger. The inward calcium currents sustain the plateau phase of the action potential.

Relaxation of the tissue is just as important as contraction for the heart to properly function as a pump. The cardiac cell stops contracting when the transmembrane potential returns to its resting potential, and calcium is cleared from the contractile elements by exchangers and pumps. The resting transmembrane potential of the cardiac myocyte is around -80mV, which is close to the Nernst potential of potassium of -90mV because potassium currents drive repolarization to near its Nernst potential. The return to the negative voltage also resets the voltage sensitive components of the ion channels which restores the excitability of the cell for the next contraction.

The shape of the cardiac action potential is complex and requires the coordination of multiple ion channels and exchangers, which are sensitive to changes in voltage and concentration, that activate and deactivate at different rates. The shape is also stable, where a stimulus larger than the intensity threshold required to activate the positive feedback loop does not change the resulting action potential shape significantly. The propagation velocity is also stable because weaker electrical signals of distant neighbors are effectively amplified and an intense stimulation is attenuated over a distance. The action potential duration, the span of time between the upstroke and return to baseline of the action potential, is also stable. After the action potential occurs, there is a period of quiescence until a new beat is initiated from a neighboring myocyte.

### 1.2.2 Arrhythmia

Cardiac arrhythmia are disruptions of the normal pattern of repeated electrical propagation within the heart. Arrhythmia can occur when the heartbeat rhythm is either too slow (bradyarrhythmia) or too fast (tachyarrhythmia). Certain types of arrhythmia can disrupt coordinated contraction to an extent that impairs or prevents the heart's ability to effectively pump blood. Arrhythmia can be caused by a change in firing rate of pacemaker tissue or from non-pacemaker cells from triggered activity (ectopy) or by reentry. Triggered activity can occur when enough cardiac cells can spontaneously excite from altered electrical properties such as from calcium or sodium overload. Reentry

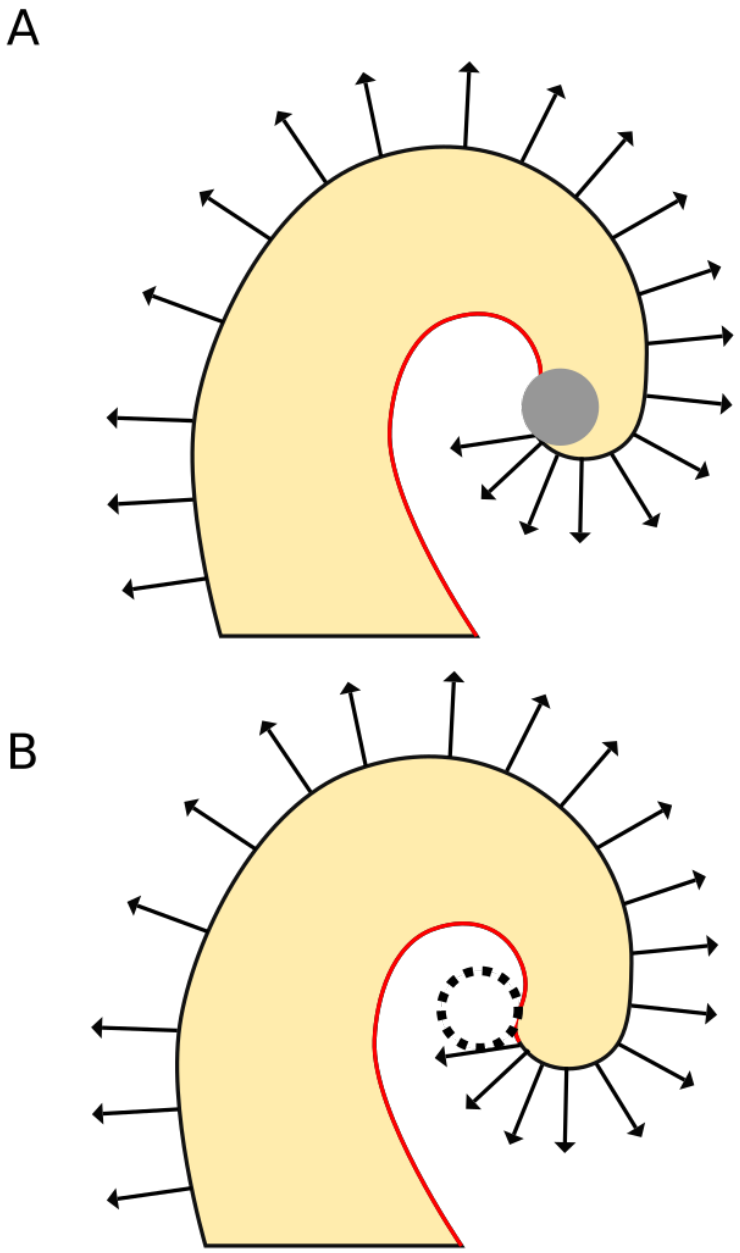


**Figure 1.3: Types of Reentry** 2D schematic representation of anatomical reentry **A.** anchored by a non-conducting region (gray) or functional reentry **B.** continuously rotating around an un-excited region (dotted circle)

is when an excitation wave returns and re-excites the same tissue. The excitation wave does not terminate and instead returns to the previously excited area. In order for reentry to occur, the previously excited regions need to recover from their refractory state. Because the path of reentry is shorter than the path of a normal excitation wave, the excitation frequency is higher and results in a higher heart beat rhythm. A persistent reentrant wave is when a reentrant wave does not terminate. The wavelength of an excitation wave is the length of the excited tissue along the direction of the wave. The length of the path of excitation wave needs to be large enough so that when it returns to the tissue that was previously excited, the tissue is no longer refractory and instead becomes re-excitable so that reentry can occur. Therefore, excitation wave conduction velocity and the dispersion of the refractory period promotes reentry.

There are two different types of reentry, anatomical and functional. Anatomical reentry is when the reentrant wave travels around an inexcitable tissue such as due to scar (Figure 1.3A). Functional reentry is when the reentrant wave travels around tissue with altered electrical properties (Figure 1.3B). A reentrant wave creates a spiral wave where the conduction velocity is higher at the edge and is zero at the center. Reentrant waves will continue to rotate around a phase singularity, which is where the activation state of tissue cannot be determined because the conduction velocity is zero. In functional reentry, the center where the reentrant wave travels around, can drift over time. Reentrant waves will terminate by colliding with other waves or by drifting into non-conducting regions. Fibrillation, the worst type of tachyarrhythmia,

occurs when a reentant wave breaks up into multiple smaller waves creating chaotic random activations that severely impair the heart's ability to pump blood.

## 1.3 Role of Mitochondria in Cardiac Arrhythmia

### 1.3.1 Ischemia/Reperfusion

Ischemic heart disease is the global number one cause of death. Sudden cardiac death (SCD) is the most common manifestation of cardiovascular disease. Most stable risk factors are not predictive enough to facilitate recommendation of therapeutic interventions prior to a cardiac event and thus transient risk factors are more likely to play a role(Zipes and Wellens, 1998). Only a small fraction of the patients who survive cardiac arrest show signs of transumural myocardial infarction and a transient ischemic event is believed to be the cause(Zipes and Wellens, 1998). Such an event might be caused by temporary occlusion from a spasm or an unstable plately thrombi(Fuster, Poon, and Willerson, 1998).

Ischemia is the interruption of the supply of oxygen and nutrients to a region of tissue. Prolongation of ischemia can result in cell death and the formation of scar tissue. Reperfusion is the restoration of blood flow to that region and prevents further damage from ischemia. Restoration of function is possible when the ischemic event was not too severe. However, reperfusion itself can cause additional damage, a phenomenon called reperfusion injury(Carry et al., 1989; Maxwell and Lip, 1997), and can even increase the risk of arrhythmia and cause sudden cardiac death(Wit and Janse, 2001).

Since energetic substrates and oxygen are important for mitochondrial function, mitochondria would be first affected by ischemia/reperfusion. Interestingly, prior to arrhythmia induced by reperfusion, there is an increase in the dispersion of refractoriness that is also concurrent with mitochondrial depolarizations of $\Delta\Psi_m$(Lyon et al., 2010; Slodzinski, Miguel a. Aon, and Brian O'Rourke, 2008; Akar et al., 2005).

### 1.3.2 Mitochondrial Network Failure

Mitochondria within cardiomyocytes organize in a dense lattice to provide the ATP generation capacity required for the high energetic demand of heart tissue. As a side effect, this high density also increases coupling between mitochondria via ROS communication. Highly coupled infrastructure networks are prone to cascading failure, where small initial shocks are able to collapse the efficiency of the entire network(Crucitti, Latora, and Marchiori, 2004). These types of failures occur in many different types of systems, including computer networks, biological networks, power transmissions, and transportations systems.

Mitochondrial networks are vulnerable to cascading failure when brought to a near critical state after exposure to oxidative stress such as during ischemia/reperfusion, exogenous ROS, or weakening of the network's scavenging capacity(Miguel a Aon, Cortassa, and Brian O'Rourke, 2004). Any additional stress introduced to a local region would cause local mitochondrial depolarizations that propagate to the rest of the network within the cell. Depolarized mitochondria represent mitochondrial failure because they cannot produce

ATP for the cell. Propagation of this failure to the rest of the network diminishes the ATP available for the cell to use. Mitochondrial network failure has been shown to lead to arrhythmia(Brown et al., 2010) but findings from ischemia/reperfusion experiments in monolayers and computational models have only began to reveal the linking mechanisms(Solhjoo et al., 2015; Zhou, Solhjoo, et al., 2014).

Mitochondrial network failure requires mechanisms for synchronization and propagation of membrane depolarizations. Electrical coupling of neighboring mitochondria might be such a mechanism(Amchenkova et al., 1988) given the connected appearance from 3D high resolution focused ion beam scanning electron microscopy images(Glancy et al., 2015). However, experimental observations of local depolarizations of mitochondrial membrane potential that only propagate after a long delay from a local stimulus suggest a different, slower mechanism(Miguel a. Aon et al., 2003). Given that depolarization propagations are rapid but the rate of synchronization of the network is slow and can have a delay(Miguel a. Aon et al., 2003; Zhou, Miguel a. Aon, et al., 2010), a mechanism that relies on diffusion of chemical messengers would need to account for short and long range communication between mitochondria.

### 1.3.3 Network Communication Mechanisms

The fact that the depolarization rate is rapid compared to repolarization rate, and that propagation occurs rapidly, suggests a short range communication mechanism that relies on an energy dissipating ion channel that is opening.

Since mitochondria respond to elevated ROS concentrations by producing or releasing additional ROS, termed ROS-induced-ROS-release (RIRR)(Brady et al., 2006), a channel that opens in response to ROS and can simultaneously release ROS and depolarize the membrane would be a possible mechanism. The permeability transistion pore, a large non-selective ion channel that can irreversibly depolarize the mitochondria, was ruled out experimentally(Miguel a. Aon et al., 2003; B O'Rourke, Ramza, and Marban, 1994). Instead, based on pharmacological evidence, a ROS-sensitive inner membrane anion channel (IMAC) is believed to underly RIRR(A D Beavis, 1989; Andrew D Beavis, 1992; Miguel a. Aon et al., 2003).

IMAC is sensitive to the specific ROS, superoxide (SO). Sufficient SO near a mitochondrion can diffuse through the mitochondrial outer membrane and into the mitochondrial intermembrane space, and trigger an opening of IMAC(Cortassa et al., 2004). Opening of the IMAC releases stored SO and other anions out of the mitochondrial matrix, resulting in $\Delta\Psi_m$ depolarization. RIRR via IMAC can be extended throughout the network when most of the mitochondria contain a near critical amount of SO within the matrix(M. A. Aon et al., 2006). Propagation occurs as SO released from one mitochondrion diffuses to a neighboring mitochondrion and initiates additional IMAC openings and release of accumulated SO. Waves of SO release and its corresponding propagation of $\Delta\Psi_m$ depolarization have been demonstrated in the intact heart in laser flash experiments(Miguel a. Aon et al., 2003). Ejection of SO enables rapid conversion of SO into hydrogen peroxide, a less reactive ROS, via additional scavenging support of cytoplasmic super-oxide dismutase (SOD).

After the elevated SO levels surrounding a mitochondrion have subsided, the IMACs close and the mitochondrion can repolarize its membrane potential. Thus, SO diffusion and IMAC opening is the short range communication mechanism used between mitochondria.

What remains unknown is how these short range communications, which depend on SO, a messenger with a short half-life, can scale to the rest of the cell. Interestingly, laser flash experiments, where a localized stimulus of oxidative stress can gradually spread throughout the mitochondrial network and eventually form a localized oscillatory region, showed a delay before the first cascade of mitochondrial depolarizations(Cortassa et al., 2004; Miguel a. Aon et al., 2003; Miguel a Aon, Cortassa, and Brian O'Rourke, 2004). Models by Zhou et al(Zhou, Miguel a. Aon, et al., 2010) and Yang et al(Yang et al., 2010), which demonstrated RIRR propagation of $\Delta\Psi_m$ depolarization and its corresponding wave of SO release from the mitochondrial matrices across the network, and the stochastic model of the mitochondrial network developed by Nivala et al(Nivala et al., 2011), failed to reproduce the delay. A common property of these previous models was that they relied on SO as the main communicator of oxidative stress. Further, these models assumed a near threshold level of oxidative stress throughout the network, and thus, could not capture what initiates the distribution of oxidative stress. Since communication via SO can only occur during IMAC induced depolarizations, a different communicator of oxidative stress that does not induce an IMAC opening seems likely to be involved.

While SO plays a key role in mitochondrial network failure via the RIRR

mechanism, the contribution of hydrogen peroxide, another ROS molecule, has not been explored. Hydrogen peroxide has a longer lifetime than SO and can more easily diffuse throughout the cytoplasm because of its lack of charge. In this dissertation, we hypothesized that hydrogen peroxide is an important communicator of oxidative stress and plays a key role in mitochondrial network failure by distributing mitochondrial dysfunction.

### 1.3.4 Mitochondrial Failure and Electrophysiology

Mitochondrial failure can scale to the whole heart and cause arrhythmia(Akar et al., 2005), but the detailed mechanisms of the process are not clear. ROS reactivity is non-selective, and can react with many electrophysiological components. For example, ROS can alter calcium cycling by increasing the activity of the ryanodine receptor(Zima and Mazurek, 2016). In this work, we explore a less direct mechanism. The proton pumps of the electron transport chain drive the formation of the electrochemical gradient, which is both the membrane potential $\Delta\Psi_m$ and the gradient of protons across the inner membrane. This potential drives ATP synthase to produce ATP from ADP. Depolarization of $\Delta\Psi_m$ results in loss of ATP production, and since the ATP synthase reaction is reversible, induces consumption of ATP to restore the lost potential(Sasaki et al., 2001). When enough mitochondria are depolarized in the network, the ATP levels can drop low enough to activate ATP-sensitive potassium channels that induce a large outward current that decreases excitability of the cell and APD(Noma, 1983; Lederer, Nichols, and Smith, 1989). Experimental work has been done to quantify these effects in isolated cardiomyocytes subjected to

metabolic stress(B O'Rourke, Ramza, and Marban, 1994). How these changes can produce reentry and the role of the distribution of mitochondrial failure remain unclear. In this dissertation, we hypothesize that a rapid change in excitability and refractoriness synchronized by mitochondrial oscillations, can create reentry. Further, the distributions of mitochondrial failure increase the likelihood of this reentry mechanism.

# References


Wiemerslage, Lyle and Daewoo Lee (2016). "Quantification of Mitochondrial Morphology in Neurites of Dopaminergic Neurons using Multiple Parameters". In: *Journal of neuroscience methods* 262, pp. 56–65. ISSN: 0165-0270. DOI: 10.1016/j.jneumeth.2016.01.008. URL: http://www.ncbi.nlm.nih.gov/pmc/articles/PMC4775301/.

Frey, Terrence G and Carmen A Mannella (2000). "Mannella - The Internal Structure of Mitochondria". In: *Trends Biochem Sci* 0004.July, pp. 1–6. URL: papers2://publication/uuid/07A16125-F493-43E7-8CEE-EF344B83E701.

O'Rourke, Brian, Sonia Cortassa, Fadi Akar, and Miguel Aon (2007). "Mitochondrial ion channels in cardiac function and dysfunction." In: *Novartis Foundation symposium* 287, 140–51, discussion 152–6. ISSN: 1528-2511. URL: http://www.pubmedcentral.nih.gov/articlerender.fcgi?artid=2692520%7B%5C&%7Dtool=pmcentrez%7B%5C&%7Drendertype=abstract.

Schatz, Gottfried (1996). "The Protein Import System of Mitochondria". In: *Journal of Biological Chemistry* 271.50, pp. 31763–31766. URL: http://www.jbc.org/content/271/50/31763.short.

Neupert, Walter (1997). "Protein Import into Mitochondria". In: *Annual Review of Biochemistry* 66.1, pp. 863–917. ISSN: 0066-4154. DOI: 10.1146/annurev.biochem.66.1.863. URL: https://doi.org/10.1146/annurev.biochem.66.1.863.

Zipes, D P and H J Wellens (1998). "Sudden cardiac death." In: *Circulation* 98, pp. 2334–2351. ISSN: 0009-7322. DOI: 10.1161/01.CIR.98.21.2334.

Fuster, V., M. Poon, and J. T. Willerson (1998). "Learning from the transgenic mouse: Endothelium, adhesive molecules, and neointimal formation". In: *Circulation* 97.1, pp. 16–18. ISSN: 00097322. DOI: 10.1161/01.CIR.97.1.16.

Carry, M M, R E Mrak, M L Murphy, C F Peng, K D Straub, and E P Fody (1989). "Reperfusion injury in ischemic myocardium: protective effects of ruthenium red and of nitroprusside". eng. In: *The American journal*

*of cardiovascular pathology* 2.4, pp. 335–344. ISSN: 0887-8005. URL: http://europepmc.org/abstract/MED/2477045.

Maxwell, Simon R J and Gregory Y H Lip (1997). "Reperfusion injury: a review of the pathophysiology, clinical manifestations and therapeutic options". In: *International Journal of Cardiology* 58.2, pp. 95–117. ISSN: 0167-5273. DOI: 10.1016/S0167-5273(96)02854-9. URL: https://doi.org/10.1016/S0167-5273(96)02854-9.

Wit, Al and Mj Janse (2001). "Reperfusion Arrhythmias and Sudden Cardiac Death A Century of Progress Toward an Understanding of the Mechanisms". In: *Circulation Research*, pp. 741–743. DOI: 10.1161/hh2101.099661. URL: http://circres.ahajournals.org/content/89/9/741.short.

Lyon, Alexander R., Paul J. Joudrey, Dongzhu Jin, Robert D. Nass, Miguel a. Aon, Brian 'Rourke, and Fadi G. Akar (2010). "Optical imaging of mitochondrial function uncovers actively propagating waves of mitochondrial membrane potential collapse across intact heart". In: *Journal of Molecular and Cellular Cardiology* 49.4, pp. 565–575. ISSN: 00222828. DOI: 10.1016/j.yjmcc.2010.07.002. URL: http://dx.doi.org/10.1016/j.yjmcc.2010.07.002.

Slodzinski, Martin K., Miguel a. Aon, and Brian O'Rourke (2008). "Glutathione oxidation as a trigger of mitochondrial depolarization and oscillation in intact hearts". In: *Journal of Molecular and Cellular Cardiology* 45.5, pp. 650–660. ISSN: 00222828. DOI: 10.1016/j.yjmcc.2008.07.017. URL: http://dx.doi.org/10.1016/j.yjmcc.2008.07.017.

Akar, Fadi G., Miguel a. Aon, Gordon F. Tomaselli, and Brian O'Rourke (2005). "The mitochondrial origin of postischemic arrhythmias". In: *Journal of Clinical Investigation* 115.12, pp. 3527–3535. ISSN: 00219738. DOI: 10.1172/JCI25371.

Crucitti, Paolo, Vito Latora, and Massimo Marchiori (2004). "Model for cascading failures in complex networks." In: *Physical review. E, Statistical, nonlinear, and soft matter physics* 69, p. 045104. ISSN: 1539-3755. DOI: 10.1103/PhysRevE.69.045104. arXiv: 0309141 [cond-mat].

Aon, Miguel a, Sonia Cortassa, and Brian O'Rourke (2004). "Percolation and criticality in a mitochondrial network." In: *Proceedings of the National Academy of Sciences of the United States of America* 101.13, pp. 4447–4452. ISSN: 0027-8424. DOI: 10.1073/pnas.0307156101.

Brown, David a., Miguel a. Aon, Chad R. Frasier, Ruben C. Sloan, Andrew H. Maloney, Ethan J. Anderson, and Brian O'Rourke (2010). "Cardiac arrhythmias induced by glutathione oxidation can be inhibited by preventing

mitochondrial depolarization". In: *Journal of Molecular and Cellular Cardiology* 48.4, pp. 673–679. ISSN: 00222828. DOI: 10.1016/j.yjmcc.2009.11.011. URL: http://dx.doi.org/10.1016/j.yjmcc.2009.11.011.

Solhjoo, Soroosh, Brian O'Rourke, Author Manuscript, and Tract Structures (2015). "Mitochondrial Instability during Regional Ischemia-Reperfusion Underlies Arrhythmias in Monolayers of Cardiomyocytes". In: *Journal of molecular and cellular cardiology*, pp. 90–99. ISSN: 0022-2828. DOI: 10.1016/j.yjmcc.2014.09.024. arXiv: NIHMS150003. URL: http://www.ncbi.nlm.nih.gov/pmc/articles/PMC4268014/.

Zhou, Lufang, Soroosh Solhjoo, Brent Millare, Gernot Plank, M. Roselle Abraham, Sonia Cortassa, Natalia Trayanova, and Brian O'Rourke (2014). "Effects of regional mitochondrial depolarization on electrical propagation: Implications for arrhythmogenesis". In: *Circulation: Arrhythmia and Electrophysiology* 7.1, pp. 143–151. ISSN: 19413084.

Amchenkova, A A, L E Bakeeva, Y S Chentsov, V P Skulachev, and D B Zorov (1988). "Coupling membranes as energy-transmitting cables. I. Filamentous mitochondria in fibroblasts and mitochondrial clusters in cardiomyocytes." In: *The Journal of Cell Biology* 107.2, 481 LP –495. URL: http://jcb.rupress.org/content/107/2/481.abstract.

Glancy, Brian, Lisa M. Hartnell, Daniela Malide, Zu-Xi Yu, Christian a. Combs, Patricia S. Connelly, Sriram Subramaniam, and Robert S. Balaban (2015). "Mitochondrial reticulum for cellular energy distribution in muscle". In: *Nature* 523.7562, pp. 617–620. ISSN: 0028-0836. DOI: 10.1038/nature14614. URL: http://www.nature.com/doifinder/10.1038/nature14614.

Aon, Miguel a., Sonia Cortassa, Eduardo Marbán, and Brian O'Rourke (2003). "Synchronized Whole Cell Oscillations in Mitochondrial Metabolism Triggered by a Local Release of Reactive Oxygen Species in Cardiac Myocytes". In: *Journal of Biological Chemistry* 278, pp. 44735–44744. ISSN: 00219258. DOI: 10.1074/jbc.M302673200.

Zhou, Lufang, Miguel a. Aon, Tabish Almas, Sonia Cortassa, Raimond L. Winslow, and Brian O'Rourke (2010). "A reaction-diffusion model of ROS-induced ROS release in a mitochondrial network". In: *PLoS Computational Biology* 6.1. ISSN: 1553734X. DOI: 10.1371/journal.pcbi.1000657.

Brady, Nathan R, Anne Hamacher-Brady, Hans V Westerhoff, and Roberta a Gottlieb (2006). "A wave of reactive oxygen species (ROS)-induced ROS release in a sea of excitable mitochondria." In: *Antioxidants & redox signaling* 8, pp. 1651–1665. ISSN: 1523-0864. DOI: 10.1089/ars.2006.8.1651.

O'Rourke, B, B M Ramza, and E Marban (1994). "Oscillations of membrane current and excitability driven by metabolic oscillations in heart cells". In: *Science* 265.5174, 962 LP –966. URL: http://science.sciencemag.org/content/265/5174/962.abstract.

Beavis, A D (1989). "On the inhibition of the mitochondrial inner membrane anion uniporter by cationic amphiphiles and other drugs." In: *Journal of Biological Chemistry* 264.3, pp. 1508–1515. URL: http://www.jbc.org/content/264/3/1508.abstract.

Beavis, Andrew D (1992). "Properties of the inner membrane anion channel in intact mitochondria". In: *Journal of Bioenergetics and Biomembranes* 24.1, pp. 77–90. ISSN: 1573-6881. DOI: 10.1007/BF00769534. URL: https://doi.org/10.1007/BF00769534.

Cortassa, Sonia, Miguel a Aon, Raimond L Winslow, and Brian O'Rourke (2004). "A mitochondrial oscillator dependent on reactive oxygen species." In: *Biophysical journal* 87.3, pp. 2060–2073. ISSN: 00063495. DOI: 10.1529/biophysj.104.041749. URL: http://dx.doi.org/10.1529/biophysj.104.041749.

Aon, Miguel Antonio, Sonia Cortassa, Fadi Gabriel Akar, and Brian O'Rourke (2006). "Mitochondrial criticality: A new concept at the turning point of life or death". In: *Biochimica et Biophysica Acta - Molecular Basis of Disease* 1762.2, pp. 232–240. ISSN: 09254439. DOI: 10.1016/j.bbadis.2005.06.008.

Yang, Ling, Paavo Korge, James N. Weiss, and Zhilin Qu (2010). "Mitochondrial oscillations and waves in cardiac myocytes: Insights from computational models". In: *Biophysical Journal* 98.8, pp. 1428–1438. ISSN: 00063495. DOI: 10.1016/j.bpj.2009.12.4300. URL: http://dx.doi.org/10.1016/j.bpj.2009.12.4300.

Nivala, Melissa, Paavo Korge, Michael Nivala, James N. Weiss, and Zhilin Qu (2011). "Linking flickering to waves and whole-cell oscillations in a mitochondrial network model". In: *Biophysical Journal* 101.9, pp. 2102–2111. ISSN: 00063495. DOI: 10.1016/j.bpj.2011.09.038. URL: http://dx.doi.org/10.1016/j.bpj.2011.09.038.

Zima, Aleksey V and Stefan R Mazurek (2016). "Functional Impact of Ryanodine Receptor Oxidation on Intracellular Calcium Regulation in the Heart". In: *Reviews of physiology, biochemistry and pharmacology* 171, pp. 39–62. ISSN: 0303-4240. DOI: 10.1007/112_2016_2. URL: http://www.ncbi.nlm.nih.gov/pmc/articles/PMC5033687/.

Sasaki, N, T Sato, E Marbán, and B O'Rourke (2001). "ATP consumption by uncoupled mitochondria activates sarcolemmal K(ATP) channels in cardiac

myocytes." In: *American journal of physiology. Heart and circulatory physiology* 280.4, H1882–H1888. ISSN: 0363-6135.

Noma, A (1983). "ATP-regulated K+ channels in cardiac muscle". In: *Nature* 305, p. 147. URL: http://dx.doi.org/10.1038/305147a0%20http://10.0.4.14/305147a0.

Lederer, W J, C G Nichols, and G L Smith (1989). "The mechanism of early contractile failure of isolated rat ventricular myocytes subjected to complete metabolic inhibition." In: *The Journal of Physiology* 413, pp. 329–349. ISSN: 0022-3751. URL: http://www.ncbi.nlm.nih.gov/pmc/articles/PMC1189104/.

# Chapter 2

# General Methods

## 2.1 Computational Modeling

Computational models are a useful tool for studying complex systems that are difficult to experimentally measure at high spatial and temporal resolution. They are also easy to manipulate and control for variables that would be difficult to do experimentally. We developed and used computational models to study the complex systems within and of the heart, that scale from mitochondria, to mitochondrial networks, to cardiac tissue.

## 2.2 Mitochondrial Models

### 2.2.1 Single Mitochondrion

Our single mitochondrion model is composed of ordinary differential equations (ODE) that represent the changes in chemical concentrations in different compartments of the mitochondrion caused by chemical reactions and transport between compartments. The equations that describe the reactions and transport can be complex, and be dependent on multiple state variables.

### 2.2.2 Network

Our mitochondrial network model is composed of multiple single mitochondrion models and where each mitochondrion can interact with its neighbors by chemical diffusion of ROS. The change of ROS over time within a mitochondrion is dependent on both the net amount of ROS influx/efflux, and the net ROS generated/converted within the mitochondrion, and thus is described by a reaction-diffusion partial differential equation (PDE). We used the finite difference method to solve the PDE describing the mitochondrial network.

## 2.3 Cardiac Electrophysiology Modeling

Modeling of the electrophysiology of cardiac tissue is similar to modeling the mitochondrial network in that both are described by reaction-diffusion equations. Hodgkin Huxley in 1952 (Hodgkin and Huxley, 1952) constructed the first computational model to reproduce the action potential of the squid giant axon. Denis Noble in 1962 (D., 1962) constructed the first cardiac action potential model. Since then, multiple models were created to study different cell types, species, and conditions.

## 2.4 Single Myocyte

The net transmembrane membrane current of a single myocyte is a combination of the currents from the capacitive effect of the cell, the ionic currents, and any externally applied electrical stimulus. Ionic currents are from the

different ion channels, exchangers, and pumps for sodium, calcium, potassium, and any other relevant ions. The equations of the transporters can itself be quite complex, requiring multiple ODEs and state variables that are part of a Markov model representation. A Markov model is a state transition model with different rates between different model states. Each transition rate can depend on multiple state variables such as ion concentration within a compartment and the transmembrane potential. Each state can have different conductive properties.

## 2.5 Cardiac Tissue

When modeling the electrophysiology of a single myocyte, only the ODEs describing the ionic, capacitive, and stimulus currents are needed. Modeling at the tissue scale requires accounting for propagation of electrical activity. A bidomain formulation is needed to describe the current density through both the gap junctions and through the extracellular space(Vigmond et al., 2003). We used a simpler and easier method to compute the monodomain formulation(Leon and Horáček, 1991; Potse et al., 2006) since we did not model any extracellular heterogeneities. We used the finite element method to numerically solve the reaction-diffusion equations. We leveraged operator splitting, where we applied different numerical approaches to the different physics of different time scales to improve the computational tractability. The ionic currents operate under faster time scales compared to diffusion currents and were computed using CVODE. CVODE uses finer adaptive time steps compared to the larger constant time step used for solving the diffusion

component.

# References


Hodgkin, A L and A F Huxley (1952). "A quantitative description of membrane current and its application to conduction and excitation in nerve". In: *The Journal of Physiology* 117.4, pp. 500–544. ISSN: 0022-3751. URL: http://www.ncbi.nlm.nih.gov/pmc/articles/PMC1392413/.

D., Noble (1962). "A modification of the Hodgkin-Huxley equations applicable to Purkinje fibre action and pacemaker potentials". In: *The Journal of Physiology* 160.2, pp. 317–352. ISSN: 0022-3751. DOI: 10.1113/jphysiol.1962.sp006849. URL: https://doi.org/10.1113/jphysiol.1962.sp006849.

Vigmond, Edward J, Matt Hughes, G Plank, and L.Joshua Leon (2003). "Computational tools for modeling electrical activity in cardiac tissue". In: *Journal of Electrocardiology* 36, pp. 69–74. ISSN: 0022-0736. DOI: 10.1016/j.jelectrocard.2003.09.017. URL: https://doi.org/10.1016/j.jelectrocard.2003.09.017.

Leon, L.Joshua and B.Milan Horáček (1991). "Computer model of excitation and recovery in the anisotropic myocardium: I. Rectangular and cubic arrays of excitable elements". In: *Journal of Electrocardiology* 24.1, pp. 1–15. ISSN: 0022-0736. DOI: https://doi.org/10.1016/0022-0736(91)90077-Y. URL: http://www.sciencedirect.com/science/article/pii/002207369190077Y.

Potse, M, B Dube, J Richer, A Vinet, and R M Gulrajani (2006). "A Comparison of Monodomain and Bidomain Reaction-Diffusion Models for Action Potential Propagation in the Human Heart". In: *IEEE Transactions on Biomedical Engineering* 53.12, pp. 2425–2435. ISSN: 0018-9294 VO - 53. DOI: 10.1109/TBME.2006.880875.

# Chapter 3

# Mitochondrial network dysfunction

## 3.1 Introduction

The organization of the mitochondrial network plays an important role in the normal functioning of the adult ventricular myocyte(Sasaki et al., 2001; Miguel a Aon, Cortassa, and Brian O'Rourke, 2004; Nivala et al., 2011). In order to meet the high energy demands of contraction and ion homeostasis, mitochondria in cardiomyocytes are organized in a dense regular lattice proximal to both the myofilaments and the $Ca^{2+}$ release apparatus(Stanley, Recchia, and Lopaschuk, 2005; Saks et al., 2006). This topological arrangement can also support propagation of mitochondrial membrane potential $\Delta\Psi_m$ changes over large distances, which has been proposed to occur either through local diffusion of signaling molecules, such as $Ca^{2+}$(Ichas, Jouaville, and Mazat, 1997) or reactive oxygen species (ROS)(Romashko, Marban, and Brian O'Rourke, 1998; Zorov et al., 2000; Miguel a. Aon, Cortassa, Marbán, et al., 2003), or by direct physical connections between mitochondria (Amchenkova et al., 1988; Glancy

et al., 2015). Since communication networks comprising strongly coupled nodes and high connectivity are prone to cascading failures(Crucitti, Latora, and Marchiori, 2004), the mitochondrial networks of ventricular myocytes are also inherently vulnerable to such failures. These complex spatiotemporal aspects of mitochondrial organization have consequences, as they can scale to affect myocyte electrical and contractile function(Miguel a. Aon, Cortassa, Marbán, et al., 2003; Lufang Zhou, Solhjoo, et al., 2014), organ level emergent phenomena, such as arrhythmias(Akar et al., 2005), or even the sudden death of the organism(Jeong et al., 2012; Dey et al., 2018).

Mitochondrial failure can manifest as mitochondrial membrane potential ($\Delta\Psi_m$) depolarizations in the intact heart(Slodzinski, Miguel a. Aon, and Brian O'Rourke, 2008; Brown and Brian O'Rourke, 2010; Lyon et al., 2010) or in isolated cardiomyocytes subjected to oxidative or metabolic stress(Romashko, Marban, and Brian O'Rourke, 1998; Miguel a. Aon, Cortassa, Marbán, et al., 2003; Zorov et al., 2000; Hou et al., 2014; Wang et al., 2008; Lu et al., 2016). These depolarizations are observed when the mitochondrial ROS scavenging system responsible for removing excess superoxide (SO) and hydrogen peroxide ($H_2O_2$) is overwhelmed, either by excess ROS production or by limited antioxidant replenishment capacity(L. Zhou and B. O'Rourke, 2012; Kusama, Bernier, and Hearse, 1989). Accumulation of SO near a mitochondrion is thought to trigger the opening of SO-sensitive mitochondrial inner membrane anion channels (IMAC)(Cortassa et al., 2004) or sensitize other ROS-sensitive channels to opening, such as the permeability transition pore (PTP)(Zorov et al., 2000; Zorov et al., 2000). Opening of such channels generates and releases

additional SO from the mitochondrial matrix, resulting in $\Delta\Psi_m$ depolarization. This triggering and release process has been termed ROS-induced ROS release (RIRR)(Zorov et al., 2000). Further, when the mitochondrial network is oxidatively stressed and the antioxidant capacity is depleted, RIRR can propagate throughout the network(Lufang Zhou, Miguel a. Aon, et al., 2010). Propagation occurs as SO released from one mitochondrion diffuses to a neighboring mitochondrion and initiates additional IMAC openings and release of accumulated SO. Superoxide dismutase (SOD) or SOD mimetics(Zorov et al., 2000; Miguel a. Aon, Cortassa, Marbán, et al., 2003) mitigate RIRR by facilitating the rapid conversion of SO into $H_2O_2$, which is subsequently removed by peroxidases in the cytoplasm and mitochondrial matrix. Network instability (failure) due to this mechanism is often characterized by regions of mitochondria with synchronized oscillating membrane potential. Mitochondrial SO release resulting in propagation of $\Delta\Psi_m$ depolarizations has been studied in experimental and computational models(Lufang Zhou, Miguel a. Aon, et al., 2010; Yang et al., 2010). Nevertheless, the mechanisms underlying propagation and synchronization within the network, and the extent and strength of coupling of network elements across the length of the heart cell (100-150 micrometers), are poorly understood. Recently, the idea that mitochondria may be electrically coupled(Amchenkova et al., 1988) across large cellular distances has been reintroduce(Glancy et al., 2015); however, this model is incompatible with a number of experimental observations. For example, local perturbations of $\Delta\Psi_m$ propagate through cardiac cells only after a long delay (minutes) between a local stimulus and the cell-wide $\Delta\Psi_m$ response(Miguel a.

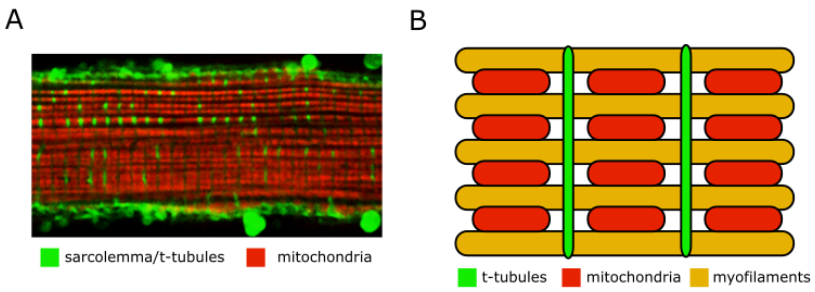


**Figure 3.1: Mitochondrial arrangement in a myocyte.** **A.** Example confocal microscopy image of canine cardiomyocyte with green stained sarcolemma and t-tubules, and red stained mitochondria. **B.** Zoomed in schematic of mitochondrial arrangement with myofilaments colored yellow

Aon, Cortassa, Marbán, et al., 2003), spatial clusters of $\Delta\Psi_m$ oscillation dynamically evolved over time and are modulated by substrate availability(Felix T. Kurz, Derungs, et al., 2015; Felix T. Kurz, Miguel a. Aon, et al., 2014; Felix T Kurz et al., 2010a; Felix T Kurz et al., 2010b), and highly localized spontaneous oscillations in $\Delta\Psi_m$ can occur in small clusters(Romashko, Marban, and Brian O'Rourke, 1998) or individual mitochondria(Hou et al., 2014; Wang et al., 2008) without propagating to neighboring mitochondria, which in the adult heart cell are physically separated laterally, by intervening myofilaments, and longitudinally, by t-tubules at each z-line (Figure 3.1). Hence, it remains to be determined if physical connections contribute to cell-wide propagating or synchronized phenomena.

Synchronization of the mitochondrial network by diffusible messengers would require a mechanism that takes into account both short and long range interactions among mitochondria. A key question is how short range mitochondrial neighbor-neighbor interactions that depend on messengers with a brief half-life, such as SO, can scale across the cell. In this study, we describe

how the sensitivity to local SO-induced RIRR depends on the longer range effects of $H_2O_2$, which has a longer lifetime than SO and can more easily diffuse throughout the cytoplasm. We show, by developing a novel computational model of the mitochondrial network, that $H_2O_2$ diffusion underlies the transmission of mitochondrial network failure by distributing oxidative stress and subsequently depleting ROS scavenging capacity, thus sensitizing mitochondria across the network to RIRR. The model provides a deeper understanding of the mechanisms of mitochondrial network failure associated with cardiac pathophysiologies such as ischemia/reperfusion injury(Akar et al., 2005) or sudden death associated with chronic heart failure(Dey et al., 2018).

## 3.2 Methods

### 3.2.1 Computational Model Summary

The model developed uses as its basis the mitochondrial network model by Zhou et al(Lufang Zhou, Miguel a. Aon, et al., 2010), which describes self-organized $\Delta\Psi_m$ oscillations mediated by $Ca^{2+}$-independent RIRR via IMAC. It does not incorporate $Ca^{2+}$-dependent activation of PTP, which can be sensitized to open by higher levels of sustained oxidative stress(Miguel a. Aon, Cortassa, Maack, et al., 2007). The model represents the mitochondrial network as a collection of closely apposed nodes (mitochondria), with interconnections represented by SO diffusion. Each individual mitochondrion is represented by the model of Cortassa et al(Cortassa et al., 2004), where ordinary differential equations describe the evolution of the mitochondrial

matrix and intermitochondrial space. The model includes descriptions of the TCA cycle, oxidative phosphorylation, $Ca^{2+}$ handling, SO production, SO transport via IMAC from matrix to intermitochondrial space, and both SO and $H_2O_2$ scavenging.

We added new components to the single mitochondrion model (Fig. 2A) to enable us to better represent ROS scavenging. First, we added a representation of the mitochondrial matrix scavenger superoxide dismutase (SOD) to address its possible role in $H_2O_2$ dynamics, as matrix SO is converted to $H_2O_2$. Second, the $H_2O_2$ scavenging system was further developed to include the thioredoxin system, as described by Kembro et al(Kembro et al., 2013), since it supplements the glutathione (GSH) system in scavenging $H_2O_2$ and thus affects $H_2O_2$ dynamics. Third, we incorporated parameterized formulations of nicotinamide adenine dinucleotide phosphate (NADPH) dynamics. NADPH drives the production of GSH and thioredoxin and thus plays a role in maintaining $H_2O_2$ scavenging capacity. We parameterized the size of the NADPH pool and its replenishment rate to set limits on the transient and steady state capacity for maintaining a functioning $H_2O_2$ scavenging system. Finally, we removed the representation of catalase to highlight the effects of the energetically driven $H_2O_2$ scavenging systems, because the catalase content in the cardiac ventricular myocyte is low(Chance, Sies, and Boveris, 1979), and because local catalase concentrations within the different cell compartments are not known.

In addition to further developing ROS scavenging, we redefined some and added other ROS production components to the single mitochondrion

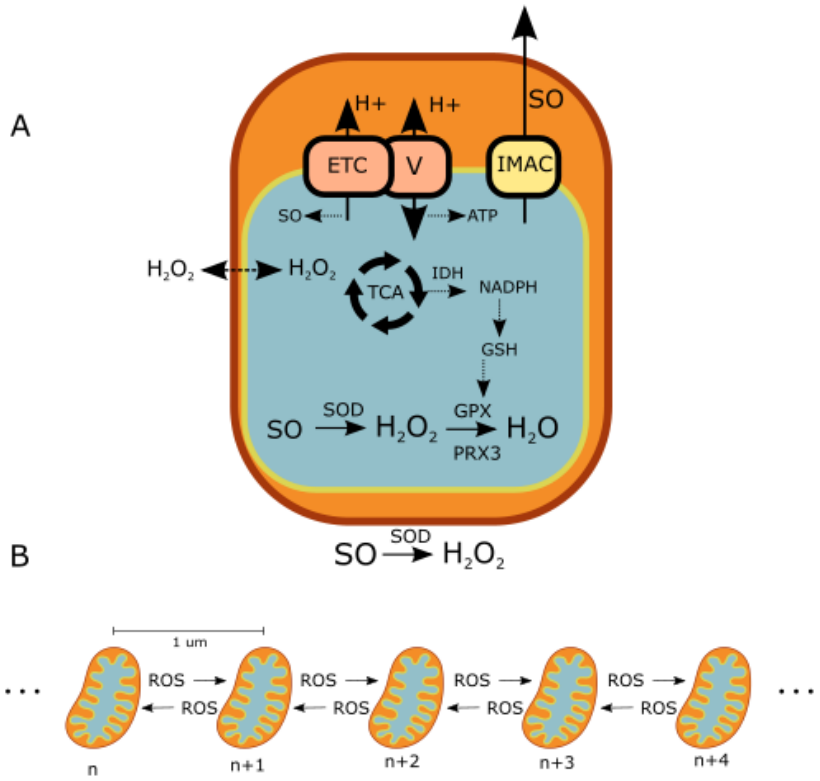


**Figure 3.2: Model Schematics.** **A.** Single mitochondrial model: TCA cycle, ROS scavenging, ROS transport via IMAC, and SO production from the electron transport chain. **B.** 1-dimensional mitochondrial network model: ROS can diffuse between neighboring mitochondria

model. In their model, Cortassa et al represented the basal SO produced from the electron transport chain as a function of oxygen consumed. However, to control for the contributions of SO production rate, we redefined the mitochondrial intrinsic SO production rate to be parameterized as $SO_{base}$. By doing so, we excluded electron transport chain driven oscillatory pressure and instead highlighted the pressure due to scavenging dynamics. We also added the two parameters for ROS stimulation, $HP_{stim}$ and $SO_{stim}$, which are the respective $H_2O_2$ and SO production rates during any given stimulation protocol.

Completing model development, we added $H_2O_2$ diffusion between mitochondria to enable $H_2O_2$ to act as a communicator of oxidative stress across the network (Figure 3.1B). We used a higher diffusion coefficient for $H_2O_2$, as compared to SO, to represent the higher diffusibility of $H_2O_2$ over SO between mitochondria(Han et al., 2003; Bienert and Chaumont, 2014). Similar to Zhou et al(Lufang Zhou, Miguel a. Aon, et al., 2010), mitochondria in our network model were arranged in a line and spaced 1 µm apart, the average distance measured experimentally in cells(Birkedal, Shiels, and Vendelin, 2006). A total of 100 mitochondria were represented in the model. This number was determined iteratively to be sufficiently large to observe all the morphological changes in the depolarization patterns of the network while simultaneously minimizing computational expense. Similar to Zhou et al(Lufang Zhou, Miguel a. Aon, et al., 2010), we assumed a no flux boundary condition for SO diffusion and reapplied this assumption for $H_2O_2$ diffusion. Previous mitochondrial network models had assumed the same boundary condition

for $H_2O_2$ diffusion(Yang et al., 2010).

### 3.2.2 Oxidative Stress Stimulation Protocol

To test our hypothesis, we simulated an oxidatively stressed mitochondrial network for 300 seconds. 300 seconds is a typical time span to observe network failure progression in oxidative stress experiments(Lufang Zhou, Miguel a. Aon, et al., 2010; Miguel a. Aon, Cortassa, Marbán, et al., 2003). We introduced oxidative stress to the network by stimulating a small group of three neighboring mitochondria in the network (Figure 3.3A). Stimulation of these mitochondria was represented by assigning a value to their SO and $H_2O_2$ production rate ($SO_{stim}$ and $HP_{stim}$ respectively). The value of the stimulus was maintained constant during the entire simulation duration (300 seconds). To be able to compare simulation results to experimental, our stimulation protocol mimicked the stimulation protocol used in laser flash experiments, where a brief (~500ms) localized laser flash induces sustained ROS production in a localized region of the networkAon 2003. The central mitochondrion in the group of three was assigned the largest $SO_{stim}$ of 5x10$^{-5}$mM ms$^{-1}$ (Figure 3.3A), which was iteratively determined to be the smallest value needed to induce a permanent depolarization in that mitochondrion. The remaining 2 stimulated mitochondria were assigned a smaller $SO_{stim}$ of 1.4x10$^{-5}$mM ms$^{-1}$ to represent the reduced laser intensity from being located at the edge of the laser flash region. Production of $H_2O_2$ was represented by assigning the center mitochondrion's $HP_{stim}$ equal to 2x10$^{-3}$mM ms$^{-1}$. To determine the effect of $H_2O_2$ transport on the progression

of mitochondrial network failure, we performed this stimulation protocol with and without $H_2O_2$ diffusion. Further, to explore the effect of different ROS stimulus makeups, we repeated these simulations with different $HP_{stim}$ rates of 1x10$^{-3}$mM ms$^{-1}$, 1.5x10$^{-3}$mM ms$^{-1}$, and 2x10$^{-3}$mM ms$^{-1}$, and different $SO_{stim}$ rates of 12x10$^{-6}$mM ms$^{-1}$, 14x10$^{-6}$mM ms$^{-1}$, and 16x10$^{-6}$mM ms$^{-1}$. These alterations to the previous stimulus rates were iteratively determined to be just large enough to demonstrate a large enough change in network behavior.

## 3.3 Results

### 3.3.1 Mitochondrial Network Response to ROS Stimulus

Figure 3.3 presents the simulations without $H_2O_2$ diffusion. At time 0, all the mitochondria were polarized with a $\Delta\Psi_m$ around 150mV. After 3 seconds, the central stimulated mitochondrion (Figure 3.3A) depolarized. Interestingly, only the central stimulated mitochondrion (Figure 3.3A) depolarized substantially (>95% reduction in $\Delta\Psi_m$). The stimulated mitochondria at the edge of the region (the immediate neighbors of the central mitochondrion) only partially depolarized to 115mV after 10 seconds, and only a bit further to 105mV after 100 seconds (Figure 3.3B). The remaining mitochondria in the network did not depolarize for the whole simulation duration of 300 seconds (Figure 3.3C). Figure 3.3C shows the evolution of the membrane potential of each mitochondrion in the network.

Figure 3.4 presents the simulations with $H_2O_2$ diffusion. Like before, the stimulation protocol involved 3 mitochondria in the center of the network with

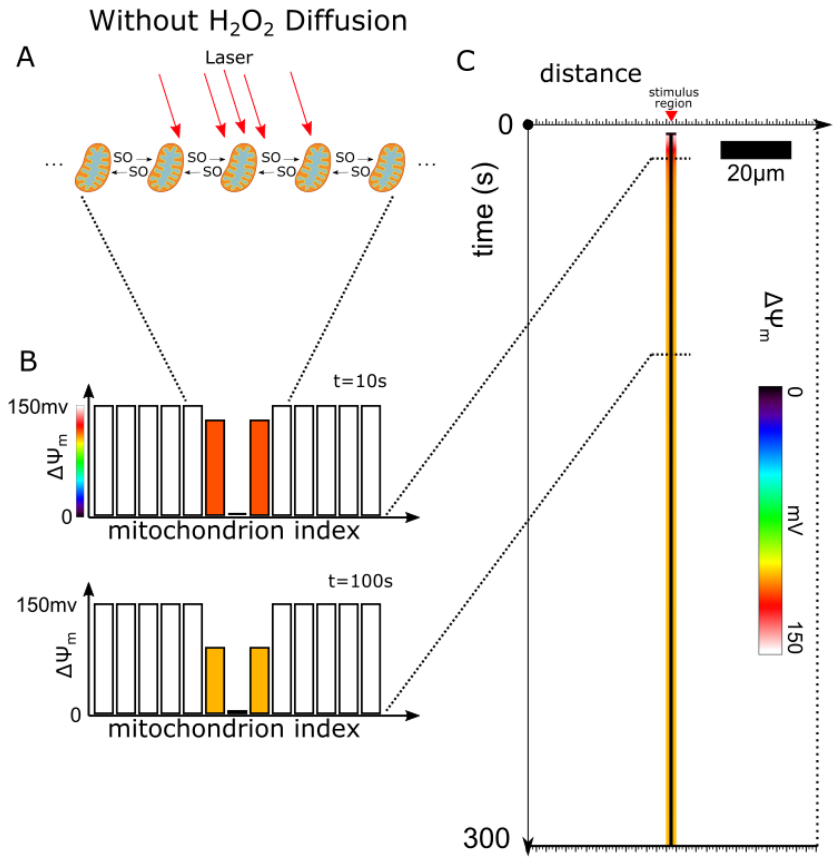


**Figure 3.3: ROS Stimulated Mitochondrial Network Without $H_2O_2$ Diffusion. A.** Schematic of the mitochondrial network with a region of mitochondria stimulated to produce ROS over time and with only SO diffusion between mitochondria. The red arrows pointing at the mitochondria represent the laser stimulation. The central mitochondrion has the largest density of arrows and representing the largest $SO_{stim}$ of 5x10$^{-5}$mM ms$^{-1}$. The other two mitochondria are on the edge of the laser stimulation region, thus receive less laser stimulation, and have a lower $SO_{stim}$ of 1.4x10$^{-5}$mM ms$^{-1}$. **B.** Bar plots of the $\Delta\Psi_m$ of mitochondria in the network at 2 different time points, 10 and 100s. **C.** Time-line plot of evolution of $\Delta\Psi_m$ of the mitochondria in the network. The plot presents a 2D representation of the time evolution of the 1D mitochondrial network, where color represents the $\Delta\Psi_m$ value. The horizontal axis represents the spatial extent of the 1D mitochondrial network, and the vertical axis represents time. The white space in the plot represents the mitochondria at spans of time where they are polarized and have a normal membrane potential around 150mV. Mitochondria that depolarized had a reduced membrane potential and are represented by the different colors depending on depolarization magnitude. The central mitochondrion, which is permanently depolarized, is represented as a black vertical line in this plot.

elevated $SO_{stim}$ (Figure 3.4A). Unlike the simulations without $H_2O_2$ diffusion, multiple mitochondria depolarized (Figure 3.4B). First, at time 0, all mitochondria were polarized. Next, the 3 stimulated mitochondria depolarized after 4 seconds. The middle mitochondrion, which had the largest SO generation rate, permanently depolarized. The behavior of this mitochondrion matched the behavior found in experiments, where laser flash stimulated mitochondria irreversibly depolarized after a few seconds(Miguel a. Aon, Cortassa, Marbán, et al., 2003; Miguel a Aon, Cortassa, and Brian O'Rourke, 2004). In contrast to the central mitochondrion, the surrounding two mitochondria were stimulated to a lesser degree and exhibited sustained depolarizations only 201 seconds after the laser flash. At 4 seconds in the simulation, these two mitochondria first underwent a transient depolarization lasting 2.5 seconds. Afterwards, the two mitochondria displayed partial depolarizations. Unlike the results of the simulations without $H_2O_2$ diffusion, these mitochondria continued to gradually depolarize and eventually fully depolarized after 201 seconds. Thus, the response of the 3 stimulated mitochondria is represented by the thick vertical black line in Figure 3.4C. Collectively, these simulation results reproduced the experimental observations where mitochondria gradually irreversibly depolarized within the laser flash stimulated region(Miguel a. Aon, Cortassa, Marbán, et al., 2003; Miguel a Aon, Cortassa, and Brian O'Rourke, 2004).

The black horizontal extrusions starting at 147 seconds in Figure 3.4C represent the mitochondrial depolarizations that propagated outward from the stimulated mitochondria. This delay in the response of the bulk of the network

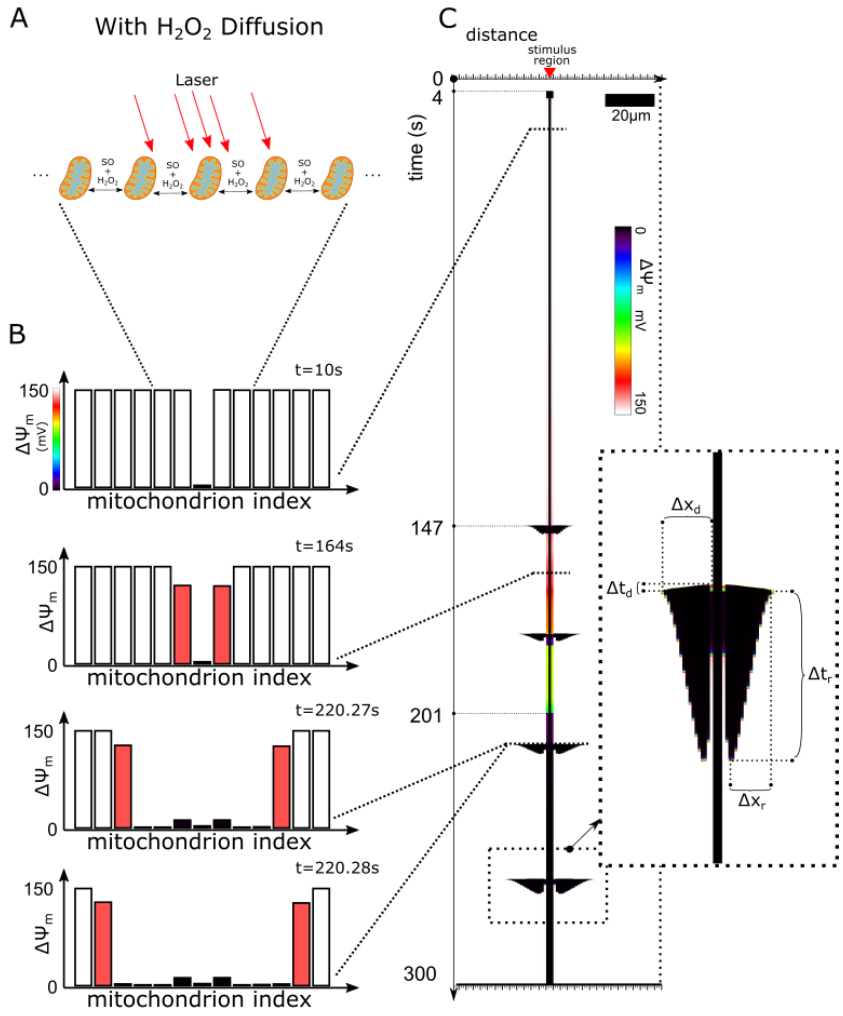


**Figure 3.4: ROS Stimulated Mitochondrial Network with $H_2O_2$ diffusion. A.** Schematic of mitochondrial network with a region of mitochondria stimulated to produce ROS over time and with both SO and $H_2O_2$diffusion between mitochondria. **B.** Bar plots of the $\Delta\Psi_m$ of mitochondria in the network at different time points. **C.** Time-line plot of evolution of $\Delta\Psi_m$ of the mitochondria in the network. The inset displays a zoomed in view of the last propagating depolarization and repolarization pattern. The propagating depolarization pattern's duration is marked by dashed line $\Delta t_d$ and the pattern's length is marked by the dashed line marked $\Delta x_d$. Similarly, the repolarization pattern's duration and length are also marked by the dashed lines $\Delta t_r$ and $\Delta x_r$ respectively.

to oxidative stress has been consistently observed in both laser flash stimulated mitochondrial networks and chemically stressed mitochondrial networks (The paper by Zhou et al demonstrated such behavior in their supplemental video (S3))(Lufang Zhou, Miguel a. Aon, et al., 2010). In our simulation results, the extent of the propagating depolarizations (Figure 3.4C inset length $\Delta x_r$ and $\Delta x_d$) gradually increased after each consecutive depolarization wave (Figure 3.4C). This network behavior is consistent with behavior in the stimulation experiments where depolarization propagations did not, at first, extend globally throughout the network. The depolarization waves in our simulations repeated roughly every 30s, which was within the range of normal frequencies found in experiments. Each of these outward propagating depolarization waves were then followed by inwardly-directed repolarization waves. This time-space depolarization/repolarization pattern exhibited a compressed diamond like shape (Figure 3.4C). Our simulation results reproduced the bias in faster depolarization propagation velocity versus the repolarization propagation velocity (Figure 3.4C inset $(\Delta x_d/\Delta t_d)$:$(\Delta x_r/\Delta t_r)$). The total time frame of the depolarization wave and repolarization wave took 3 seconds at the first oscillation, and increased to 5 seconds for the last observed oscillation. This trend of increasing the average depolarization duration of the mitochondria in these depolarization waves was also observed in experiments(Lufang Zhou, Miguel a. Aon, et al., 2010; Miguel a. Aon, Cortassa, Marbán, et al., 2003; Miguel a Aon, Cortassa, and Brian O'Rourke, 2004).

### 3.3.2 Mechanisms Driving Mitochondrial Network Failure Patterns

From the simulation with $H_2O_2$ diffusion, Figure 3.5A displays the evolution of $\Delta\Psi_m$ alongside the evolution of ROS accumulation. We found that the mitochondrial network accumulated $H_2O_2$ around the stimulus location (Figure 3.5A $H_2O_2$). The $H_2O_2$ concentration monotonically increased in the stimulus region over time for the entire simulation duration (300 seconds). The center mitochondrion had an average $H_2O_2$ accumulation rate of 1.7uM/s. The immediate neighboring mitochondria had a similar average $H_2O_2$ accumulation rate but only after a delay of 3-5 seconds, and remained lower in concentration by 25 uM compared with the stimulus region. This pattern of delay and reduced $H_2O_2$ concentration was repeated for successive neighboring mitochondria with roughly the same step decrease of 25 uM per mitochondrion. This pattern ended when the next successive neighboring $H_2O_2$ concentration reached the baseline (<~10nM) and thus marked the boundary of the extent of $H_2O_2$ accumulation. A roughly linear $H_2O_2$ gradient formed, extending from this boundary to the stimulus location. Altogether, both the size of the $H_2O_2$ accumulation region and the $H_2O_2$ of the mitochondria within the region increased over time.

In contrast, the patterns of SO accumulation did not form a simple linear gradient over time and instead displayed complex fluctuating patterns both along the string of mitochondria (i.e. horizontal direction in Figure 3.5A) and over time (vertically in Figure 3.5A), both in the matrix and the inter-mitochondrial space ($SO_m$ & $SO_i$). The laser flash stimulated mitochondria

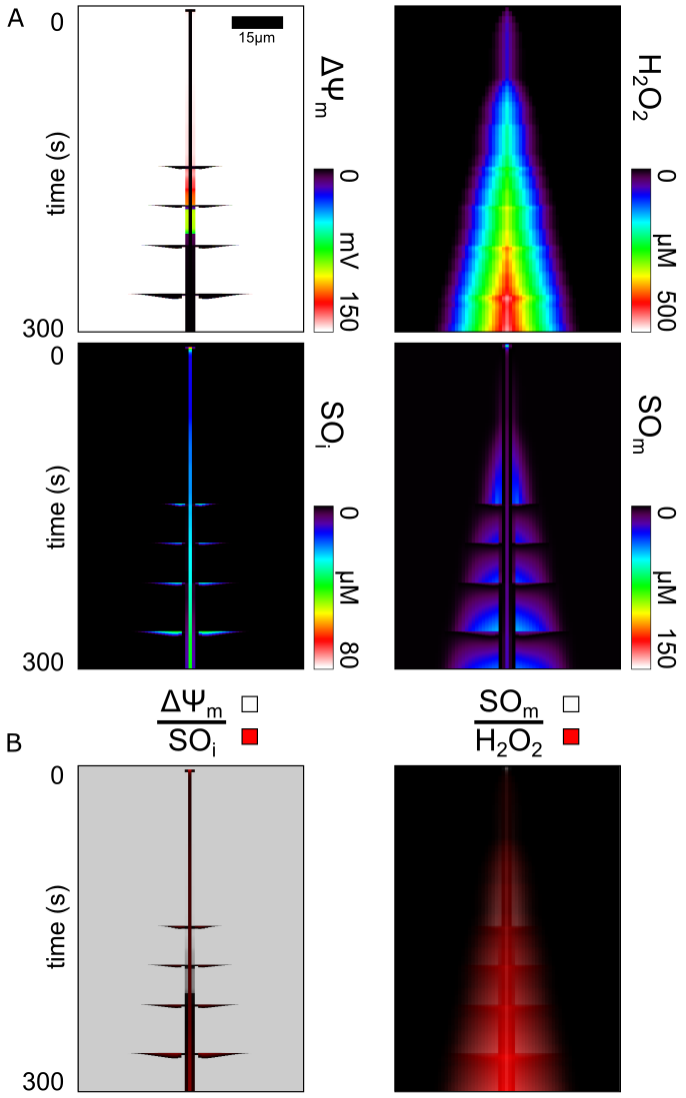


**Figure 3.5: Evolution of the Region Vulnerable to Failure and Regions of ROS Accumulation in the Mitochondrial Network. A.** From the same simulation run shown in Figure 3.4, shown are the plots of mitochondrial membrane potential ($\Delta\Psi_m$), hydrogen peroxide ($H_2O_2$), inter-mitochondrial superoxide ($SO_i$), and matrix superoxide ($SO_m$). **B.** Pairs of time-line plots from (A) created using a partially transparent overlay to highlight encasement or overlap of accumulation regions. The top overlayed plot uses varying transparent shades of white to a maximum of 80% opaque to represent different quantities specified above the line. Likewise, the bottom plot uses varying transparent shades of red to a maximum of 100% opaque to represent different concentrations of the species below the line

generated ROS at the start of the simulation and as a result, the matrix SO of the central mitochondrion quickly increased to above 150uM. At this concentration, the SO leakage into the intermembrane space triggered the central mitochondrion's depolarization at 4 seconds. The central mitochondrion then released more SO into the intermitochondrial space, reducing its matrix SO to 13.6uM. This SO concentration remained relatively stable, and only increased at a rate of 113nM/s as long as the oxidative stress stimulus was maintained, reaching an observed maximum of 45uM after 300 seconds. Interestingly, besides the initial release of SO at the onset of the central mitochondrion's depolarization, the mitochondria directly adjacent to the central mitochondrion exhibited low matrix SO (<1uM) compared to its outer neighbors for the first 221 seconds of simulation. These mitochondria displayed partial depolarizations, where only a slight reduction of $\Delta\Psi_m$ (from 151mV to 148mV) occurred. These partial depolarizations were caused by the partial conductance increase of IMAC, which was caused by SO stimulation that diffused from the central mitochondrion. SO generated in these partially stimulated mitochondria continuously escaped and prevented matrix SO accumulation. The generated SO instead transferred to the intermitochondrial space, raising the concentration of SO in that space to ~50nM, which was substantially larger than the <1nM of the more distant polarized neighbors, but not large enough to induce positive feedback of RIRR bursting. The remaining mitochondria in the network displayed matrix SO accumulation patterns similar to their $H_2O_2$ accumulation patterns, but only prior to their next depolarization event. Also, during this period before the next depolarization, intermitochondrial SO did not accumulate. Only the region of mitochondria with enough accumulated

matrix SO (>1nM) depolarized. Sufficient accumulation of matrix SO was required such that a triggered release of matrix SO into the intermitochondrial space would induce further self-release, which then needed to be large enough to trigger depolarizations in neighboring mitochondria. This transport process resulted in a rapid transient increase in intermitochondrial SO depending on the amount of accumulated stored SO, and also a rapid decrease in matrix SO. After sufficient SO scavenging, the depolarized mitochondria repolarized once the intermitochondrial SO returned to baseline levels. These patterns of matrix SO accumulation and release continued after each subsequent depolarization propagation. Further, the length of the extent of the accumulation region increased with each cycle where the additional number of mitochondria recruited per depolarization ranged between 2 and 4. Interestingly, the extent of matrix SO accumulation region was contained within the extent of the $H_2O_2$ accumulation region and the extent of intermitochondrial SO accumulation was contained within the depolarized region (Figure 3.5B).

The $H_2O_2$ scavenging system component GSH formed a depletion zone (Figure 3.6A GSH) that enveloped the $H_2O_2$ accumulation region (Figure 3.6B GSH | $H_2O_2$). NADPH, the energetic supplier to that system, also formed a depletion zone but was instead enveloped by the GSH depletion region (Figure 3.6B GSH | NADPH). Interestingly, the growth of the GSH depletion zone underwent two phases. First, a depletion zone of ~12 um formed at the center over the first 40 seconds while NADPH was elevated. After the NADPH of that region depleted, the second phase of GSH depletion occurred and the GSH and NADPH depletion region gradually increased in extent

over time. This change in extent growth is denoted by the dashed red line in Figure 3.6A. Thus, depletion of the cascaded energetic drivers of the $H_2O_2$ scavenging system was required for initiating $H_2O_2$ accumulation and for further increasing the extent of this $H_2O_2$ accumulation region.

### 3.3.3 Dependence of Mitochondrial Network Response on ROS Stimulus Makeup

Figure 3.7 presents the results of simulations where the $HP_{stim}$ and $SO_{stim}$ rates were varied independently to compare different ratios of $H_2O_2$ and SO generation rates. Like before, the $HP_{stim}$ was only assigned to the central laser flash stimulated mitochondrion. The different $SO_{stim}$ rates were assigned to the immediate neighboring stimulated mitochondria since the central mitochondrion's $SO_{stim}$ was defined by depolarization status protocol like described before. The case shown in Figure 3.7 second row & second column involved the same stimulation parameters as in Figure 3.4 where $SO_{stim}$ was 1.4x10$^{-5}$ and $HP_{stim}$ was 2x10$^{-3}$. Reducing $HP_{stim}$ to 1.5x10$^{-3}$ resulted in the $\Delta\Psi_m$ patterns presented in Figure 3.7 second row & first column. Reducing $HP_{stim}$ from 2x10$^{-3}$ to 1.5x10$^{-3}$ increased the delay of the first propagating depolarization by ~77 seconds, decreased the number of observed propagating depolarizations by over half, increased the time between depolarizations by ~30 seconds, and decreased the size of the extent of depolarizing mitochondria by ~30%. The start times for all propagating depolarization waves in each plot were different for each ROS combination (Table 3.1). No propagating depolarization waves were observed when $HP_{stim}$ was reduced to 1x10$^{-3}$. Increasing $SO_{stim}$ decreased the delay in the first propagating depolarization wave by

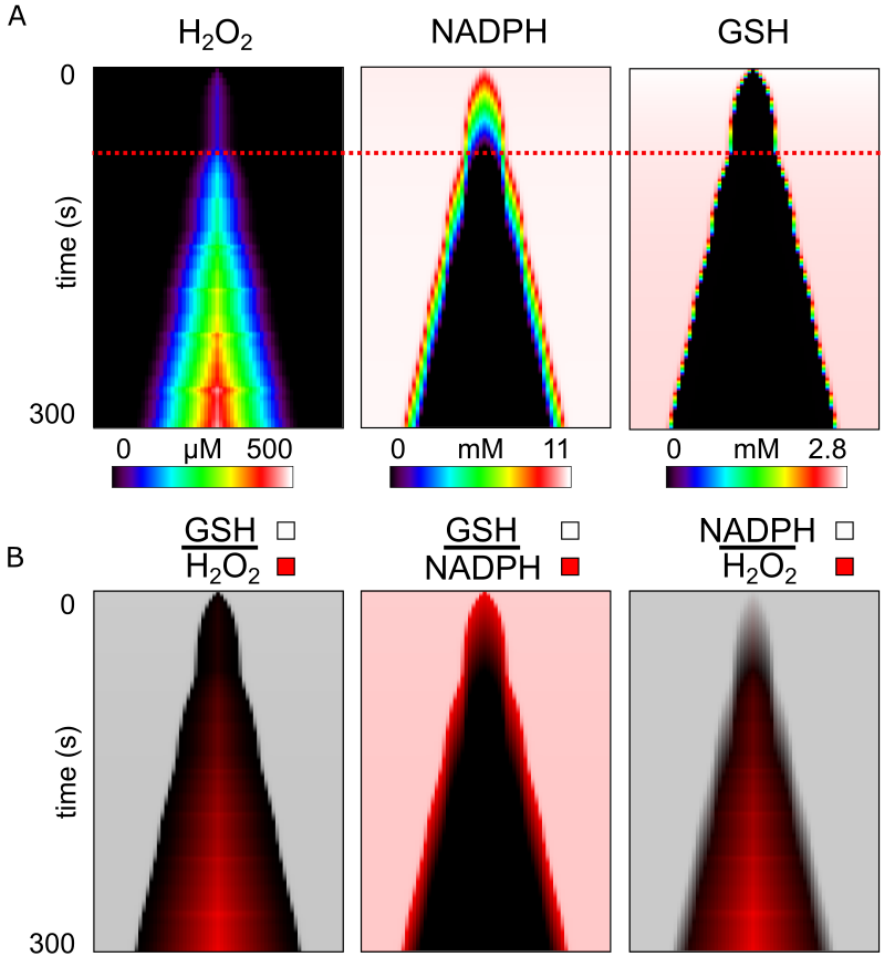


**Figure 3.6: Evolution of $H_2O_2$ Accumulation and $H_2O_2$ Scavenging Capacity Depletion in the Mitochondrial Network. A.** From the same simulation run shown in Figure 3.4 and Figure 3.5, show are the plots over time of hydrogen peroxide ($H_2O_2$), glutathione (GSH) which is the energetic driver of the $H_2O_2$ scavenger enzyme glutathione peroxidase, and nicotinamide adenine dinucleotide phosphate (NADPH) which is the energetic driver of the GSH producing enzyme glutathione reductase. The red dashed line marks the time when the respective extent of accumulation or depletion resumes outward growth towards the rest of the network after a ~10 second hiatus. **B.** Pairs of time-line plots from (A) created using a partially transparent overlay to highlight encasement or overlap of accumulation and depletion regions. The top overlayed plot uses varying transparent shades of white to a maximum of 80% opaque to represent different concentrations of the species listed above the line. Likewise, the bottom plot uses varying transparent shades of red to a maximum of 100% opaque to represent different concentrations of the species below the line.

~8 seconds. This decrease was explained by the increased rate of matrix SO accumulation of the stimulated mitochondria, which causes increased leak to the intermitochondrial space sooner, which causes intermitochondrial SO to reach the IMAC opening trigger threshold sooner. This additional flux into the intermitochondrial space can also reduce the matrix SO accumulation of neighbors while their neighbor's matrix SO levels are still low. The additional intermitochondrial SO slightly increases their neighbor's IMAC conductance that leaks out some matrix SO. This results in an increased time between subsequent depolarization waves by ~10 seconds, thus reducing the frequency of oscillations. In contrast, increasing $HP_{stim}$ from 1.5x10$^{-3}$ to 2x10$^{-3}$ decreased the time between depolarizations by about ~30 seconds, and therefore increased the propagating depolarization wave frequency. Since $H_2O_2$ diffused more readily to the mitochondria near the $H_2O_2$ source, those mitochondria accumulated $H_2O_2$ and thus also matrix SO more rapidly.

## 3.4 Discussion

In this study we tested the hypothesis that $H_2O_2$ diffusion underlies the progression of mitochondrial network failure. To do so, we used a computational model of a mitochondrial network. The model included a detailed representation of the ROS scavenging system, ROS production from both intrinsic origins and external stimuli, and ROS diffusion between mitochondria. We regionally stimulated the network with ROS and observed the network behavior with and without $H_2O_2$ diffusion. We found that $H_2O_2$ diffusion was necessary to reproduce the mitochondrial network behavior observed in oxidative

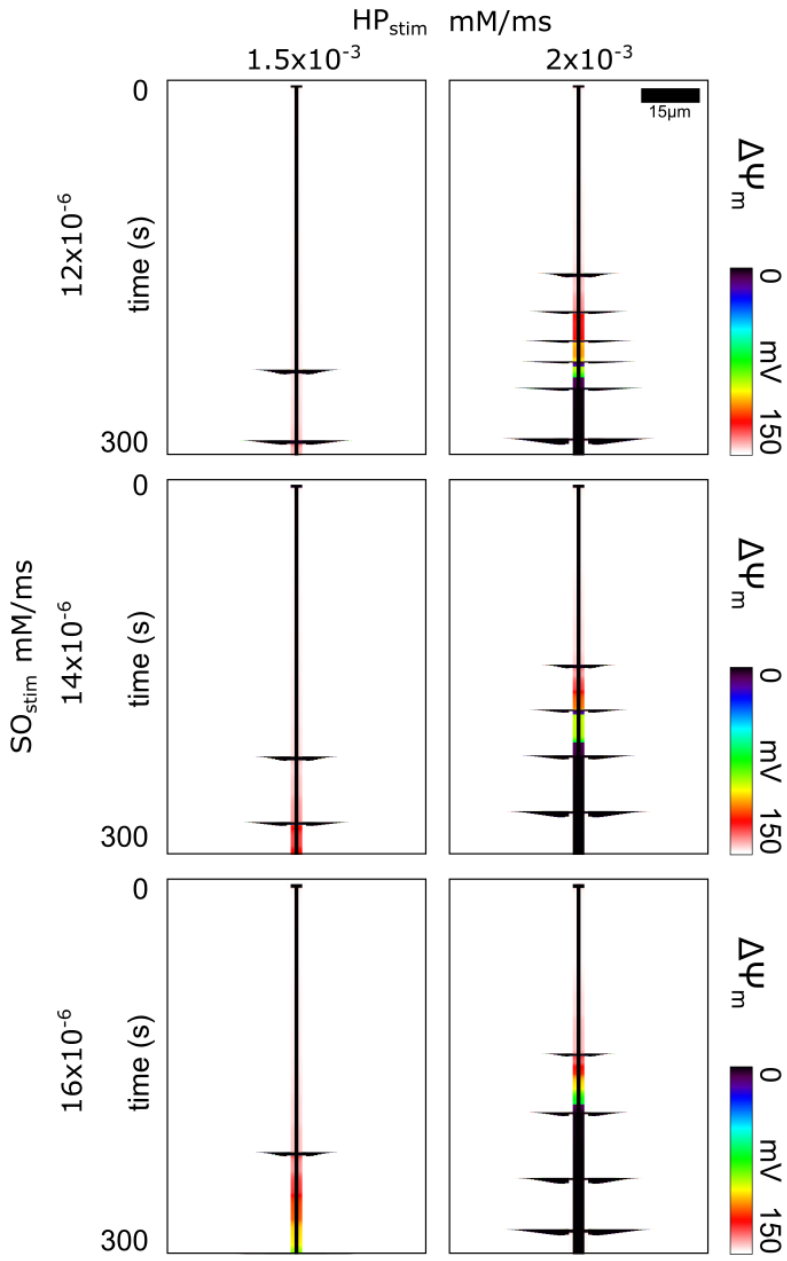


**Figure 3.7: Variations in Mitochondrial Network Oscillation Frequency and Timing Depending on the ROS Stimulus Makeup.** ime-line plots of $\Delta\Psi_m$ of the mitochondria in the network for different  and  rates. Propagating depolarization waves of varying frequency and extent are visible in each of the plots depending on the ROS stimulus rates.

| | HPstim (nM/ms) | | |
|---|---|---|---|
| | | 1.5 | 2 |
| SOstim (pM/ms) | 1.2 | 231<br>287 | 154<br>184<br>207<br>224<br>245<br>286 |
| | 1.4 | 221<br>273 | 147<br>183<br>220<br>264 |
| | 1.5 | 218<br>299 | 139<br>186<br>238<br>279 |

**Table 3.1: Propagating Wave Depolarization Start Times (seconds)**

stress experiments. $H_2O_2$ diffused from the stimulus region and gradually depleted the $H_2O_2$ scavenging capacity of the local mitochondria. Growth of the region of scavenging capacity depletion enabled growth of the region of $H_2O_2$ accumulation. These findings demonstrate that $H_2O_2$ is an important communicator of oxidative stress that can distribute stress throughout the network prior to any signs of network failure from $\Delta\Psi_m$ depolarizations.

### 3.4.1 Hydrogen Peroxide Communication & Accumulation Enables SO Accumulation & Communication

Depending on the tissue and cell type, different specific ROS were believed to play a more significant role in underlying mitochondrial network failure. In a modeling study by Park et al(Park, Lee, and Choi, 2011), the dominant key messenger molecule of a ROS signaling network transitioned from the

ROS SO to $H_2O_2$ as the distance between mitochondria increased. Thus, $H_2O_2$, with its improved diffusivity and longer lifetime over SO, was believed to play a comparatively more significant role in neurons, where the spacing between mitochondria was large. In ventricular cells, where there is less space between mitochondria versus neuronal cells, the dominant key messenger molecule in the RIRR phenomenon was found to be SO(Zorov et al., 2000; Miguel a. Aon, Cortassa, Marbán, et al., 2003). Propagating RIRR, where ROS release of a mitochondrion induces ROS release of a neighboring mitochondrion, occurs in ventricular cells when SO emission from a mitochondrion triggers opening of the IMAC of a neighboring mitochondrion(M. A. Aon et al., 2006; Miguel a. Aon, Cortassa, Marbán, et al., 2003). The resulting expulsions of stored SO and other anions also depolarize the mitochondria's $\Delta\Psi_m$, which is a mitochondrial failure. Thus, SO transport was believed to play the dominant role in producing mitochondrial network failure(M. A. Aon et al., 2006; Miguel a Aon, Cortassa, and Brian O'Rourke, 2004; Miguel a. Aon, Cortassa, Marbán, et al., 2003). However, propagation of this RIRR process relies on SO transport between neighbors that is large enough to trigger another IMAC opening(Lufang Zhou, Miguel a. Aon, et al., 2010). Any initial SO release dissipates in magnitude over distance according to the laws of diffusion, and thus continuation of this propagation requires regenerative SO release across the network.

A mitochondrial network where enough oxidative stress has accumulated, such that any triggering of SO release can cause a cascade of SO releases across the network, has been termed "mitochondrial criticality"(M. A. Aon

et al., 2006). However, a chicken-and-egg problem arises when assuming SO is responsible for bringing the network to criticality because propagation of SO releases depends on prior SO accumulation. A different communicator of oxidative stress was required to bring the network to criticality prior to mitochondrial depolarization. In agreement with the observation that widespread CM-DCF oxidation (primarily an indicator of $H_2O_2$) precedes the first cell-wide depolarization (Miguel a Aon, Cortassa, and Brian O'Rourke, 2004), the present results show that $H_2O_2$ can function as this alternative communicator of oxidative stress. Further, since $H_2O_2$ diffusion was necessary to observe mitochondrial depolarizations across the network, $H_2O_2$ communication underlies SO accumulation. As $H_2O_2$ diffused and accumulated throughout the network, scavenging of SO via SOD was inhibited(Bray et al., 1974; Liochev and Fridovich, 2002), which enabled SO to accumulate within the mitochondria matrices to produce a "critical" network. Thus, $H_2O_2$ still plays an important role in cell types where SO was believed to be the most important ROS in governing mitochondrial network failure.

### 3.4.2 Delay in Network Response to Oxidative Stress is from Scavenging Capacity Depletion Time Course

While $H_2O_2$ diffusion is the mechanism for how oxidative stress can communicate and spread throughout the network prior to mitochondrial depolarizations, it is unknown how this form of oxidative stress determines the progression of the network failure behavior. Laser stimulus- induced oxidative stress in a small region of the mitochondrial network consistently shows a delay of more than a minute before a cell-wide depolarization is

observed(Lufang Zhou, Miguel a. Aon, et al., 2010; Miguel a. Aon, Cortassa, Marbán, et al., 2003). Previous mitochondrial network models have been unable to reproduce this delayed behavior. Some type of "counter" mechanism must exist for any time-invariant system to display a delay effect, where the counter is some pool that is depleted or accumulated over time. Consistent with the behavior of a relaxation oscillator, when the counter crosses a threshold, downstream effects are triggered. Given a steady input of ROS to the mitochondrial network, we looked for patterns of system quantities gradually accumulating or depleting.

The mitochondrial network within ventricular cells contains a complex scavenging system that has a cascaded topology(Kembro et al., 2013). SO, which is an intrinsic by-product of the processes of the electron transport chain and the production of ATP, is continuously reduced by SOD to produce $H_2O_2$(Cortassa et al., 2004). $H_2O_2$ is then scavenged by GSH peroxidase and thioredoxin-dependent peroxiredoxins to prevent $H_2O_2$ accumulation(Cortassa et al., 2004). Regeneration of reduced GSH and thioredoxin is accomplished through NADPH-driven reductases, while NADPH redox potential ultimately depends on mitochondrial intermediates provided by the Krebs cycle. Modeling helps to reveal the dynamics of these redox-coupled reactions, and our results demonstrated that, indeed, GSH and NADPH are gradually depleted over time and across the network, prior to observing mitochondrial depolarizations. Further, our simulations also displayed the delay in response of the network to oxidative stress. SO accumulation and therefore the sensitivity of the network to perturbation, are potentiated by

$H_2O_2$ accumulation, which occurs prior to GSH and NADPH depletion. The encasement of the region of matrix SO accumulation within the regions of $H_2O_2$ accumulation (Figure 3.6B) and the NADPH and GSH depletion regions (Figure 3.5B), demonstrates the sequential cascaded topology of the scavenging system. Thus, the delay in response of the network is caused by the time it takes to deplete the NADPH and GSH reserves of the network, and simultaneously, to accumulate $H_2O_2$ and SO throughout the network. Our model is able to represent the evolution of a mitochondrial network gradually overwhelmed by oxidative stress.

### 3.4.3 Modeling Variations in Mitochondrial Network Failure Behavior

There are variations in the protocols for how oxidative stress is introduced to mitochondrial networks. The common methods of experiments include bathing the network in exogenous ROS solution(Lufang Zhou, Miguel a. Aon, et al., 2010), providing a laser stimulus that locally produces ROS(Miguel a. Aon, Cortassa, Marbán, et al., 2003), metabolically stressing the system via ischemia/reperfusion protocols(Brady et al., 2006; Solhjoo et al., 2015), or by reducing scavenging capacity of the system via targeted inhibitory chemicals(Slodzinski, Miguel a. Aon, and Brian O'Rourke, 2008; Miguel a. Aon, Cortassa, Maack, et al., 2007). Each method affects the distribution of oxidative stress and the overall response of the network. Models have been developed to try study these systems and reproduce some of the behavior of these experiments. A previous model by Yang(Yang et al., 2010) examined how the short range effects of SO and the longer range effects of $H_2O_2$ could participate to

independently activate IMAC and PTP, respectively; however, the impact of $H_2O_2$ accumulation (with consequent NADPH and GSH depletion) on the SO triggering mechanism was not explored. In a subsequent model from Nivala et al (Nivala et al., 2011), SO-mediated IMAC activation was modeled as a stochastic process that caused local propagations that could, depending on SO levels, sum to produce propagating waves of dpsi depolarization, but the effect of $H_2O_2$ was not included. Also, models from our lab(Lufang Zhou, Miguel a. Aon, et al., 2010) have been used to study propagation mechanisms during oxidatively stressed conditions. These models, however, do not capture the delay in response of the network to oxidative stress or demonstrate the relationship between $H_2O_2$ diffusion, the SO accumulation, or the ultrasensitive nature of the dpsi oscillations. By varying the ratio of $H_2O_2$ and SO, our model shows that altering the $H_2O_2$ stimulus modulates the growth rate of the oscillatory region, whereas altering the SO stimulus alters the frequency of oscillations. Full validation of the model will require accurate measurements of the different distributions of ROS across the network of a cell and examination of the impact of network topology on propagations and synchronization. Nevertheless, we believe that the specific dependencies of $H_2O_2$ and SO on long- and short-range coherent behavior, respectively, should remain.

The present model supports the feasibility of long range ROS-dependent communication in the mitochondrial network, but does not exclude the possibility of direct physical communication between mitochondria, for example, through nanotunnel structures(Lavorato et al., 2017). However, such structures have only been shown to span distances of ~1-5 mm (roughly 1 - 2

sarcomeres) within cardiomyocytes, which could not account for synchronization of oscillations over the entire length of the adult heart cell (>100 mm).

Further study is also needed to see how the effects of $H_2O_2$ communication are important in experiments with ischemia/reperfusion protocols, and how this network behavior scales up in tissue and in the whole heart. We hypothesize that the high mobility of $H_2O_2$ is important in distributing oxidative stress at the tissue and whole heart levels and may be important for producing the heterogenous distributions of network oscillation phases that may play a role in arrhythmogenesis. Incorporating our network model into a cardiac tissue model can be used to investigate these unknowns.

## 3.5 Appendix

### 3.5.1 Methods

#### 3.5.1.1 Mitochondrial Model Additions

The following describes the details of the model additions and changes from previous models. Listed variable names correspond to the variable names in the model equations file.

We made changes to the Zhou model(Lufang Zhou, Miguel a. Aon, et al., 2010) to better represent ROS scavenging. First, we added a representation of the mitochondrial matrix SOD. We reused the same formulation of the scavenging rate via intermitochondrial SOD (VSOD_i) from the Cortassa model(Cortassa et al., 2004) for the matrix SOD scavenging rate (VSOD_m).

The concentration of matrix SOD, compared to intermitochondrial SOD, was reduced from 1.43 uM to 300 nM to represent the reduced availability of SOD in the matrix due to the differences in volume of the two spaces.

Second, we updated the parameters of the glutathione based $H_2O_2$ scavenging system. The concentration for glutathione peroxidase (E__GPX_T), the concentration for glutathione reductase (E__GR_T), the K constants for GSSG (K_GSSG_M) and NADPH (K__NADPH), and total glutathione pool (G_tot) was taken from (Laura D. Gauthier et al., 2013), Phi_2, and k_GR were taken from (Laura D Gauthier et al., 2013) because the (Laura D. Gauthier et al., 2013) supplement values appeared to have a unit conversion error.

Third, we included the thioredoxin/peroxiredoxin based $H_2O_2$ scavenging system. The equations for this component was taken from the (Laura D. Gauthier et al., 2013) supplement. Similar to the glutathione changes, the values for Phi were taken from the (Laura D Gauthier et al., 2013) supplement.

Finally, we parameterized the size of the NADPH pool, using a starting capacity value of 12mM and a replenishment rate of 7.5nM/ms (NADPH_gen).

In addition to SO diffusion, we added $H_2O_2$ diffusion. The resulting equations for ROS flux were:

$$\begin{aligned} neighborSO\_flux &= (SOi\_left + SOi\_right - 2 * SOi\_self)/C\_SO \\ neighborHP\_flux &= (HP\_left + HP\_right - 2 * HP\_self)/C\_HP \end{aligned} \tag{3.1}$$

SOi_(left | right) was the SO concentration of the neighbors. HP_(left | right) was the $H_2O_2$ concentration of the neighboring mitochondria. The diffusion coefficient for SO (C_SO) was unchanged from the Zhou model(Lufang Zhou,

Miguel a. Aon, et al., 2010) and 4mM/ms/um was used for the diffusion coefficient for $H_2O_2$ (C_HP).

With the changes just described, the resulting differential equations for the affected state variables were:

$$\begin{aligned} dSOm/dt &= SO\_stim - VSOD\_m - IMAC\_flux \\ dSOi/dt &= IMAC\_flux - VSOD\_i + neighborSO\_flux \\ dNADPH/dt &= NADPH\_gen - VGR - VTRXR \\ dH2O2/dt &= HP\_stim + VSOD\_m + VSOD - VGPX - VPRX + neighborHP\_flux \end{aligned} \tag{3.2}$$

VGR is the rate of production of glutathione from glutathione reductase using NADPH and the precursor GSSG. Similarly, VTRXR is for replenishment of thioredoxin. VGPX and VPRX are the $H_2O_2$ scavenging rates from the scavenging systems governed by GSH and thioredoxin respectively. The constants used for VGR in the Zhou et al model(Lufang Zhou, Miguel a. Aon, et al., 2010) were updated to the more recent values in Gauthier et al 2013 ((Laura D. Gauthier et al., 2013; Laura D Gauthier et al., 2013)) with the changes for the constants described above. VTRXR and VPRX was also added from the Gauthier models.

#### 3.5.1.2 Computational Methods

The nonlinear system of partial differential equations describing ROS communication between nodes was spatially discretized using the finite difference method. The aggregated ODEs of all the nodes were numerically integrated using the solver CVODE, a multistep stiff ODE solver that uses a banded backward differentiation formula method and a direct linear solver to implement

newton iteration. A maximum time step of 0.1 ms was used to stably simulate the model on a desktop computer.

### 3.5.2 Model Equations

```
//Parameterizing: VpSO, EtSOD, and NADPH

EtSOD = EtSOD_parameter;//1.43e-3;//0.0003;
Kki = 0.5;
k5_SOD = 2.5E-4;
k3_SOD = 24.0;
k1_SOD = 1.2e3;

VSOD = 2.0*k1_SOD*k5_SOD*(k1_SOD+k3_SOD*(1.0+H2O2/Kki))*EtSOD *SOi /(
    k5_SOD*(2.0*k1_SOD+k3_SOD*(1+H2O2/Kki))+k1_SOD*k3_SOD*(1.0+H2O2/Kki)*
    SOi);
// uses state: SOm
// uses state: H2O2
// outputs: SOm
EtSODm = EtSODm_parameter;
VSODm = ((2*k1_SOD*k5_SOD*(k1_SOD+(k3_SOD*(1+(H2O2/Kki))))*EtSODm*SOm)
    /((k5_SOD*((2*k1_SOD)+(k3_SOD*(1+(H2O2/Kki)))))+(k1_SOD*k3_SOD*(1+(
    H2O2/Kki))*SOm)));


E__GPX_T = E__GPX_T_parameter;
Phi_1 = 5e-3; //s
Phi_2 = 0.75; //s
E__GR_T = 5.10e-3;
k_GR = 2.5E-3; //s
K__GSSG_M = 0.12; // vs 0.06
K__NADPH_M = 0.015; // match
G_tot = 3.0;
E__Prx_T = 1.0;
Phi_P1 = 3.83;//6.3833e-6;
Phi_P2 = 1.85;//3.0833e-7;
K__TrxSS_M = 0.006;
K__TNADPH_M = 0.012;
k_TrxR = 0.022;//1.32e3;
E__TrxR_T = 0.01;
```

```
k_TxPx = 2.5;//1.5e5;
Trx_tot = 0.025;
Prx_tot = 0.15;

GSSG = 0.5*(G_tot-GSH);
TrxSS = Trx_tot-TrxSH2;
PrxSS = Prx_tot-PrxSH2;

VGPX = E__GPX_T*H2O2*GSH/(Phi_1*GSH+Phi_2*H2O2);
VGR = k_GR*E__GR_T*GSSG*NADPH/(GSSG*NADPH+K__GSSG_M*NADPH+K__NADPH_M*
    GSSG+K__GSSG_M*K__NADPH_M);
VPRX = E__Prx_T*H2O2*pow(PrxSH2,2)/(Phi_P2*PrxSH2+Phi_P1*H2O2);
VTRXR = k_TrxR*E__TrxR_T*TrxSS*NADPH/(TrxSS*NADPH+K__TrxSS_M*NADPH+
    K__TNADPH_M*TrxSS+K__TrxSS_M*K__TNADPH_M);
VTXPX = k_TxPx*TrxSH2*PrxSS;

Cdiff_H2O2 = Cdiff_H2O2_parameter;
left_H2O2 = ((n_idx == 0) ? H2O2 : map(H2O2,n_idx-1));
right_H2O2 = ((n_idx == (num_nodes-1)) ? H2O2 : map(H2O2,n_idx+1));
V_diff_H2O2 = (left_H2O2 + right_H2O2 - 2*H2O2) * Cdiff_H2O2;

// uses state: SOi
// outputs: SOi
Cdiff_SOi = Cdiff_SOi_parameter;
left_SOi = (((n_idx==0)) ? SOi : map(SOi,(n_idx-1)));
right_SOi = (((n_idx==(num_nodes-1))) ? SOi : map(SOi,(n_idx+1)));
V_diff = (((left_SOi+right_SOi)-(2*SOi))*Cdiff_SOi);

// uses state: NADH
// uses state: AKG
// uses state: Cam
// outputs: NADH
// outputs: AKG
// outputs: SCoA
CPN = 10.0;
NAD = (CPN-NADH);
KmIDNAD = 0.923;
KmIDNAD_NAD = (KmIDNAD/NAD);
KmKG = 1.94;
nKG = 1.2;
KmKGNAD = 38.7;
```

```
KmKGNAD_KmIDNAD = (KmKGNAD/KmIDNAD);
Kca = 0.00127;
Mg = 0.4;
Kmg = 0.0308;
Mg_Kmg_1 = ((Mg/Kmg)+1.0);
Mg_Kmg_1_Kca = (Mg_Kmg_1/Kca);
a = (AKG*(Mg_Kmg_1+(Mg_Kmg_1_Kca*Cam)));
EtKG = 0.5;
kKGDH = 0.075;
kKGDH_EtKG = (kKGDH*EtKG);
VKGDH = ((kKGDH_EtKG*a)/(a+KmKG+(AKG*pow((KmKGNAD_KmIDNAD*KmIDNAD_NAD),
    nKG))));

// uses state: ADPm
// uses state: Succ
// uses state: SCoA
// outputs: ADPm
// outputs: Succ
// outputs: SCoA
CoA = 0.02;
KSLeq = 3.115;
CoA_KSLeq = (CoA/KSLeq);
kfSL = 0.005;
Cm = 1.5;
ATPm = (Cm-ADPm);
VSL = (kfSL*((SCoA*ADPm)-(CoA_KSLeq*Succ*ATPm)));

// uses state: Dpsi
// outputs: Dpsi
kresf = 5.765E13;
rb = 1.762E-16;
g = 0.85;
ra = 6.394E-13;
r3 = 1.059E-26;
RT_over_F = 26.7292465926919;
FRT_6_g = ((6.0*g)/RT_over_F);
FADH2 = 1.24;
FAD = 0.01;
AREF = (RT_over_F*log((kresf*sqrt((FADH2/FAD)))));
Dpsio = 50.0;
exp_6_FRT_Dpsio = exp(((6.0*Dpsio)/RT_over_F));
```

```
r1 = 2.077E-18;
exp_AREF_FRT = exp((AREF/RT_over_F));
VFO_VHFe_C1 = ((1.0+(r1*exp_AREF_FRT))*exp_6_FRT_Dpsio);
DpH = (-0.2);
DmuH_Constant = ((-2.303)*RT_over_F*DpH);
DmuH = (DmuH_Constant+Dpsi);
exp_FRT_6_g_DmuH = exp((FRT_6_g*DmuH));
r2 = 1.728E-9;
ra_rb = (4.0*(ra+rb));
rhoREF = 3.75E-4;
ra_exp_AREF_FRT = (4.0*ra*exp_AREF_FRT);
r2_r3_exp_AREF_FRT = (r2+(r3*exp_AREF_FRT));
VHFe = ((ra_exp_AREF_FRT-(ra_rb*exp_FRT_6_g_DmuH))*(rhoREF/(VFO_VHFe_C1
    +(r2_r3_exp_AREF_FRT*exp_FRT_6_g_DmuH))));

// uses state: SOi
// uses state: SOm
// uses state: Dpsi
// uses alg: RT_over_F
// outputs: SOi
// outputs: SOm
Kappa = 0.07;
Kcc = 0.01;
Em = 4.0;
af = 10000.0;
G_L = 3.5E-8;
j_Vt2SO2m = 0.1;
G_max = 3.9085E-6;
Vt2SO2m = ((-j_Vt2SO2m)*((((-1.0)*Dpsi)-(RT_over_F*log((SOm/SOi))))/Dpsi
    )*((-1)*(0.001+(af/(1+(Kcc/SOi))))*(G_L+(G_max/(1.0+exp((Kappa*(Em
    -((-1.0)*Dpsi)))))))*((-1.0)*Dpsi)));

// uses state: Dpsi
// uses alg: RT_over_F
// outputs: Cam
// outputs: Dpsi
F_over_RT = (1.0/RT_over_F);
FRT2 = (2.0*F_over_RT);
ktrans = 0.019;
inv_ktrans = (1.0/ktrans);
Cai = 1.0E-4;
```

```
Cai_ktrans_plus1 = (1.0+(Cai*inv_ktrans));
kact = 3.8E-4;
inv_kact = (1.0/kact);
na = 2.8;
Vmuni = 0.0275;
Cai_ktrans_plus1_p3 = (Cai_ktrans_plus1*Cai_ktrans_plus1*
    Cai_ktrans_plus1);
Vmuni_ktrans = (Vmuni/ktrans);
FRT2_Dpsi = (FRT2*(Dpsi-91.0));
L = 110.0;
Vuni = ((Vmuni_ktrans*Cai*FRT2_Dpsi*Cai_ktrans_plus1_p3)/(((
    Cai_ktrans_plus1_p3*Cai_ktrans_plus1)+(L/pow((1.0+(Cai*inv_kact)),na)
    ))*(1.0-exp((-FRT2_Dpsi)))));

// uses state: Oaa
// outputs: Oaa
EtCS = 0.4;
AcCoA = 1.0;
KCS = 0.5;
KmAcCoA = 0.0126;
VCS_C1 = ((KCS*EtCS*AcCoA)/(KmAcCoA+AcCoA));
KmOaa = 6.4E-4;
VCS = ((VCS_C1*Oaa)/(Oaa+KmOaa));

// uses state: VpSO
// outputs: SOm
// uses state: NADH
// uses state: Dpsi
// uses alg: DpH
// uses alg: r1
// uses alg: DmuH_Constant
// uses alg: Dpsio
// uses alg: DmuH
// uses alg: RT_over_F
// uses alg: exp_6_FRT_Dpsio
// uses alg: r2
// uses alg: exp_FRT_6_g_DmuH
// uses alg: FRT_6_g
// uses alg: r3
// uses alg: ra
// uses alg: g
```

```
// uses alg: CPN
// uses alg: KmIDNAD_NAD
// uses alg: KmIDNAD
// uses alg: NAD
// outputs: NADH
rc1 = 2.656E-22;
r1_exp_6_FRT_Dpsio = (r1*exp_6_FRT_Dpsio);
rc2 = 8.632E-30;
rhoREN = 1.0E-4;
rhoREN_rc2 = (0.5*rhoREN*rc2);
kres = 1.35E18;
kres_sq_KmIDNAD = ((kres*kres)/KmIDNAD);
AREN = sqrt((NADH*kres_sq_KmIDNAD*KmIDNAD_NAD));
ra_rc1_exp_6_FRT_Dpsio = (ra+(rc1*exp_6_FRT_Dpsio));
rhoREN_ra_rc1_exp_6_FRT_Dpsio = (0.5*rhoREN*ra_rc1_exp_6_FRT_Dpsio);
rhoREN_ra = (0.5*rhoREN*ra);
denominator1 = (1.0/((exp_6_FRT_Dpsio+(r1_exp_6_FRT_Dpsio*AREN))+((r2+(
    r3*AREN))*exp_FRT_6_g_DmuH)));
VNO = ((((rhoREN_ra_rc1_exp_6_FRT_Dpsio+(rhoREN_rc2*exp_FRT_6_g_DmuH))*
    AREN)-(rhoREN_ra*exp_FRT_6_g_DmuH))*denominator1);

// uses state: MAL
// uses state: FUM
// outputs: MAL
// outputs: FUM
KFHeq = 1.0;
kfFH = 0.00332;
kfFH_KFHeq = (kfFH/KFHeq);
VFH = ((kfFH*FUM)-(kfFH_KFHeq*MAL));

// uses state: SOi
// uses state: Dpsi
// uses alg: G_max
// uses alg: G_L
// uses alg: af
// uses alg: Em
// uses alg: Kcc
// uses alg: Kappa
// outputs: Dpsi
VIMAC2 = ((-1.0)*(0.001+(af/(1.0+(Kcc/SOi))))*(G_L+(G_max/(1+exp((Kappa
    *(Em-((-1.0)*Dpsi)))))))*((-1.0)*Dpsi));
```

```
// uses state: Succ
// uses state: ISOC
// uses state: Oaa
// uses state: AKG
// uses state: MAL
// uses state: FUM
// uses state: SCoA
// outputs: ISOC
KACOeq = 2.22;
one_inv_KACOeq = (1.0+(1.0/KACOeq));
CIK = 1.0;
kfACO = 0.0125;
VACO = (kfACO*(CIK-AKG-SCoA-Succ-FUM-MAL-Oaa-(ISOC*one_inv_KACOeq)));

// uses state: Oaa
// uses state: NADH
// uses state: MAL
// uses alg: CPN
// uses alg: NAD
// outputs: Oaa
// outputs: NADH
// outputs: MAL
Kh2 = 26.7;
KmmNAD = 0.2244;
Kh1 = 1.131E-5;
Kioaa = 0.0031;
Koff = 0.0399;
EtMD = 0.154;
Kmal = 1.493;
Kmal_Kioaa = (Kmal/Kioaa);
H = 2.5E-5;
kMDH = 0.111;
Kh3 = 6.68E-9;
Kh4 = 5.62E-6;
kMDH_Fh_EtMD = ((1.0/(1.0+(Kh3/H)+((Kh3*Kh4)/H*H)))*(1.0/(1.0+(Kh3/H)+((
    Kh3*Kh4)/H*H)))*((1.0/(1.0+(H/Kh1)+(H*H/(Kh1*Kh2))))+Koff)*kMDH*EtMD)
    ;
VMDH = ((kMDH_Fh_EtMD*MAL*NAD)/((MAL+Kmal+(Oaa*Kmal_Kioaa))*(KmmNAD+NAD)
    ));
```

```
// uses state: Cam
// uses state: Dpsi
// uses alg: Cai
// uses alg: RT_over_F
// uses alg: FRT2_Dpsi
// uses alg: F_over_RT
// uses alg: FRT2
// outputs: Cam
// outputs: Dpsi
Nai = 7.0;
VmNC = 1.0E-4;
b = 0.5;
Knca = 3.75E-4;
Kna = 9.4;
b_05 = (b*0.5);
n = 3.0;
VnaCa = ((VmNC*exp((b_05*FRT2_Dpsi))*Cam)/(Cai*pow((1.0+(Kna/Nai)),n)
    *(1.0+(Knca/Cam))));

// uses state: NADH
// uses state: Dpsi
// uses alg: DpH
// uses alg: r1
// uses alg: kres
// uses alg: DmuH_Constant
// uses alg: Dpsio
// uses alg: DmuH
// uses alg: rhoREN
// uses alg: denominator1
// uses alg: RT_over_F
// uses alg: exp_6_FRT_Dpsio
// uses alg: r2
// uses alg: exp_FRT_6_g_DmuH
// uses alg: kres_sq_KmIDNAD
// uses alg: AREN
// uses alg: FRT_6_g
// uses alg: r3
// uses alg: ra
// uses alg: g
// uses alg: r1_exp_6_FRT_Dpsio
// uses alg: CPN
```

```
// uses alg: KmIDNAD_NAD
// uses alg: KmIDNAD
// uses alg: rb
// uses alg: NAD
// outputs: Dpsi
rhoREN_6_ra = (6.0*rhoREN*ra);
rhoREN_6_ra_rb = (6.0*rhoREN*(ra+rb));
VHNe = (((rhoREN_6_ra*AREN)-(rhoREN_6_ra_rb*exp_FRT_6_g_DmuH))*
    denominator1);

// uses state: ADPm
// uses state: Dpsi
// uses alg: Cm
// uses alg: ATPm
// uses alg: RT_over_F
// uses alg: F_over_RT
// outputs: ADPm
// outputs: Dpsi
VmDT = 0.005;
VmDT_75 = (0.75*VmDT);
VmDT_20 = (20.0*VmDT);
hm = 0.5;
hm_F_over_RT = (hm*F_over_RT);
ADPm_ATPm = (ADPm/ATPm);
tenDiv9 = (10.0/9.0);
ADP = 0.05;
ATPi = 6.25;
ATPi_ADP = (ATPi/ADP);
VANT = ((VmDT_75-(VmDT_20*ATPi_ADP*ADPm_ATPm*exp(((-F_over_RT)*Dpsi))))
    /((1.0+(tenDiv9*ATPi_ADP*exp(((-hm_F_over_RT)*Dpsi))))*(1.0+(18*
    ADPm_ATPm))));

// uses state: ADPm
// uses state: Dpsi
// uses alg: Cm
// uses alg: DpH
// uses alg: ATPm
// uses alg: DmuH_Constant
// uses alg: Dpsio
// uses alg: DmuH
// uses alg: RT_over_F
```

```
// outputs: ADPm
kf1 = 17100.0;
Pi = 2.0;
kf1_Pi = (kf1/Pi);
AF1 = ((kf1_Pi*ATPm)/ADPm);
pa = 1.656E-8;
p3 = 6.65E-15;
FRT_3 = (3.0/RT_over_F);
exp_3FRT_DmuH = exp((FRT_3*DmuH));
p1 = 1.346E-8;
pc2 = 4.585E-17;
p2 = 7.739E-7;
rhoF1 = 0.05;
pc1 = 9.651E-17;
exp_3_FRT_Dpsio = exp(((3.0*Dpsio)/RT_over_F));
VATPase_C1 = ((100.0*pa)+(pc1*exp_3_FRT_Dpsio));
p1_exp_3_FRT_Dpsio = (p1*exp_3_FRT_Dpsio);
denominator = ((-rhoF1)/(exp_3_FRT_Dpsio+(p1_exp_3_FRT_Dpsio*AF1)+((p2+(
    p3*AF1))*exp_3FRT_DmuH)));
VATPase = ((((VATPase_C1+(pc2*exp_3FRT_DmuH))*AF1)-(pa*exp_3FRT_DmuH))*
    denominator);

// uses state: ADPm
// uses state: Dpsi
// uses alg: p1_exp_3_FRT_Dpsio
// uses alg: denominator
// uses alg: Cm
// uses alg: exp_3_FRT_Dpsio
// uses alg: DpH
// uses alg: FRT_3
// uses alg: ATPm
// uses alg: DmuH_Constant
// uses alg: Dpsio
// uses alg: DmuH
// uses alg: Pi
// uses alg: RT_over_F
// uses alg: rhoF1
// uses alg: p2
// uses alg: kf1
// uses alg: p1
// uses alg: kf1_Pi
```

```
// uses alg: exp_3FRT_DmuH
// uses alg: p3
// uses alg: pa
// uses alg: AF1
// outputs: Dpsi
pb = 3.373E-10;
pa_300 = (300.0*pa);
pa_pb_3 = (3.0*(pa+pb));
Vhu = (((pa_300+(pa_300*AF1))-(pa_pb_3*exp_3FRT_DmuH))*denominator);

// uses state: Dpsi
// uses alg: DpH
// uses alg: DmuH_Constant
// uses alg: DmuH
// uses alg: RT_over_F
// outputs: Dpsi
gh = 1.0E-8;
Vhleak = (gh*DmuH);

// outputs: Dpsi
Cmito = 0.001812;
inv_Cmito = (1.0/Cmito);

// outputs: Cam
fm = 3.0E-4;

// uses state: Oaa
// uses state: AKG
// outputs: Oaa
// outputs: AKG
kfAAT = 6.44E-4;
GLU = 1.0;
KAATeq = 6.6;
kcnsASP = 1.5E-6;
VAAT_Constant = ((kfAAT*GLU*kcnsASP*KAATeq)/kfAAT);
kcnsASP_KAATeq_kfAAT = ((kcnsASP*KAATeq)/kfAAT);
VAAT = ((VAAT_Constant*Oaa)/(kcnsASP_KAATeq_kfAAT+AKG));

// uses state: ADPm
// uses state: ISOC
// uses state: NADH
```

```
// uses state: Cam
// uses alg: H
// uses alg: CPN
// uses alg: KmIDNAD_NAD
// uses alg: KmIDNAD
// uses alg: NAD
// outputs: ISOC
// outputs: NADH
// outputs: AKG
KidhNADH = 0.19;
inv_KidhNADH = (1.0/KidhNADH);
Fi = (1.0+(NADH*inv_KidhNADH));
kIDH = 0.05;
EtID = 0.109;
kIDH_EtID = (kIDH*EtID);
KaCa = 5.0E-4;
inv_KaCa = (1.0/KaCa);
KADP = 0.62;
inv_KADP = (1.0/KADP);
Kmiso = 1.52;
nID = 2.0;
Fa = (1.0/((1.0+(ADPm*inv_KADP))*(1.0+(Cam*inv_KaCa))));
kh_1 = 8.1E-5;
kh_2 = 5.98E-5;
VIDH_Constant = (1.0+(H/kh_1)+(kh_2/H));
VIDH = (kIDH_EtID/(VIDH_Constant+(KmIDNAD_NAD*Fi)+(pow((Kmiso/ISOC),nID)
    *Fa*(1.0+(KmIDNAD_NAD*Fi)))));

// uses alg: b
// outputs: Dpsi
two_b = (2.0*b);

// uses state: Succ
// uses state: Oaa
// uses state: FUM
// outputs: Succ
// outputs: FUM
KiOxaa = 0.15;
inv_KiOxaa = (1.0/KiOxaa);
KiFUM = 1.3;
KmSucc = 0.03;
```

```
KmSucc_KiFUM = (KmSucc/KiFUM);
EtSDH = 0.5;
kSDH = 0.005;
kSDH_EtSDH = (kSDH*EtSDH);
VSDH = ((kSDH_EtSDH*Succ)/(Succ+((KmSucc+(KmSucc_KiFUM*FUM))*(1.0+(
    inv_KiOxaa*Oaa)))));

Cam_init                                                = 1.6026754051804608e
    -004;
ADPm_init                                               = 4.3787214656881651e
    -002;
Dpsi_init                                               = 1.5110923886716841e
    +002;
NADH_init                                               = 9.1262431574514160e
    +000;
ISOC_init                                               = 6.1526822463370678e
    -001;
AKG_init                                                = 6.3382927748632811e
    -005;
SCoA_init                                               = 8.7883773193026898e
    -002;
Succ_init                                               = 2.3466416517868308e
    -004;
FUM_init                                                = 1.1827903208965811e
    -002;
MAL_init                                                = 6.0357471749036560e
    -003;
Oaa_init                                                = 6.2317155371649292e
    -008;

H2O2gen_init = 0.0;
SOgen_init = 0.0;
SOm_init = 3.0352618104833946e-005;
SOi_init = 3.0900363134336965e-006;
H2O2_init = 6.9776447602637735e-007;
GSH_init = 2.8;
TrxSH2_init = 0.002;
PrxSH2_init = 0.0281;
NADPH_init = 1.0;
```

```
VpSO = SOgen;
VpH2O2 = H2O2gen;

diff_Cam                                                =  fm * (Vuni - VnaCa)
    ;
diff_ADPm                                               =  VANT - VATPase -
    VSL;
diff_Dpsi                                               =  -(-VHNe - VHFe +
    Vhu + VANT + Vhleak + two_b * VnaCa + 2.0 * Vuni + VIMAC2) *
    inv_Cmito;
diff_NADH                                               =  -VNO + VIDH + VKGDH
     + VMDH;
diff_ISOC                                               =  VACO - VIDH;
diff_AKG                                                =  VIDH + VAAT - VKGDH
    ;
diff_SCoA                                               =  VKGDH - VSL;
diff_Succ                                               =  VSL - VSDH;
diff_FUM                                                =  VSDH - VFH;
diff_MAL                                                =  VFH - VMDH;
diff_Oaa                                                =  VMDH - VCS - VAAT;

diff_H2O2gen = 0.0;
diff_SOgen = 0.0;
diff_SOm = VpSO - VSODm - Vt2SO2m;
diff_SOi = Vt2SO2m - VSOD + V_diff;
diff_H2O2 = VpH2O2 + VSODm + VSOD - VPRX - VGPX + V_diff_H2O2;
diff_GSH = VGR - VGPX;
diff_TrxSH2 = VTRXR - VTXPX;
diff_PrxSH2 = VTXPX - VPRX;

VpNADPH = VpNADPH_parameter;
diff_NADPH = VpNADPH - VGR - VTRXR;

//
    ---------------------------------------------------------------------
```

# References


Sasaki, N, T Sato, E Marbán, and B O'Rourke (2001). "ATP consumption by uncoupled mitochondria activates sarcolemmal K(ATP) channels in cardiac myocytes." In: *American journal of physiology. Heart and circulatory physiology* 280.4, H1882–H1888. ISSN: 0363-6135.

Aon, Miguel a, Sonia Cortassa, and Brian O'Rourke (2004). "Percolation and criticality in a mitochondrial network." In: *Proceedings of the National Academy of Sciences of the United States of America* 101.13, pp. 4447–4452. ISSN: 0027-8424. DOI: 10.1073/pnas.0307156101.

Nivala, Melissa, Paavo Korge, Michael Nivala, James N. Weiss, and Zhilin Qu (2011). "Linking flickering to waves and whole-cell oscillations in a mitochondrial network model". In: *Biophysical Journal* 101.9, pp. 2102–2111. ISSN: 00063495. DOI: 10.1016/j.bpj.2011.09.038. URL: http://dx.doi.org/10.1016/j.bpj.2011.09.038.

Stanley, William C, Fabio A Recchia, and Gary D Lopaschuk (2005). "Myocardial Substrate Metabolism in the Normal and Failing Heart". In: *Physiological reviews*. ISSN: 0031-9333. DOI: 10.1152/physrev.00006.2004..

Saks, Valdur, Petras Dzeja, Uwe Schlattner, Marko Vendelin, Andre Terzic, and Theo Wallimann (2006). "Cardiac system bioenergetics: metabolic basis of the Frank-Starling law". In: *The Journal of Physiology* 571.2, pp. 253–273. ISSN: 00223751. DOI: 10.1113/jphysiol.2005.101444. URL: http://doi.wiley.com/10.1113/jphysiol.2005.101444.

Ichas, François, Laurence S Jouaville, and Jean-Pierre Mazat (1997). "Mitochondria Are Excitable Organelles Capable of Generating and Conveying Electrical and Calcium Signals". In: *Cell* 89.7, pp. 1145–1153. ISSN: 0092-8674. DOI: 10.1016/S0092-8674(00)80301-3. URL: https://doi.org/10.1016/S0092-8674(00)80301-3.

Romashko, Dmitry N, Eduardo Marban, and Brian O'Rourke (1998). "Subcellular metabolic transients and mitochondrial redox waves in heart cells".

In: *Proceedings of the National Academy of Sciences* 95.4, 1618 LP –1623. URL: http://www.pnas.org/content/95/4/1618.abstract.

Zorov, D B, C R Filburn, L O Klotz, J L Zweier, and S J Sollott (2000). "Reactive oxygen species (ROS)-induced ROS release: a new phenomenon accompanying induction of the mitochondrial permeability transition in cardiac myocytes." In: *The Journal of experimental medicine* 192.7, pp. 1001–1014. ISSN: 00221007. DOI: 10.1084/jem.192.7.1001.

Aon, Miguel a., Sonia Cortassa, Eduardo Marbán, and Brian O'Rourke (2003). "Synchronized Whole Cell Oscillations in Mitochondrial Metabolism Triggered by a Local Release of Reactive Oxygen Species in Cardiac Myocytes". In: *Journal of Biological Chemistry* 278, pp. 44735–44744. ISSN: 00219258. DOI: 10.1074/jbc.M302673200.

Amchenkova, A A, L E Bakeeva, Y S Chentsov, V P Skulachev, and D B Zorov (1988). "Coupling membranes as energy-transmitting cables. I. Filamentous mitochondria in fibroblasts and mitochondrial clusters in cardiomyocytes." In: *The Journal of Cell Biology* 107.2, 481 LP –495. URL: http://jcb.rupress.org/content/107/2/481.abstract.

Glancy, Brian, Lisa M. Hartnell, Daniela Malide, Zu-Xi Yu, Christian a. Combs, Patricia S. Connelly, Sriram Subramaniam, and Robert S. Balaban (2015). "Mitochondrial reticulum for cellular energy distribution in muscle". In: *Nature* 523.7562, pp. 617–620. ISSN: 0028-0836. DOI: 10.1038/nature14614. URL: http://www.nature.com/doifinder/10.1038/nature14614.

Crucitti, Paolo, Vito Latora, and Massimo Marchiori (2004). "Model for cascading failures in complex networks." In: *Physical review. E, Statistical, nonlinear, and soft matter physics* 69, p. 045104. ISSN: 1539-3755. DOI: 10.1103/PhysRevE.69.045104. arXiv: 0309141 [cond-mat].

Zhou, Lufang, Soroosh Solhjoo, Brent Millare, Gernot Plank, M. Roselle Abraham, Sonia Cortassa, Natalia Trayanova, and Brian O'Rourke (2014). "Effects of regional mitochondrial depolarization on electrical propagation: Implications for arrhythmogenesis". In: *Circulation: Arrhythmia and Electrophysiology* 7.1, pp. 143–151. ISSN: 19413084.

Akar, Fadi G., Miguel a. Aon, Gordon F. Tomaselli, and Brian O'Rourke (2005). "The mitochondrial origin of postischemic arrhythmias". In: *Journal of Clinical Investigation* 115.12, pp. 3527–3535. ISSN: 00219738. DOI: 10.1172/JCI25371.

Jeong, Euy-Myoung, Man Liu, Megan Sturdy, Ge Gao, Susan T. Varghese, Ali a. Sovari, and Samuel C. Dudley (2012). "Metabolic stress, reactive oxygen species, and arrhythmia". In: *Journal of Molecular and Cellular Cardiology*

52.2, pp. 454–463. ISSN: 00222828. DOI: 10.1016/j.yjmcc.2011.09.018. URL: http://dx.doi.org/10.1016/j.yjmcc.2011.09.018.

Dey, Swati, Deeptankar DeMazumder, Agnieszka Sidor, D B Foster, and Brian O'Rourke (2018). "Mitochondrial ROS Drive Sudden Cardiac Death and Chronic Proteome Remodeling in Heart Failure". In: *Circulation Research*, CIRCRESAHA.118.312708. ISSN: 0009-7330. DOI: 10.1161/CIRCRESAHA.118.312708. URL: http://circres.ahajournals.org/lookup/doi/10.1161/CIRCRESAHA.118.312708.

Slodzinski, Martin K., Miguel a. Aon, and Brian O'Rourke (2008). "Glutathione oxidation as a trigger of mitochondrial depolarization and oscillation in intact hearts". In: *Journal of Molecular and Cellular Cardiology* 45.5, pp. 650–660. ISSN: 00222828. DOI: 10.1016/j.yjmcc.2008.07.017. URL: http://dx.doi.org/10.1016/j.yjmcc.2008.07.017.

Brown, David a. and Brian O'Rourke (2010). "Cardiac mitochondria and arrhythmias". In: *Cardiovascular Research* 88, pp. 241–249. ISSN: 00086363. DOI: 10.1093/cvr/cvq231.

Lyon, Alexander R., Paul J. Joudrey, Dongzhu Jin, Robert D. Nass, Miguel a. Aon, Brian 'Rourke, and Fadi G. Akar (2010). "Optical imaging of mitochondrial function uncovers actively propagating waves of mitochondrial membrane potential collapse across intact heart". In: *Journal of Molecular and Cellular Cardiology* 49.4, pp. 565–575. ISSN: 00222828. DOI: 10.1016/j.yjmcc.2010.07.002. URL: http://dx.doi.org/10.1016/j.yjmcc.2010.07.002.

Hou, Tingting, Xianhua Wang, Qi Ma, and Heping Cheng (2014). "Mitochondrial flashes: new insights into mitochondrial ROS signalling and beyond". In: *The Journal of Physiology* 592.Pt 17, pp. 3703–3713. ISSN: 0022-3751. DOI: 10.1113/jphysiol.2014.275735. URL: http://www.ncbi.nlm.nih.gov/pmc/articles/PMC4192698/.

Wang, Wang, Huaqiang Fang, Linda Groom, Aiwu Cheng, Wanrui Zhang, Jie Liu, Xianhua Wang, Kaitao Li, Peidong Han, Ming Zheng, Jinhu Yin, Weidong Wang, Mark P Mattson, Joseph P Y Kao, Edward G Lakatta, Shey-Shing Sheu, Kunfu Ouyang, Ju Chen, Robert T Dirksen, and Heping Cheng (2008). "Superoxide Flashes in Single Mitochondria". In: *Cell* 134.2, pp. 279–290. ISSN: 0092-8674. DOI: 10.1016/j.cell.2008.06.017. URL: https://doi.org/10.1016/j.cell.2008.06.017.

Lu, Xiyuan, Jennifer Kwong, Jeffery D Molkentin, and Donald M Bers (2016). "Individual Cardiac Mitochondria Undergo Rare Transient Permeability Transition Pore Openings". In: *Circulation research* 118.5, pp. 834–841. ISSN:

0009-7330. DOI: 10.1161/CIRCRESAHA.115.308093. URL: http://www.ncbi.nlm.nih.gov/pmc/articles/PMC4779382/.

Zhou, L. and B. O'Rourke (2012). "Cardiac mitochondrial network excitability: insights from computational analysis". In: *AJP: Heart and Circulatory Physiology* 302, H2178–H2189. ISSN: 0363-6135. DOI: 10.1152/ajpheart.01073.2011.

Kusama, Y, M Bernier, and D J Hearse (1989). "Singlet oxygen-induced arrhythmias. Dose- and light-response studies for photoactivation of rose bengal in the rat heart." In: *Circulation* 80, pp. 1432–1448. ISSN: 0009-7322. DOI: 10.1161/01.CIR.80.5.1432.

Cortassa, Sonia, Miguel a Aon, Raimond L Winslow, and Brian O'Rourke (2004). "A mitochondrial oscillator dependent on reactive oxygen species." In: *Biophysical journal* 87.3, pp. 2060–2073. ISSN: 00063495. DOI: 10.1529/biophysj.104.041749. URL: http://dx.doi.org/10.1529/biophysj.104.041749.

Zhou, Lufang, Miguel a. Aon, Tabish Almas, Sonia Cortassa, Raimond L. Winslow, and Brian O'Rourke (2010). "A reaction-diffusion model of ROS-induced ROS release in a mitochondrial network". In: *PLoS Computational Biology* 6.1. ISSN: 1553734X. DOI: 10.1371/journal.pcbi.1000657.

Yang, Ling, Paavo Korge, James N. Weiss, and Zhilin Qu (2010). "Mitochondrial oscillations and waves in cardiac myocytes: Insights from computational models". In: *Biophysical Journal* 98.8, pp. 1428–1438. ISSN: 00063495. DOI: 10.1016/j.bpj.2009.12.4300. URL: http://dx.doi.org/10.1016/j.bpj.2009.12.4300.

Kurz, Felix T., Thomas Derungs, Miguel A. Aon, Brian O'Rourke, and Antonis A. Armoundas (2015). "Mitochondrial Networks in Cardiac Myocytes Reveal Dynamic Coupling Behavior". In: *Biophysical Journal* 108.8, pp. 1922–1933. ISSN: 0006-3495. DOI: 10.1016/j.bpj.2015.01.040. URL: https://doi.org/10.1016/j.bpj.2015.01.040.

Kurz, Felix T., Miguel a. Aon, Brian O'Rourke, and Antonis a. Armoundas (2014). "Cardiac mitochondria exhibit dynamic functional clustering". In: *Frontiers in Physiology* 5.September, pp. 1–8. ISSN: 1664-042X. DOI: 10.3389/fphys.2014.00329. URL: http://journal.frontiersin.org/article/10.3389/fphys.2014.00329/abstract.

Kurz, Felix T, Miguel a Aon, Brian O'Rourke, and Antonis a Armoundas (2010a). "Spatio-temporal oscillations of individual mitochondria in cardiac myocytes reveal modulation of synchronized mitochondrial clusters." In:

*Proceedings of the National Academy of Sciences of the United States of America* 107.32, pp. 14315–14320. ISSN: 0027-8424. DOI: 10.1073/pnas.1007562107.

Kurz, Felix T, Miguel a Aon, Brian O'Rourke, and Antonis a Armoundas (2010b). "Wavelet analysis reveals heterogeneous time-dependent oscillations of individual mitochondria." In: *American journal of physiology. Heart and circulatory physiology* 299.September 2010, H1736–H1740. ISSN: 0363-6135. DOI: 10.1152/ajpheart.00640.2010.

Aon, Miguel a., Sonia Cortassa, Christoph Maack, and Brian O'Rourke (2007). "Sequential opening of mitochondrial ion channels as a function of glutathione redox thiol status". In: *Journal of Biological Chemistry* 282.30, pp. 21889–21900. ISSN: 00219258. DOI: 10.1074/jbc.M702841200.

Kembro, Jackelyn M., Miguel a. Aon, Raimond L. Winslow, Brian O'Rourke, and Sonia Cortassa (2013). "Integrating mitochondrial energetics, redox and ROS metabolic networks: A two-compartment model". In: *Biophysical Journal* 104.2, pp. 332–343. ISSN: 00063495. DOI: 10.1016/j.bpj.2012.11.3808. URL: http://dx.doi.org/10.1016/j.bpj.2012.11.3808.

Chance, B, H Sies, and A Boveris (1979). "Hydroperoxide metabolism in mammalian organs." In: *Physiological reviews* 59.3, pp. 527–605. ISSN: 0031-9333.

Han, Derick, Fernando Antunes, Raffaella Canali, Daniel Rettori, and Enrique Cadenas (2003). "Voltage-dependent anion channels control the release of the superoxide anion from mitochondria to cytosol". In: *Journal of Biological Chemistry* 278.8, pp. 5557–5563. ISSN: 00219258. DOI: 10.1074/jbc.M210269200.

Bienert, Gerd P. and François Chaumont (2014). "Aquaporin-facilitated transmembrane diffusion of hydrogen peroxide". In: *Biochimica et Biophysica Acta - General Subjects* 1840.5, pp. 1596–1604. ISSN: 18728006. DOI: 10.1016/j.bbagen.2013.09.017. URL: https://www.sciencedirect.com/science/article/pii/S030441651300398X?via%7B%5C%%7D3Dihub.

Birkedal, Rikke, Holly a Shiels, and Marko Vendelin (2006). "Three-dimensional mitochondrial arrangement in ventricular myocytes: from chaos to order." In: *American journal of physiology. Cell physiology* 291.6, pp. C1148–C1158. ISSN: 0363-6143. DOI: 10.1152/ajpcell.00236.2006.

Park, Junseong, Jungsul Lee, and Chulhee Choi (2011). "Mitochondrial network determines intracellular ROS dynamics and sensitivity to oxidative stress through switching inter-mitochondrial messengers". In: *PLoS ONE* 6.8. ISSN: 19326203. DOI: 10.1371/journal.pone.0023211.

Aon, Miguel Antonio, Sonia Cortassa, Fadi Gabriel Akar, and Brian O'Rourke (2006). "Mitochondrial criticality: A new concept at the turning point of life or death". In: *Biochimica et Biophysica Acta - Molecular Basis of Disease* 1762.2, pp. 232–240. ISSN: 09254439. DOI: 10.1016/j.bbadis.2005.06.008.

Bray, Robert C, Stephen A Cockle, E Martin Fielden, Peter B Roberts, Giuseppe Rotilio, and Lilia Calabrese (1974). "Reduction and inactivation of superoxide dismutase by hydrogen peroxide". In: *Biochemical Journal* 139.1, 43 LP –48. URL: http://www.biochemj.org/content/139/1/43.abstract.

Liochev, Stefan I and Irwin Fridovich (2002). "Copper, Zinc Superoxide Dismutase and H2O2 : EFFECTS OF BICARBONATE ON INACTIVATION AND OXIDATIONS OF NADPH AND URATE, AND ON CONSUMPTION of H2O2 ". In: *Journal of Biological Chemistry* 277.38, pp. 34674–34678. DOI: 10.1074/jbc.M204726200. URL: http://www.jbc.org/content/277/38/34674.abstract.

Brady, Nathan R, Anne Hamacher-Brady, Hans V Westerhoff, and Roberta a Gottlieb (2006). "A wave of reactive oxygen species (ROS)-induced ROS release in a sea of excitable mitochondria." In: *Antioxidants & redox signaling* 8, pp. 1651–1665. ISSN: 1523-0864. DOI: 10.1089/ars.2006.8.1651.

Solhjoo, Soroosh, Brian O'Rourke, Author Manuscript, and Tract Structures (2015). "Mitochondrial Instability during Regional Ischemia-Reperfusion Underlies Arrhythmias in Monolayers of Cardiomyocytes". In: *Journal of molecular and cellular cardiology*, pp. 90–99. ISSN: 0022-2828. DOI: 10.1016/j.yjmcc.2014.09.024. arXiv: NIHMS150003. URL: http://www.ncbi.nlm.nih.gov/pmc/articles/PMC4268014/.

Lavorato, Manuela, V Ramesh Iyer, Williams Dewight, Ryan R Cupo, Valentina Debattisti, Ludovic Gomez, Sergio De la Fuente, Yan-Ting Zhao, Héctor H Valdivia, György Hajnóczky, and Clara Franzini-Armstrong (2017). "Increased mitochondrial nanotunneling activity, induced by calcium imbalance, affects intermitochondrial matrix exchanges". In: *Proceedings of the National Academy of Sciences* 114.5, E849 LP –E858. URL: http://www.pnas.org/content/114/5/E849.abstract.

Gauthier, Laura D., Joseph L. Greenstein, Sonia Cortassa, Brian O'Rourke, and Raimond L. Winslow (2013). "A Computational model of reactive oxygen species and redox balance in cardiac mitochondria". In: *Biophysical Journal* 105.4, pp. 1045–1056. ISSN: 00063495. DOI: 10.1016/j.bpj.2013.07.006. URL: http://dx.doi.org/10.1016/j.bpj.2013.07.006.

Gauthier, Laura D, Joseph L Greenstein, Brian O'Rourke, and Raimond L Winslow (2013). "An Integrated Mitochondrial ROS Production and Scavenging Model: Implications for Heart Failure". In: *Biophysical Journal* 105.12, pp. 2832–2842. ISSN: 0006-3495. DOI: 10.1016/j.bpj.2013.11.007. arXiv: arXiv:1011.1669v3. URL: http://www.ncbi.nlm.nih.gov/pmc/articles/PMC3882515/.

# Chapter 4

# Effect of Multiple Non-coherent Clusters of Oscillating Mitochondria on Electrical Propagation

## 4.1 Introduction

Sudden cardiac death is usually preceded by an arrhythmia that can be caused by an increase in dispersion of refractoriness(Zipes and Wellens, 1998). Regional heterogeneity of the refractory period of cardiac tissue depends on the APD of the individual cardiomyocytes and the conduction velocity(Zhou, Solhjoo, et al., 2014). Unidirectional block can occur when the repolarization gradient is greater than 3.2ms/mm(Laurita and Rosenbaum, 2000; Qu, Garfinkel, and Weiss, 2006). Dispersion of repolarization is also seen during reperfusion of the heart, after ischemia(Levites, Banka, and Helfant, 1975) and is concurrent with an increase in spatiotemporal heterogeneity of the mitochondrial membrane potential(Lyon et al., 2010; Slodzinski, Miguel a.

Aon, and O'Rourke, 2008). Further, the timing of $\Delta\Psi_m$ depolarization and ventricular fibrillation during reperfusion coincide(Akar et al., 2005).

The mechanistic link between mitochondrial dysfunction and electrical instability in the heart is incomplete. One possible mechanism is via ATP-sensitive potassium channels ($K_{ATP}$), which open when ATP is low and can cause APD shortening(George E. Billman, 2008). Indeed, blocking these channels reduces the APD shortening during ischemia and can prevent arrhythmia induced during reperfusion(G E Billman, Englert, and Schölkens, 1998). Also, mutations in $K_{ATP}$ are associated with arrhythmia in humans(Antzelevitch and Barajas-Martinez, 2010; Medeiros-Domingo et al., 2010; Tester et al., 2011).

Understanding what causes $K_{ATP}$ channel activation is important for understanding the link between metabolic stress and arrhythmia. Mitochondrial ROS-Induced-ROS-Release (RIRR) is the autocatalytic burst release of ROS from either increased ROS production from the electron transport chain when subjected to exogenous sources of ROS, or when antioxidant defense of the mitochondria are compromised(Miguel a. Aon, Cortassa, Maack, et al., 2007). The RIRR event is a key component of depolarization of $\Delta\Psi_m$ in cardiac cells during oxidative stress(Zorov et al., 2000). RIRR can be synchronized across entire mitochondrial network from local ROS diffusion as described in the previous study and produces a propagating depolarization wave(Zhou, Miguel a. Aon, et al., 2010). $\Delta\Psi_m$ depolarization causes ATPase to operate in reverse, consuming ATP rather than producing, which drops the ATP/ADP ratio and, with enough failing mitochondria, activates the $K_{ATP}$ channels that cause APD shortening(Sasaki et al., 2001).

In this work, we first looked at how mitochondrial oscillations in $\Delta\Psi_m$ from oxidative stress can create an APD shortening pattern in tissue that results in reentry in a computational model of a paced tissue slab. Second, we investigated how distributions of mitochondrial failure state can evolve and increase the chance of creating reentry. We used a phenomenological based reaction-diffusion system to model the evolution of the distribution of mitochondrial state and modified the first tissue model to accept the distribution parameters. Our findings demonstrated that oscillations in mitochondrial state are pro-arrhythmic and how the evolution of the distribution of mitochondrial oscillation parameters is important for increasing the amount of arrhythmogenic risk.

## 4.2 Methods

### 4.2.1 Computational Model

The cardiomyocyte model used in this study was the ECME-RIRR model(Zhou, Cortassa, et al., 2009), based on experimental observations of oxidative stress-iinduced metabolic oscillations in intact guinea pig cardiomyocytes, where a $\Delta\Psi_m$ depolarization is triggered by a ROS-activated inner membrane anion channel(Miguel a Aon, Cortassa, and O'Rourke, 2004; Miguel a. Aon, Cortassa, Marbán, et al., 2003). The general scheme of the myocyte model is displayed in Figure 4.1. To investigate how mitochondrial oscillations present in the cardiac tissue can increase the risk of arrhythmia, we incorporated the ECME-RIRR myocyte model into a 2D finite element model (5x5$cm^2$ slab) of ventricular tissue. Electrical activity of the myocardial sheet was described by the

monodomain equation(Plank et al., 2008). No-flux conditions for membrane myocyte voltage were used at the slab boundaries.

### 4.2.2 Simulation Protocol

The tissue slab was divided into two regions, an oxidatively stressed region in the center of the slab, and the normal tissue surrounding it (Figure 4.2.) This represented a region of tissue undergoing oxidative stress from reperfusion. The oxidatively stressed region produced additional ROS compared to the normal tissue, which could induce RIRR, reduce ATP levels, and activate $K_{ATP}$ channels. The tissue was paced every second for 30 stimulations. Variations in $K_{ATP}$ channel density ($\sigma_{KATP}$) and size of the stressed zone were explored to determine their effect on reentry inducibility.

In the second part, the stimulation protocol was the same but the cell model was modified to parameterize the oscillation properties of the mitochondria. These properties include depolarization frequency, duration, and initial depolarization delay (phase). As a simplification, since the time scale for reentry is much shorter than the cycle length of a mitochondrial oscillation, only the phase was manipulated (Figure 4.3). Thus, a mitochondrion would change state, from polarized to depolarized or depolarized to polarized, at some predetermined time during the window where an electrical wave was propagating through the tissue. Since ROS generation was no longer coupled to the model, ROS generation and scavenging were removed along with their equation dependencies. The stimulation protocol from part one was used in part two but the mitochondrial oscillation phase distribution of the stressed

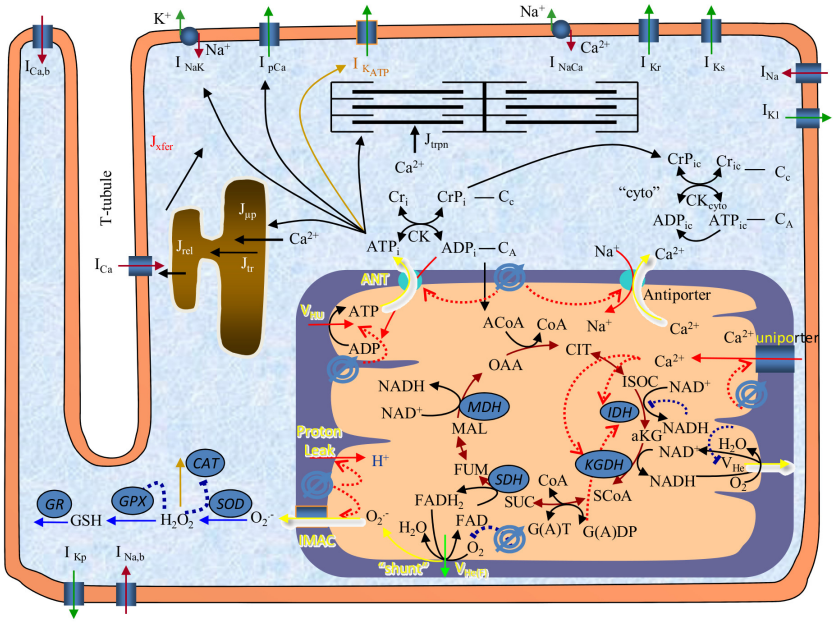


**Figure 4.1: ECME-RIRR Model Schematic.** Schematic of E-C coupling, Mitochondrial Energetics and ROS Induced ROS Release (ECME-RIRR) model. The electrophysiological module describes the major ion channels underlying the action potential and the processes involved in $Ca^{2+}$ handling, and the inner mitochondrial membrane channels. The mitochondrial module accounts for the major components of mitochondrial energetics. The RIRR module describes ROS production, transport and scavenging. The mitochondrial energetics and ROS are linked to cellular electrical activity through the energy sensitive K ATP current. This model displays many of the features observed in whole-cell experiments carried out in guinea pig myocytes. In particular, the ECME- RIRR model recapitulates the close coupling between mitochondrial energy state, ROS bursting, and APD shortening observed in myocytes subjected to oxidative stress(Zhou, Cortassa, et al., 2009). It is the first cardiac cell model to consider the links between ion fluxes, energy-consuming reactions (e.g. myosin ATPase), energy production, and ROS balance, thereby allowing us to investigate how mitochondrial dysfunction translates into electrophysiological alterations that could lead to arrhythmias. It is worthy to point out that various experimental studies have demonstrated that many ion channels and transporters are sensitive to both redox state and phosphorylation state. However, as our major objective was to investigate whether and how mitochondrial dysfunction, particularly depolarization and increased ATP turnover associated with KATP channel activation, could influence AP propagation in cell monolayers, only some of these components are linked to ATP/ADP levels in the present model (i.e., the KATP channel and the energy-dependent pumps and ATPases).

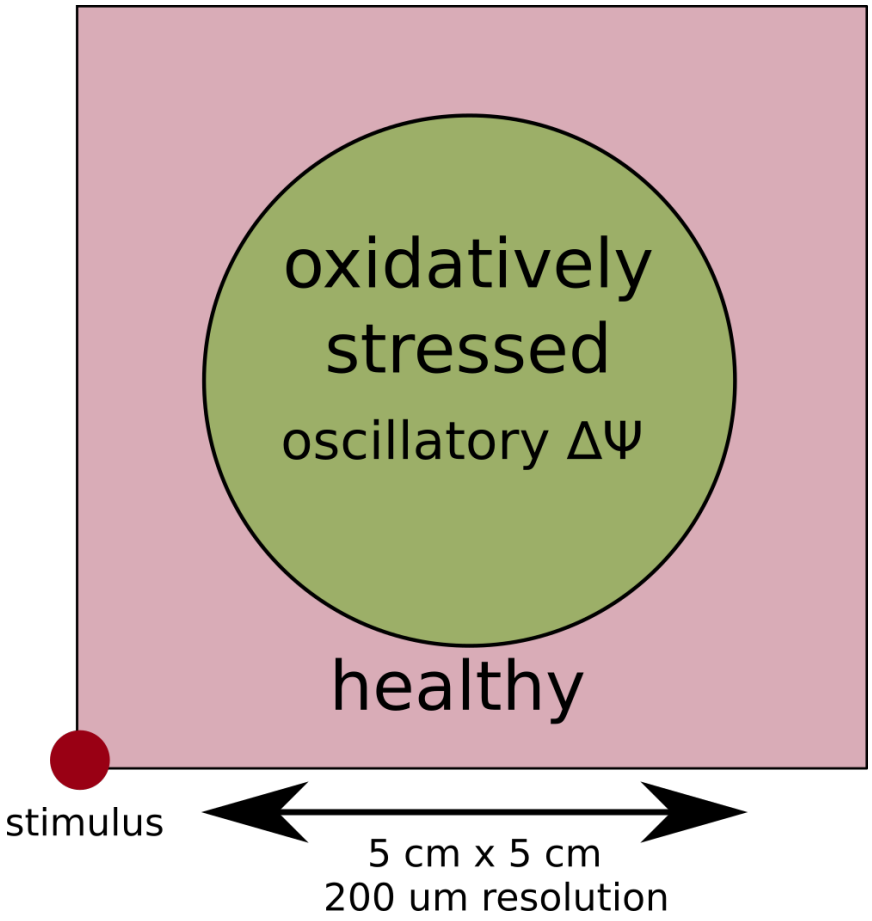


**Figure 4.2: Tissue Slab Protocol Scheme.**

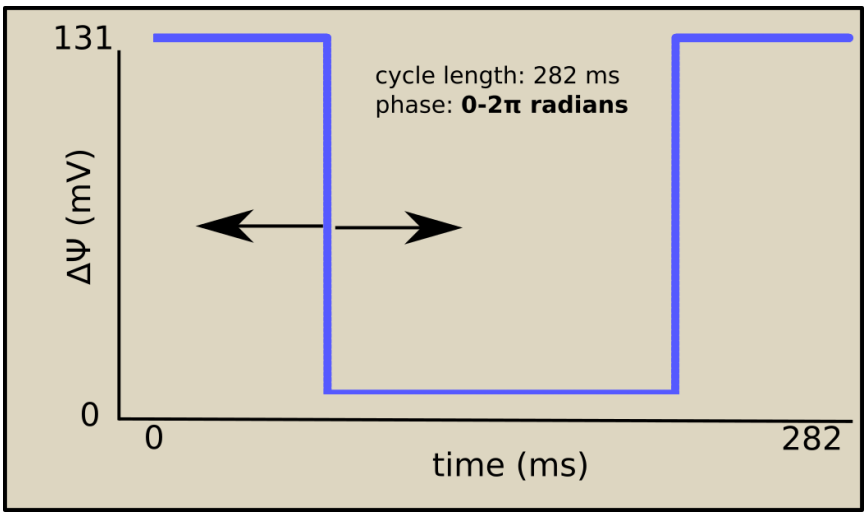


**Figure 4.3: Parameterization of Mitochondrial Oscillation State.** A change in phase is a shifting of the depolarization start time or repolarization start time

region was varied. The first distribution was chosen to replicate the conditions in part one where the mitochondria in each cell would start depolarized and would repolarize when the propagating wave was at the middle of the stressed region. The second distribution was a uniformly random phase for each myocyte. Using the distribution evolution algorithm described below, a new phase distribution was derived from each iteration of the algorithm. The iterative algorithm generated distributions that formed clusters of similar phases. We ran simulations with distributions that were acquired after 5, 10, 100, and 500 iterations. These different distributions visually differed in cluster size.

### 4.2.3 Phase Distribution Algorithm

An uniformly random distribution of phase values were assigned to all the mesh nodes that were marked as oxidatively stressed to act as the initial

distribution. To perform a step in the algorithm, for each neighboring mesh node, a reaction function would compute a phase displacement based on the difference between the current node's phase and the neighbor's phase. When a neighbor was depolarized, the current node would depolarize earlier if the current node is polarized. This action represents the additional ROS from a neighboring cell that would cause the current cell to accumulate additional ROS faster. If the current node was already depolarized, however, this would delay repolarization of the current node because of the additional ROS to scavenge. Each of these effects would be averaged to represent the diffusion aspect of the reaction-diffusion system. Because the input domain is a cyclic range of values, we used the centroid method as the method of computing an average. This is where phase is converted to a vector on a unit circle based on the radian value, and the sum of the vectors divided by the magnitude of the sum returns a new vector on the unit circle pointing to the new phase to use.

## 4.3 Results

### 4.3.1 Formation of Inexcitable Region

After enough electrical stimuli, all of the oxidatively stressed tissue had dramatically reduced APD and would repolarize faster than the surrounding normal tissue, resulting in a region of polarized tissue surrounded by polarized tissue 200 ms after a stimulus (Figure 4.4A). Increasing the $\sigma_{KATP}$ reduced APD (Figure 4.4B) and resulted in different levels of excitation of the oxidatively stressed region when compared at the same time after excitation (Figure 4.4C). Decreasing the APD also decreased the time for the j-gate of the sodium

channel to recover from inactivation (Figure 4.4D). The effect was dramatic enough with $\sigma_{KATP}$=3.8 that the j-gate could recover before the wave outside the metabolic sink had finished passing through the region, making the tissue vulnerable to re-excitation. The tissue did not re-excite, however, due to the strong outward currents of the $K_{ATP}$ channels preventing depolarization. Changing $\sigma_{KATP}$ had no effect on $\Delta\Psi_m$.

### 4.3.2 Recovery of Mitochondrial Energetics Induces Spontaneous Arrhythmia

With additional pacings, eventually the mitochondria in the oxidative stress region repolarized, which restored ATP levels, deactivating the $K_{ATP}$ channels and restoring excitability in the stressed region. If the mitochondrial repolarization event occured while a propagating wave passed through the stressed region, the tissue at the back of the wave (within the stressed region) would re-excite and propagate in the reverse direction (Figure 4.5A). This reverse wave would continue moving in the reverse direction. If the size of the stressed region was small enough (r=0.5 cm), the reverse wave would travel until it collided with the still excited normal tissue at the edge of the stressed tissue boundary (Figure 4.5A top row). If the region was large enough (r=1 and 2cm), the reverse wave would encounter repolarized normal tissue that was excitable and would thus continue propagation, forming a reentrant circuit (Figure 4.5A middle and bottom row). The reentrant propagation persisted longer with the larger radius (r=2cm) and thus size increases the risk of arrhythmia (Figure 4.5B).

The mitochondria repolarize rapidly (<80ms) and at 132ms results in 90%

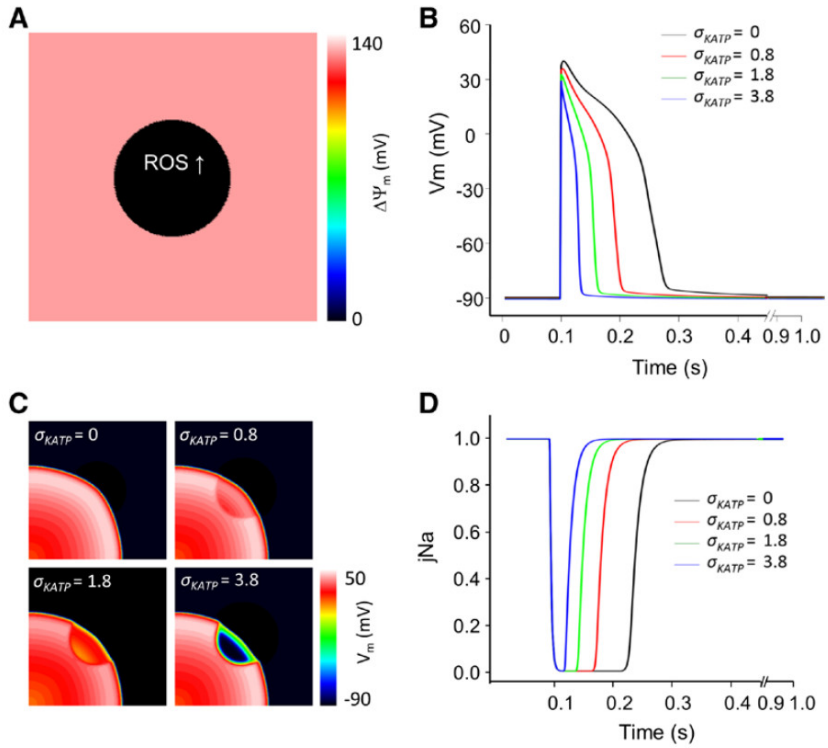


**Figure 4.4: Effect of reactive oxygen species (ROS)-induced regional mitochondrial depolarization on metabolic sink formation and electrical wave propagation in a 2-dimensional (2D) tissue model.** **A.** Regional mitochondrial inner membrane potential ($\Delta\Psi_m$) depolarization in the central region occurs spontaneously when fractional ROS generation by the electron transport chain is increased (ROS shunt increased from the nominal level of 2% to 14% in the central zone). **B.** Effects of changing $\sigma_{KATP}$ ($0/um^2$ , $0.8/um^2$ , $1.8/um^2$ , and $3.8/um^2$) throughout the model on the action potential at the center of the metabolic sink (action potentials outside of the sink were not affected). **C.** Propagation of the electrical wave through the metabolic sink at 90 ms after the stimulus (1 Hz stimulus applied at lower left corner). **D.** Sodium channel availability (jNa; inactivation gate parameter) with different $K_{ATP}$ channel densities. 2D tissue model size, 5x5 $cm^2$, 63 000 nodes; sink zone radius, r=1 cm; tissue conductivity, 0.1 S/m. Excitation-contraction coupling, mitochondrial energetics, and ROS-induced ROS release model parameters were otherwise identical to those in the study by Zhou et al(Zhou, Miguel a. Aon, et al., 2010)

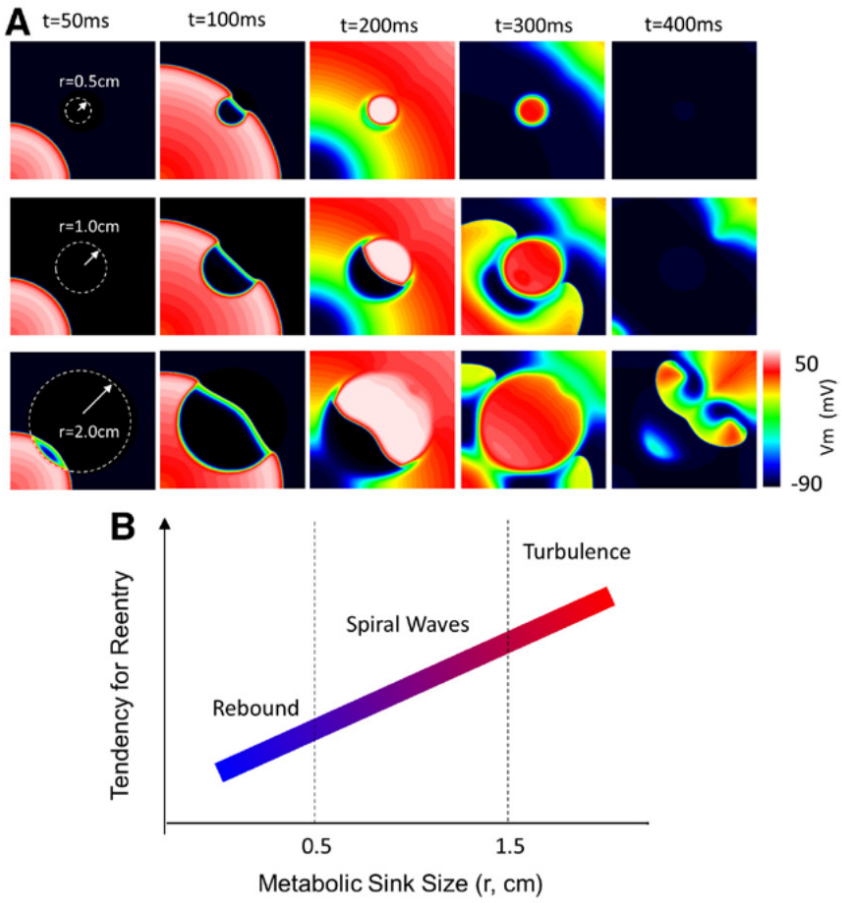


**Figure 4.5: Effect of recovery of mitochondrial inner membrane potential ($\Delta\Psi_m$) on electrical propagation.** **A.** $\Delta\Psi_m$ repolarization in the metabolic sink induced either a rebound excitation contained within the sink, re-entry, or fibrillation in the 2-dimensional tissue model, depending on the sink size (r=0.5, 1, and 2cm, respectively). **B.** Scheme of the effect of sink size on the genesis of abnormal electrical activity. $\sigma_{KATP}$=3.8/$um^2$.

recovery of $\Delta\Psi_m$, which almost completely inactivates the $K_{ATP}$ channels in the stressed region (Figure 4.6A). Because the wavelength of the forward propagating wave is short, the stressed region has a short refractory period. Rapid inactivation of $K_{ATP}$ channels (Figure 4.6C) results in a change of excitability of the tissue while the stressed region is within a propagating wave. Reentry from the rapid change in excitability is not exclusive to the reverse wave propagation but also from the sides (Figure 4.7. $K_{ATP}$ current is also present at the stressed region boundary, preventing excitation when a propagating wave is passing through the whole tissue slab (Figure 4.6A).

### 4.3.3 Dynamic Excitability of Small Clusters Induces Spontaneous Arrhythmia

To obtain different distributions of mitochondrial oscillation phase, we first assigned a random phase to each node in the mesh. This phase determined whether the mitochondria in the cell model would start polarized or depolarized, and at what time they would transition to the other state. A randomly distributed phase simulates the effects of the initially unsynchronized mitochondrial oscillators like those found in neonatal rat ventricular myocyte monolayers during coverslip reperfusion(Solhjoo et al., 2015). Applying the phase generation algorithm to this distribution resulted in a new, slightly different distribution. Figure 4.8 shows that clusters of nodes with similar phases formed and grew in size with additional iterations. Increasing the iterations beyond 500 did not appear to qualitatively alter the distribution.

Applying the stimulation protocol to a tissue slab with a stressed region with an identically uniform phase resulted in the same propagation pattern

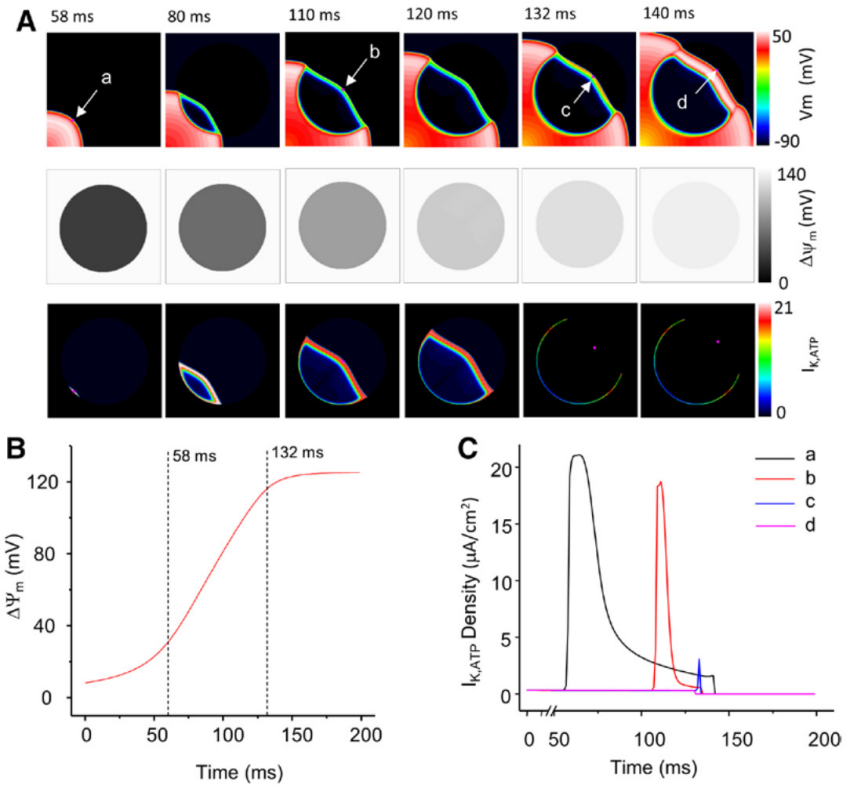


**Figure 4.6: Electrical wave, mitochondrial inner membrane potential ($\Delta\Psi_m$) recovery, and $I_{KATP}$ during waveback breakthrough.** **A.** Propagation of the electrical wave (top), recovery of $\Delta\Psi_m$ (middle), and K ATP current (bottom). **B.** The time course of $\Delta\Psi_m$ recovery at the sink center. **C.** Inactivation of K ATP currents accompanying mitochondrial repolarization. $\sigma_{KATP}$=3.8/$um^2$, r=2cm.

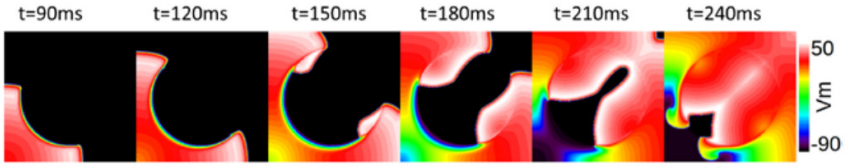


**Figure 4.7: Reentry from the side.** Induction of re-entry during recovery of mitochondrial inner membrane potential under the conditions of reduced tissue conductivity (gap junction uncoupling) in the metabolic sink (conductivity decreased from 0.1 S/m in normal tissue to 0.03 S/m in the central region). $\sigma_{KATP}$=3.8/$um^2$, r=2 cm. Similar behavior can be achieved with tissue conductivities in the interval 0.1 to 0.03 S/m and $\sigma_{KATP}$>3.8/$um^2$.

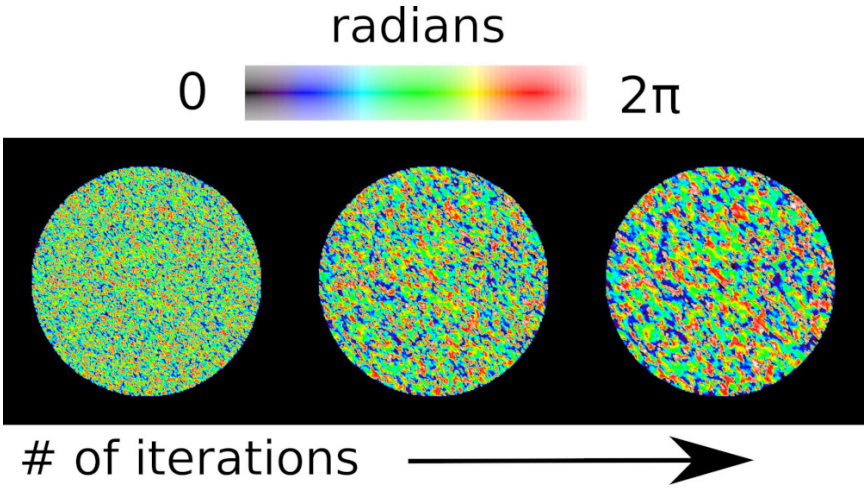


**Figure 4.8: Iterative Phase Distribution Generation.** Additional iterations of the phase generation algorithm produces clusters of similar phase with increasing size. The number of iterations, from left to right are 0, 10, and 100.

as before (Figure 4.9 Top row). Applying the stimulation protocol to a tissue slab with a phase distribution that is uniformly random resulted in a propagating wave through the stressed region with an APD and wavelength shorter than the normal tissue but longer than the identically uniform case (Figure 4.9 Middle row). This wavelength looked more like the wavelength seen in monolayer experiments(Zhou, Solhjoo, et al., 2014) without having to modify the conduction velocity by changing the tissue conductivity or the sodium channel conductivity. Applying the stimulation protocol to a tissue slab with the phase distribution acquired after 100 iterations resulted in reentry (Figure 4.9 Bottom row). With the uniformly random distribution, even though individual nodes had fully activated $K_{ATP}$ channels, they were still substantially excited from neighboring nodes. The net effect was similar to tissue simulation with intermediate $\sigma_{KATP}$ values (0.8-1.5)$/um^2$. As the cluster sized increased, enough current from the $K_{ATP}$ channels could shorten the

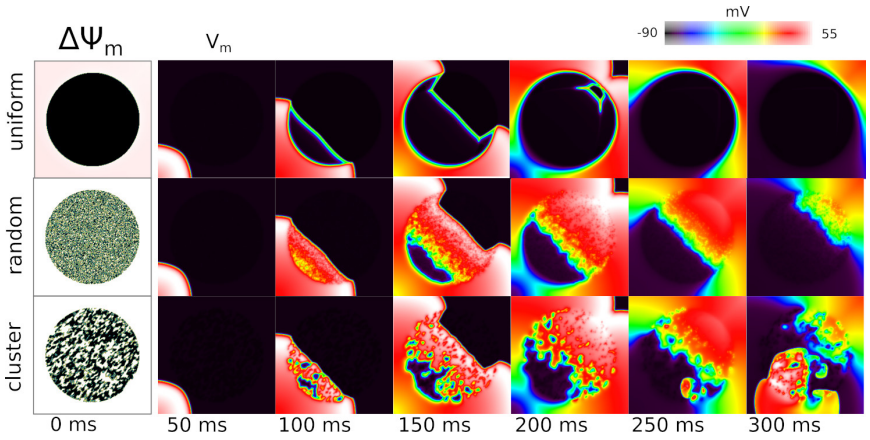


**Figure 4.9: Electrical wave propagation with generated mitochondrial oscillation phase distributions.** Top row, electrical propagation with a stressed region with the same mitochondrial oscillation phase. Middle row, oscillation phase is uniform-randomly distributed for each myocyte. Bottom row, electrical activity using a phase distribution obtained after 100 iterations of the phase generation algorithm.

APD to the levels seen in the uniformly identical distribution simulation.

In the clustered distribution simulation, after the propagating wave with shortened wavelength passed over the stressed region, small pockets of unexcited tissue were visible (Figure 4.10 150ms, a,b,c). At 230ms after stimulation, some of the clusters re-excited because of their repolarized mitochondria and local surrounding excited tissue (Figure 4.10 230ms b,c). However, only a subset of these clusters (Figure 4.10 240ms c) were able to propagate and re-excite additional tissue. A stepped sequential restoration of excitability created a gating based delay mechanism that effectively created slower propagation. Similar to the Panama canal locks, this allowed a reverse oriented propagating wave to meet the boundary of the stressed region after the normal tissue was no longer refractory. Further, because of the presence of additional clusters of still inexcitable tissue, the propagating wave had to meander around these

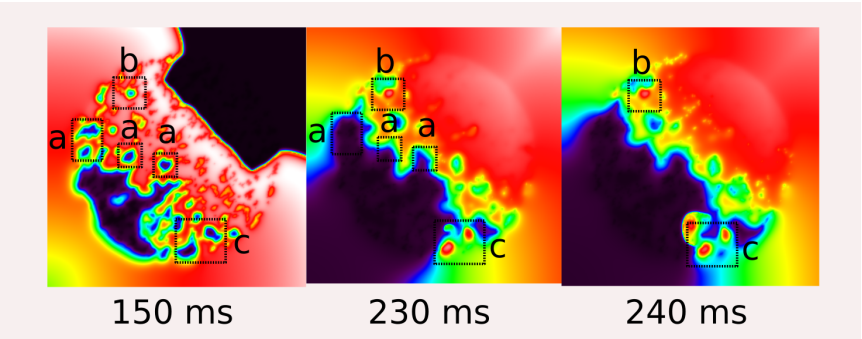


**Figure 4.10: Dynamic excitability of small tissue clusters. a** clusters are unexcited at 150ms and remain unexcited at 230ms. **b,c** clusters are unexcited at 150ms but are re-excited at 230ms and 240ms from excited neighboring tissue. Only **c** cluster is surrounded by additional re-excitable tissue such that a wave can propagate at the back of the original wave at 240ms.

clusters, further delaying the contact with the boundary. Both of these mechanisms can increase the risk of reentry by holding and delaying excitation of tissue. This can decrease the size of stressed region needed to create reentry.

## 4.4 Discussion

In this study, we showed in a 2D simulation of a tissue slab that spatiotemporal heterogeneity of the mitochondrial state across the myocytes in the tissue can cause spatiotemporal heterogentity of refractorniess, which can induce reentry and arrhythmia in the tissue. Mitochondria, which are responsible for supplying ATP to the cell, are linked to the electrical properties of the myocyte, through sarcolemmal $K_{ATP}$ channels. These channels are activated by a decrease in cytosolic ATP and induce an inward potassium current(Lederer, Nichols, and Smith, 1989; Noma, 1983). Mitochondrial function is compromised when the supply of the components necessary for respiration are eliminated, such as in ischemia. After 10 minutes of ischemia, the

resting membrane potential equals the Nernst potential of potassium(Kleber, 1983) and accounts for most of the AP shortening during the early phase of ischemia(Akar et al., 2005). Reperfusion is the first step in restoring function of the heart after ischemia, however, reperfusion itself can cause injury(Carry et al., 1989; Maxwell and Lip, 1997). In guinea pig hearts, reperfusion after 30 minutes of global ischemia induced reentrant arrhythmia which was prevented or reversed with 4'chlorodizepam, which is believed to block the inner membrane anion channel of the mitochondria(Akar et al., 2005). This study revealed what spatialtemporal patterns of mitochondrial energetic state that can cause reentry and revealed how the evolution of the distribution of mitochondrial oscillation properties can increase the probability of reentry.

Reentry was created through first spontaneous reactivation of tissue at the rear of the propagating wave. This tissue was able to reactivate because first, the inactivation components of the sodium channels had already recovered because this tissue had a reduced APD that had less of an influence on the inactivation component. The activation of $K_{ATP}$ channels created an outward current that reduced the APD but also increased the inward current required to initiate a new action potential. Thus, only tissue that had both recovered sodium channels and inactive $K_{ATP}$ channels could re-excite after a short period. The rapid repolarization of the mitochondrial membrane potential, which rapidly restored ATP levels, was important in order to occur within the time window of a normal APD. This rapid change could fulfill the requirements of having recovered sodium channels and inactive $K_{ATP}$ channels.

This activation at the back of the wave could only propagate if there was additional tissue to excite. Additional oxidatively stressed tissue which also had a reduced APD, were excitable, and the reverse propagation could pass through those tissue. Normal tissue had the longer APD and so once the back wave reached the stressed/normal interface, the back wave propagation would terminate unless the path to the interface was sufficiently long. However, mitochondrial networks between different myocytes, are unlikely to be perfectly synchronized in depolarization and repolarization timing due to the variations in ROS generation, ROS scavenging, spacing, and the chaotic nature of these systems.

Initially, these separate mitochondrial systems might be completely discordant. These results were similar to the simulations run with smaller $\sigma_{KATP}$ values because of the averaging effect and did not create reentry. However, Thus, while different mitochondrial systems were likely to be discordant globally, there are synchronization mechanisms between mitochondria that would make the phase of the region locally similar. A reaction-diffusion system models the balance between synchronization and alteration of oscillation properties and often produces clustered distributions(Lee et al., 1994).

Using these types of distributions, additional mechanisms were possible to increase the time for the back wave to meet the interface. First, a sequence of mitochondrial oscillation phase clusters could be cascaded in time and both contain and move the excited tissue in lock-step. This pattern is analogous to the Panamal locks which allow boats to travel in-step, across the canal, where two end points are at different heights. Essentially, phase clusters closer to

the interface reactivate relatively later. Second, from the stacking of multiple clusters, the path back to the interface is more tortuous, increasing the distance needed to travel. Together, these mechanisms decrease the required size of the metabolically stressed region and increase the risk of reentry.

### 4.4.1 Limitations

These simulations only considered the effect of low ATP on potassium currents and not the effect of low ATP on other channels and systems. Further, ROS has additional direct effects on other channels that were not accounted for. We expect these effects to only increase the risk of arrhythmia. We used a phenomenological based model of evolving mitochondrial phase distribution. There might be additional mechanisms of synchronization between cells that can produce a different phase distribution. Also the mitochondrial network was lumped as a single mitochondrion for each myocyte. A network can have multiple frequencies and different resulting levels of $K_{ATP}$ channel activation that is not completely all on or off.

Further, the actual heart is composed of a thick volume, where transmural dispersion of repolarization can lead to waves from many angles that can encounter the metabolic sink at different times. Our 2D simulation requires that every reentry start from somewhere within a thin plane and doesn't represent these additional possibilities.

### 4.4.2 Future Directions

These results provide two thereaputic targets, the $K_{ATP}$ channel and the inner membrane anion channel of the mitochondria. Indeed, $K_{ATP}$ channel inhibition prevented arrhythmia induced by the combination of acute myocardial ischemia and exercise in dogs with healed myocardial infarctions(G E Billman, Englert, and Schölkens, 1998; George E. Billman, 2008; George E Billman et al., 2004).

Extending these simulations to 3D might reveal addition mechanisms that increase the risk of reentry. In 3D, the sphere stacking problem is more complex and can further increase the path length, effectively increasing the time needed to travel to reach excitable tissue. Also, the chance of finding a sequential gating neighbor increases with additional directions to have neighbors.

# References


Zipes, D P and H J Wellens (1998). "Sudden cardiac death." In: *Circulation* 98, pp. 2334–2351. ISSN: 0009-7322. DOI: 10.1161/01.CIR.98.21.2334.

Zhou, Lufang, Soroosh Solhjoo, Brent Millare, Gernot Plank, M. Roselle Abraham, Sonia Cortassa, Natalia Trayanova, and Brian O'Rourke (2014). "Effects of regional mitochondrial depolarization on electrical propagation: Implications for arrhythmogenesis". In: *Circulation: Arrhythmia and Electrophysiology* 7.1, pp. 143–151. ISSN: 19413084.

Laurita, K R and D S Rosenbaum (2000). "Interdependence of modulated dispersion and tissue structure in the mechanism of unidirectional block." In: *Circulation research* 87.10, pp. 922–928. ISSN: 0009-7330. DOI: 10.1161/01.RES.87.10.922.

Qu, Zhilin, Alan Garfinkel, and James N Weiss (2006). "Vulnerable window for conduction block in a one-dimensional cable of cardiac cells, 1: single extrasystoles." In: *Biophysical journal* 91.3, pp. 793–804. ISSN: 00063495. DOI: 10.1529/biophysj.106.080952. URL: http://dx.doi.org/10.1529/biophysj.106.080945.

Levites, R, V S Banka, and R H Helfant (1975). "Electrophysiologic effects of coronary occlusion and reperfusion. Observations of dispersion of refractoriness and ventricular automaticity". In: *Circulation* 52.5, pp. 760–765. URL: 1175258.

Lyon, Alexander R., Paul J. Joudrey, Dongzhu Jin, Robert D. Nass, Miguel a. Aon, Brian 'Rourke, and Fadi G. Akar (2010). "Optical imaging of mitochondrial function uncovers actively propagating waves of mitochondrial membrane potential collapse across intact heart". In: *Journal of Molecular and Cellular Cardiology* 49.4, pp. 565–575. ISSN: 00222828. DOI: 10.1016/j.yjmcc.2010.07.002. URL: http://dx.doi.org/10.1016/j.yjmcc.2010.07.002.

Slodzinski, Martin K., Miguel a. Aon, and Brian O'Rourke (2008). "Glutathione oxidation as a trigger of mitochondrial depolarization and oscillation in intact hearts". In: *Journal of Molecular and Cellular Cardiology* 45.5, pp. 650–

660. ISSN: 00222828. DOI: 10.1016/j.yjmcc.2008.07.017. URL: http://dx.doi.org/10.1016/j.yjmcc.2008.07.017.

Akar, Fadi G., Miguel a. Aon, Gordon F. Tomaselli, and Brian O'Rourke (2005). "The mitochondrial origin of postischemic arrhythmias". In: *Journal of Clinical Investigation* 115.12, pp. 3527–3535. ISSN: 00219738. DOI: 10.1172/JCI25371.

Billman, George E. (2008). "The cardiac sarcolemmal ATP-sensitive potassium channel as a novel target for anti-arrhythmic therapy". In: *Pharmacology & Therapeutics* 120.1, pp. 54–70. ISSN: 01637258. DOI: 10.1016/j.pharmthera.2008.07.004. URL: http://linkinghub.elsevier.com/retrieve/pii/S0163725808001241.

Billman, G E, H C Englert, and B a Schölkens (1998). "HMR 1883, a novel cardioselective inhibitor of the ATP-sensitive potassium channel. Part II: effects on susceptibility to ventricular fibrillation induced by myocardial ischemia in conscious dogs." In: *The Journal of pharmacology and experimental therapeutics* 286.3, pp. 1465–1473. ISSN: 0022-3565.

Antzelevitch, Charles and Hector Barajas-Martinez (2010). "A gain-of-function I<sub>K-ATP</sub> mutation and its role in sudden cardiac death associated with J-wave syndromes". In: *Heart Rhythm* 7.10, pp. 1472–1474. ISSN: 1547-5271. DOI: 10.1016/j.hrthm.2010.07.027. URL: https://doi.org/10.1016/j.hrthm.2010.07.027.

Medeiros-Domingo, Argelia, Bi-Hua Tan, Lia Crotti, David J Tester, Lee Eckhardt, Alessandra Cuoretti, Stacie L Kroboth, Chunhua Song, Qing Zhou, Doug Kopp, Peter J Schwartz, Jonathan C Makielski, and Michael J Ackerman (2010). "Gain-of-function mutation S422L in the KCNJ8-encoded cardiac K<sub>ATP</sub> channel Kir6.1 as a pathogenic substrate for J-wave syndromes". In: *Heart Rhythm* 7.10, pp. 1466–1471. ISSN: 1547-5271. DOI: 10.1016/j.hrthm.2010.06.016. URL: https://doi.org/10.1016/j.hrthm.2010.06.016.

Tester, David J, Bi Hua Tan, Argelia Medeiros-Domingo, Chunhua Song, Jonathan C Makielski, and Michael J Ackerman (2011). "Loss-of-function mutations in the KCNJ8-Encoded Kir6.1 KATP channel and sudden infant death syndrome". In: *Circulation: Cardiovascular Genetics* 4.5, pp. 510–515. ISSN: 1942-3268. DOI: 10.1161/CIRCGENETICS.111.960195. URL: http://www.scopus.com/inward/record.url?scp=82955173743%7B%5C&%7DpartnerID=8YFLogxK%20http://www.scopus.com/inward/citedby.url?scp=82955173743%7B%5C&%7DpartnerID=8YFLogxK.

Aon, Miguel a., Sonia Cortassa, Christoph Maack, and Brian O'Rourke (2007). "Sequential opening of mitochondrial ion channels as a function of glutathione redox thiol status". In: *Journal of Biological Chemistry* 282.30, pp. 21889–21900. ISSN: 00219258. DOI: 10.1074/jbc.M702841200.

Zorov, D B, C R Filburn, L O Klotz, J L Zweier, and S J Sollott (2000). "Reactive oxygen species (ROS)-induced ROS release: a new phenomenon accompanying induction of the mitochondrial permeability transition in cardiac myocytes." In: *The Journal of experimental medicine* 192.7, pp. 1001–1014. ISSN: 00221007. DOI: 10.1084/jem.192.7.1001.

Zhou, Lufang, Miguel a. Aon, Tabish Almas, Sonia Cortassa, Raimond L. Winslow, and Brian O'Rourke (2010). "A reaction-diffusion model of ROS-induced ROS release in a mitochondrial network". In: *PLoS Computational Biology* 6.1. ISSN: 1553734X. DOI: 10.1371/journal.pcbi.1000657.

Sasaki, N, T Sato, E Marbán, and B O'Rourke (2001). "ATP consumption by uncoupled mitochondria activates sarcolemmal K(ATP) channels in cardiac myocytes." In: *American journal of physiology. Heart and circulatory physiology* 280.4, H1882–H1888. ISSN: 0363-6135.

Zhou, Lufang, Sonia Cortassa, An Chi Wei, Miguel a. Aon, Raimond L. Winslow, and Brian O'Rourke (2009). "Modeling cardiac action potential shortening driven by oxidative stress-induced mitochondrial oscillations in guinea pig cardiomyocytes". In: *Biophysical Journal* 97.7, pp. 1843–1852. ISSN: 00063495. DOI: 10.1016/j.bpj.2009.07.029. URL: http://dx.doi.org/10.1016/j.bpj.2009.07.029.

Aon, Miguel a, Sonia Cortassa, and Brian O'Rourke (2004). "Percolation and criticality in a mitochondrial network." In: *Proceedings of the National Academy of Sciences of the United States of America* 101.13, pp. 4447–4452. ISSN: 0027-8424. DOI: 10.1073/pnas.0307156101.

Aon, Miguel a., Sonia Cortassa, Eduardo Marbán, and Brian O'Rourke (2003). "Synchronized Whole Cell Oscillations in Mitochondrial Metabolism Triggered by a Local Release of Reactive Oxygen Species in Cardiac Myocytes". In: *Journal of Biological Chemistry* 278, pp. 44735–44744. ISSN: 00219258. DOI: 10.1074/jbc.M302673200.

Plank, Gernot, Lufang Zhou, Joseph L Greenstein, Sonia Cortassa, Raimond L Winslow, Brian O'Rourke, and Natalia A Trayanova (2008). "From mitochondrial ion channels to arrhythmias in the heart: computational techniques to bridge the spatio-temporal scales". In: *Philosophical Transactions of the Royal Society A: Mathematical, Physical and Engineering Sciences*

366.1879, 3381 LP –3409. URL: http://rsta.royalsocietypublishing.org/content/366/1879/3381.abstract.

Solhjoo, Soroosh, Brian O'Rourke, Author Manuscript, and Tract Structures (2015). "Mitochondrial Instability during Regional Ischemia-Reperfusion Underlies Arrhythmias in Monolayers of Cardiomyocytes". In: *Journal of molecular and cellular cardiology*, pp. 90–99. ISSN: 0022-2828. DOI: 10.1016/j.yjmcc.2014.09.024. arXiv: NIHMS150003. URL: http://www.ncbi.nlm.nih.gov/pmc/articles/PMC4268014/.

Lederer, W J, C G Nichols, and G L Smith (1989). "The mechanism of early contractile failure of isolated rat ventricular myocytes subjected to complete metabolic inhibition." In: *The Journal of Physiology* 413, pp. 329–349. ISSN: 0022-3751. URL: http://www.ncbi.nlm.nih.gov/pmc/articles/PMC1189104/.

Noma, A (1983). "ATP-regulated K+ channels in cardiac muscle". In: *Nature* 305, p. 147. URL: http://dx.doi.org/10.1038/305147a0%20http://10.0.4.14/305147a0.

Kleber, Andre G (1983). "Resting membrane potential, extracellular potassium activity, and intracellular sodium activity during acute global ischemia in isolated perfused guinea pig hearts." In: *Circulation research* 52 4, pp. 442–450.

Carry, M M, R E Mrak, M L Murphy, C F Peng, K D Straub, and E P Fody (1989). "Reperfusion injury in ischemic myocardium: protective effects of ruthenium red and of nitroprusside". eng. In: *The American journal of cardiovascular pathology* 2.4, pp. 335–344. ISSN: 0887-8005. URL: http://europepmc.org/abstract/MED/2477045.

Maxwell, Simon R J and Gregory Y H Lip (1997). "Reperfusion injury: a review of the pathophysiology, clinical manifestations and therapeutic options". In: *International Journal of Cardiology* 58.2, pp. 95–117. ISSN: 0167-5273. DOI: 10.1016/S0167-5273(96)02854-9. URL: https://doi.org/10.1016/S0167-5273(96)02854-9.

Lee, Kyoung-Jin, William D McCormick, John E Pearson, and Harry L Swinney (1994). "Experimental observation of self-replicating spots in a reaction-diffusion system". In: *Nature* 369, p. 215. URL: http://dx.doi.org/10.1038/369215a0%20http://10.0.4.14/369215a0.

Billman, George E, Melanie S Houle, Heinrich C Englert, and Heinz Gögelein (2004). "Effects of a Novel Cardioselective ATP-Sensitive Potassium Channel Antagonist, 1-[[5-[2-(5-Chloro-o-anisamido)ethyl]-$\beta$-methoxyethoxyphenyl 3-methylthiourea, Sodium Salt (HMR 1402), on Susceptibility to Ventricular

Fibrillati". In: *Journal of Pharmacology and Experimental Therapeutics* 309.1, 182 LP –192. URL: http://jpet.aspetjournals.org/content/309/1/182.abstract.

# Chapter 5

# Conclusion

## 5.1 Summary of findings

In this thesis work, we investigated the mechanisms governing the progression of mitochondrial network failure from exposure to oxidative stress, and further, how network failure can scale to the whole heart, manifesting as an arrhythmia. First, using a biophysically detailed model of a mitochondrial network, we showed that hydrogen peroxide was necessary for spreading stress from a local region, to the rest of the network. Superoxide could not perform this function because superoxide was only released during inner membrane anion channel opening during mitochondrial membrane potential depolarization propagations and its rapid removal limits the spatial extent of its action. Hydrogen peroxide diffusion could slowly deplete the scavenging capacity of the network, and the regions that were depleted determined the regions that would oscillate. Second, using a 2D model of tissue, mitochondrial depolarizations lead to opening of ATP sensitive potassium channels that altered the excitability and APD of the tissue. By modulating when the

tissue could become excitable, a wave could propagate from the back of an existing propagating wave, and create reentry. Further, the distribution of mitochondrial oscillation properties that could emerge over time, could increase the likelihood of reentry and even at smaller stressed region sizes.

Together, these findings highlight the importance of mitochondria in normal heart function. The highly coupled organization of mitochondria and cardiac cells enables efficient function necessary for an organisms survival but also leaves the organism vulnerable to cascading failure mechanisms. To combat these vulnerabilities, the findings in this work suggest two targets for therapeutic intervention in preventing arrhythmia in conditions of oxidative stress, the ATP sensitive potassium channel, and the inner membrane anion channel of the mitochondria.

## 5.2 Future directions

Biophysically detailed descriptions of the synchronization mechanisms between the different mitochondrial networks of neighboring myocytes are lacking. Modeling the diffusion of ROS between myocytes may lead to new emergent behavior not present in the simplified reaction-diffusion phase generation model used in this work. Further, ROS has direct effects on other channels and systems that were not accounted for, both in the mitochondria and in the cytosol. A model including these arrhythmia mechanisms from these future directions may show a dramatic increased risk of arrhythmia from oxidative stress when all combined together. Given that sudden cardiac death victims sometimes show no sign of scarring, these combined mechanisms may

be important when only a short transient ischemia/reperfusion is responsible.

# BRENT MILLARE

## Computational Modeling Resource Engineer & Scientist

@ brent.millare@gmail.com  Baltimore, MD

## EXPERIENCE

### Research Scientist

**Johns Hopkins University**

August 2009 – Ongoing  Baltimore, MD

- Mathematical modeling to investigate how mitochondrial failure can lead to life threatening ventricular arrhythmia under Dr. Natalia Trayanova at Johns Hopkins (See publications)
- Managed computer resources of the lab and led the building of over 30 desktop computers
- Built and maintained websites for two university laboratories

### Research Scientist

**University California Riverside**

Aug 2005 – May 2009  Riverside, CA

- Bioinspired approach to designing engineering materials
- Designed microfluidic based biological sensor

## PUBLICATIONS


- Vullev, V. I., Wan, J., Heinrich, V., Landsman, P., Bower, P. E., Xia, B., ... Jones, G. (2006). Nonlithographic fabrication of microfluidic devices. Journal of the American Chemical Society, 128(50), 16062–16072.
- Millare, B., Thomas, M., Ferreira, A., Xu, H., Holesinger, M., & Vullev, V. I. (2008). Dependence of the Quality of Adhesion between Poly(dimethylsiloxane) and Glass Surfaces on the Conditions of Treatment with Oxygen Plasma. Langmuir, 24(22), 13218–13224. https://doi.org/10.1021/la801965s
- Bao, D., Millare, B., Xia, W., Steyer, B. G., Gerasimenko, A. A., Ferreira, A., ... Vullev, V. I. (2009). Electrochemical oxidation of ferrocene: A strong dependence on the concentration of the supporting electrolyte for nonpolar solvents. Journal of Physical Chemistry A, 113(7), 1259–1267.
- Ashraf, M. K., Pandey, R. R., Lake, R. K., Millare, B., Gerasimenko, A. A., Bao, D., & Vullev, V. I. (2009). Theoretical design of bioinspired macromolecular electrets based on anthranilamide derivatives. In Biotechnology Progress (Vol. 25, pp. 915–922).
- Thomas, M. S., Millare, B., Clift, J. M., Bao, D., Hong, C., & Vullev, V. I. (2010). Print-and-peel fabrication for microfluidics: What's in it for biomedical applications? Annals of Biomedical Engineering, 38(1), 21–32.
- Thomas, M. S., Clift, J. M., Millare, B., & Vullev, V. I. (2010). Print-and-peel fabricated passive micromixers. Langmuir, 26(4), 2951–2957.
- Upadhyayula, S., Bao, D., Millare, B., Sylvia, S. S., Habib, K. M. M., Ashraf, K., ... Vullev, V. I. (2011). Permanent electric dipole moments of carboxyamides in condensed media: What are the limitations of theory and experiment? Journal of Physical Chemistry B, 115(30), 9473–9490.
- Chau, K., Millare, B., Lin, A., Upadhyayula, S., Nunez, V., Xu, H., & Vullev, V. I. (2011). Dependence of the quality of adhesion between poly(dimethylsiloxane) and glass surfaces on the composition of the oxidizing plasma. Microfluidics and Nanofluidics, 10(4), 907–917.


## COMPUTER SKILLS

Linux 17+ years | ArchLinux | Ubuntu | Debian | Gentoo | Clojure 7+ years | Clojurescript | Datalog | HTML5 | CSS3 | C 20+ years | Common Lisp | Bash | CUDA | Python | Matlab | R | Javascript | C++ | Java | PHP | SQL | VHDL | Git | Cloud Technologies Amazon Web Services | Datomic | Finite Element Method | Finite Difference Method

## AWARDS

- 2011 Brent Millare, PhD student, awardee, NIH pre-doctoral fellowship Recieved NIH F31 Grant for my work on Metabolic/Electrophysiological Model of the Heart under Ischemia/Reperfusion.

## EDUCATION

### Ph.D. in Biomedical Engineering

**Johns Hopkins University**

Sept 2009 – Sept 2018

### B.S. in Computer Science

**UC Riverside**

Aug 2003 – Dec 2007

- Nuñez, V., Upadhyayula, S., Millare, B., Larsen, J. M., Hadian, A., Shin, S., ... Vullev, V. I. (2013). Microfluidic space-domain time-resolved emission spectroscopy of terbium(III) and europium(III) chelates with pyridine-2,6-dicarboxylate. Analytical Chemistry, 85(9), 4567–4577. https://doi.org/10.1021/ac400200x
- B Millare, B O'Rourke, N Trayanova, Cell-wide Coordination of ROS-induced ROS Release by Hydrogen Peroxide in Mitochondrial Networks, Physiome meeting, Bar Harbor, Oct. 2013 (abstract available online at cardiacphysiome.phys.mcw.edu)
- Zhou, L., Solhjoo, S., Millare, B., Plank, G., Abraham, M. R., Cortassa, S., ... O'Rourke, B. (2014). Effects of regional mitochondrial depolarization on electrical propagation: Implications for arrhythmogenesis. Circulation: Arrhythmia and Electrophysiology, 7(1), 143–151.
- Millare, B. O'Rourke, B. and N. A. Trayanova (2014). "Cell-Wide Coordination of ROS-Induced ROS Release by Hydrogen Peroxide in Mitochondrial Networks." Biophysical Journal 106(2):183a, 2016
- Millare BM, Trayanova NA. Clusters Of Ventricular Tissue With Metabolically Induced Delayed Excitability Can Initiate A Reentrant Wave. Heart Rhythm. 2016;13(Suppl 5):S193